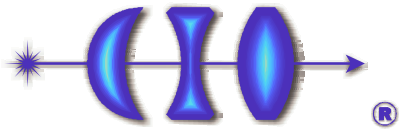

DYNAMIC OF COMPLEX SYSTEM WITH PARAMETRIC MODULATION: DUFFING OSCILLATORS AND A FIBER LASER

THESIS

Presentado por *M.C. Rider Jaimes Reátegui*

Asesor Dr. Alexander Pisarchik

COMO REQUISITO PARA OBTENER EL GRADO DE :

DOCTOR EN CIENCIAS (ÓPTICAS)

LEÓN GUANAJUATO

MÉXICO

26th August 2004

Contents

List of Figures

Dedicatoria

A mis padres Carlos Jaimes y Maria Luisa Reátegui

A mis hermanos Marcos, Carlos, Sumaya, Ruth, Luis y Susan

A toda mi familia

A la Memoria de Wilber Cordoba

Agradecimientos

A Dios que me dio vida, salud y amor.

A mi asesor el Dr. Alexander Pisarchick, que gracias a su incansable apoyo, paciencia y sobre todo su gran espíritu hacia la ciencia me motivó a realizar este trabajo.

Al Dr. Alexander Kir 'yanov por su ejemplo de trabajo, conocimientos y lo más importante colaboró activamente en el desarrollo de este trabajo.

Al Centro de Investigaciones en Óptica, A.C., donde se realizó en su totalidad este trabjo de tesis doctoral. De manera especial expreso mi agradecimiento a los doctores Victor Pinto Robledo, Luis Efraín Regalado, Ramón Rodríguez Vera y el Lic. Antonio Martínez Castillo quienes hicieron posible mi llegada al CIO.

A la Dirección de Formación Académica de Centro de Investigaciones en Optica, A.C. De manera muy especial quiero agradecer al Dr. Oracio Barbosa García y a la Lic. Guillermina Muñiz, quienes se encargaron muy gentilmente de apoyarme con los trámites administrativos que se tuvieron que realizar.

A los Investigadores, Estudiantes, Trabajadores del Centro de Investiga-

ciones en Optica, A.C., sin ellos no hubiera sido posible hacer uso de las diferentes instalaciones del Centro.

A mis amigos y compañeros: Gelacio Atondo, Manuel De la Torre, Rubén Rodríguez, Tonatiuh Saucedo, Sinhué Hinojosa, Víctor Duran, Cornelio Álvarez, Tonatiuh Echegoyén, ya que con sus espíritus de solidariada y amistad me apoyaron mucho en los momentos difíciles.

Y lo más importante agradecer a México, ya que con su enorme hospitalidad en este lindo País me hizo sentir un ambiente más humano.

Preface

This thesis collected the work I did during my Ph.D. at the Centro de Investigaciones en Óptica A.C. The work was done under the supervision of Dr. Alexander Pisarchik. I also acknowledge to Dr. Alexander Kiryanov for his help. Department of Photonics, Centro de Investigaciones en Óptica A.C. This work has been supported by Instituto Mexicano de Cooperación Internacional de la S.R.E en el marco del programa "Cuauhtémoc II " (SER-CONACYT-OEA) and also it has been partially supported by COCYTEG Convenio # 03-04-k119-019 del 2003, internal supported of Centro de Investigaciones en Óptica A.C and Instituto México-USA of the University of California (UC-MEXUS) and Consejo Nacional de Ciencia y Tecnologia-México.

Chapter 1

Introduction

More than two decades of intense studies of nonlinear dynamic have shown that the chaos occurs widely in physics, chemistry, biology, engineering, mathematical and social life [1, 2, 3]. The discovery of chaos changes our understanding of the foundation of physics, has many practical applications as well. The nonlinear dynamic sheds new light on the working of lasers, fluids, mechanical structures, and chemical reactions. It has been noted only as irregular or unpredictable behavior and often attributed to random external influences. Further studies showed that chaotic phenomena are completely deterministic and characteristic for typical nonlinear systems.

The interest in chaos and nonlinear dynamic have grown rapidly since 1963, when Lorentz published his numerical work on a simplified model of convection, and discussed its implication for weather prediction. Nowadays the researches of nonlinear dynamics are addressing to important practical applications which include communications, modelling brain and cardiac

rhythm activity, earthquake dynamics, etc. (see, e.g., [4] and references therein).

In nonlinear dynamics, the study of nonlinear oscillators has played a very important role in the understanding the chaotic phenomenon. The Duffing oscillator has been treated as paradigm of many ubiquitous system. The study of such systems is based mostly on approximate analytical approaches and detail numerical investigations.

Many systems in the nature have several stable states separated by energy barriers. When the system moves among the stables states, the dynamics becomes quite complex. A simple model that illustrates some of this features is the double-well Duffing oscillator. This model was first introduced to understand forced vibrations of industrial machinery by the German electrical engineer Duffing in 1918 [5].

The knowledge of the dynamic behavior of this oscillator under external modulation is of great importance and can be adequate to explored a variety model of physical processes such as stiffening strings, beam buckling, nonlinear electronic circuits, superconducting Josephson parametric amplifiers, and ionization waves in plasmas, as well as biological processes [6, 7, 8, 9, 10, 11, 12, 13, 14, 15],

The search of laser dynamic with chaotic and turbulent processes in other field of the nature has been carried out since last 25 years. It has become increasingly evident that misunderstood and troublesome laser properties, such as unstable emission, poor reproducibly of the laser pulse, limitation of attainable widths of ultrashort pulses and coherence lengths, and also problems

with the emission mode pattern shapes, spontaneous irregular pulsing, etc., are not caused by insufficient technical skill, but are direct consequences of the inherent nonlinearity of the laser. The improvement of these laser properties therefore requires not just diligent effort but more understanding of the physics of this particular nonlinear dissipative system.

In the past decades, revolutionary progress has been achieved in research and commercialization of erbium-doped fiber lasers (EDFLs). The exclusive advantages of these lasers are the long interaction length of pumping light with the active ions that leads to very high gain and a single transversal mode operation given by a suitable choice of the fiber core diameter and index step. These features make EDFLs excellent light sources for optical communications, reflectometry, sensing, medicine, etc. [16, 17]. Meanwhile, these lasers are quite sensitive to any external perturbation which may destabilize their normal operation. Therefore, the knowledge of the dynamic behavior of these lasers under external modulation is of great importance and can be prominent for many applications.

The mean objective of this thesis is to study nonlinear dynamic of complex system wit parametric modulation. As example of complex system, We choose Duffing oscillator and a fiber laser. Both the Duffing oscillator and laser equations model nonautonomous system, in which one of the parameters is modulated harmonically. The Duffing oscillator is commonly used as a general example in theoretical of nonautonomous system, whereas the fiber laser is the practical example of such a system.

In numerical calculation We used fourth-order Runge-Kutta algorithm.

Time series, phase space diagram, and bifurcation diagram has been used to visualize the dynamic behavior of the system.

The thesis contains seven chapters, the first and second Chapters are dedicated to Introduction and basic concept of dynamic nonlinear. The study of dynamic behavior of two double-well Duffing oscillators subjected to parametric or/and stochastic modulation is treated in Chapter 3 and 4 respectively. In Chapter 5 we dedicate to study of dynamics of an erbium-doped fiber laser with pump modulation. The general conclusion and Appendix are treated in Chapter 6 and 7 respectively.

More precisely, the thesis is organized in the following way.

Chapter 1 Introduction. It contains preceding, justification, objectives, methodology and structure of the thesis.

Chapter 2 Basic concept of nonlinear dynamics. In this chapter briefly introduces to the reader to basic concept of dynamic nonlinear, such as discreet and continuous system, autonomous and nonautonomous system, brief theory of stability and bifurcation diagram, types of dynamic control, and various class of solution of nonlinear systems.

Chapter 3 Duffing oscillators. This chapter is devoted to study of the dynamics of complex systems with parametric modulation. We star with a brief view of Duffing oscillators and synchronization, then we study the dynamics of two coupled Duffing oscillators with parametric modulation in one of them. We also identify intermittent lag synchronization in such a

system . Finally we give the main conclusion of this part of work.

Specifically studying of the dynamic of two coupled Duffing oscillators with parametric modulation, first, we search analytically for steady-state solutions of the system without modulation. Then we find numerically all solutions of the whole system with parametric excitation for different coupling strengths, modulation amplitudes and frequencies. This allows us to reveal the relation with the coupling effects on the Hopf bifurcation of the whole system and on crisis of coexisting attractors. We also demonstrate that chaotic oscillations in this system are always synchronized in phase. Finally, an interesting type of synchronization.

For studying intermittent lag synchronization in parametrically modulated of two coupled Duffing oscillators, first we make stability analyzes of equation of system, Then we constructed the codimensional-two bifurcation diagram in the parameter space of modulation amplitude and coupling strength and in the space of amplitude and frequency of modulation, the dynamic display different dynamic, such as, one-well chaos (OWC), cross-well chaos (CWC), hopping oscillations (HO), and periodic orbits (PO). Then intermittent lag synchronization is studied. Finally, the main conclusions are given at the end of the chapter.

Chapter 4 On-off Intermittency in Duffing Oscillators with Parametric and stochastic driving. First we do a brief definition and classification of intermittency phenomenon. Then we dedicate to the coexisting attractors and on-off intermittency in two coupled Duffing oscillators with

parametric and stochastic driving. We find numerically all solutions of the whole system with parametric excitation and noise for different amplitudes and frequencies of the modulation. This allows us to identify region of the coexistence of the different attractors. Then we build the basin of attraction of attractors for fixed values of modulation amplitude and frequency. We demonstrate that the system without modulation, display only steady state behavior. Finally, we consider the system without noise.

Moreover in this chapter we also dedicate to Control of on-off intermittency by slow parametric modulation. In this part we study dynamic in two coupled double-well Duffing oscillators with stochastic driving. We applying a slow harmonic modulation a system parameter, and demonstrate that the intermittent attractors can be completely eliminated. The influence of noise is also investigated. The power-law scaling of the average laminar time with a critical exponent of -1 as a function of both the amplitude and frequency of the control modulation is found near the onset of intermittency.

Finally the main conclusions are given at the end of the chapter.

Chapter 5 Dynamic of Laser. In this chapter we study dynamic of a fiber laser. At the beginning we give view laser dynamic with parametric modulation.

The chapter is organized as follows. In section 1 we give a introduction. In Section 2 we describe our model. In order to test the model, in Section 3 we simulate numerically the experiments reported in our previous works [18, 19] for the case when the modulation frequency is higher than the relaxation

oscillation frequency of the laser. Then, in Section 4 we study numerically the laser dynamics in the low-frequency range, i.e. when the modulation frequency is smaller than the relaxation oscillation frequency. We demonstrate that the low-frequency range exhibits a rather interesting insight to EDFL dynamics with external modulation because of the appearance of many "fine" dynamical phenomena that become latent at higher modulation frequencies. In Section 5 we describe the experimental setup of the diode-pumped EDFL with pump modulation and compare the results of simulations with experiments. In the course of experiments, we determine directly the structure of frequency- and phase-locked states (with respect to pump modulation) through bifurcation diagrams in space of the modulation parameters. Finally, the main conclusions are given in Section 6.

Chapter 6 General Conclusion. In this chapter we give the general conclusions of all the work.

Chapter 7 Appendix. In this last chapter we dedicated to the normalize of the erbium Doped fiber laser equations given in the chapter 5

Chapter 2

Basic Concept of Nonlinear Dynamics

This chapter briefly summarizes some facts pertaining to the behavior of nonlinear dynamic system. In §1.1 some basic concepts of dynamical system are given, such as discreet and continuous system, autonomous and nonautonomous system, etc. In §1.2 and §1.3 we introduce the reader to theory of stability and bifurcation. In §1.4 and §1.5 we describe various classes of a solution of nonlinear system The readers who are already familiar with this topics may want to skip the first chapter and jump directly to the next chapter.

The material contained in this chapter is standard and can be found in the most textbooks on nonlinear system and nonlinear dynamic, (see e.g. [1, 2, 3]).

2.1 Dynamics of Nonlinear Systems

2.1.1 Discreet and Continuous System, Autonomous and Nonautonomous System

A rough definition of nonlinear dynamic is a system whose time evolution equation are nonlinear, that is, the dynamic variables describing the properties of the system appear in the equations in a nonlinear form, and the superposition principle does not apply.

A dynamical system consists of a set of possible states, together with a rule that determines the present states in terms past states.

Two types of dynamical system we can find. If the rule is applied at discreet times, it is called discreet-time dynamic system. A discreet-time system takes the current state as input and updates the situation by producing a new state as output. By the state of the system, we mean whatever information is need so that the rule may be applied. Discreet time system is called maps.

Mathematically a map is defined as function whose domain (input) space and range (output) space are the same and the rule that govern a map is

$$x_n = f\ (x_{n-1}) \tag{2.1}$$

where the variable n stands for time and x_n is the state of the system in time n. The output of the rule is used as an input value for the next state.

The other important type of a dynamic system is essentially the limit of

discreet system with smaller and smaller update times, the governed rule is a set of differential equations and the term of a continue time dynamical system is sometimes used. In this work we considerate a continuous time dynamical system.

The general state equation for nonlinear system considered in this work is

$$\dot{u} = f\ (u), \qquad u\ (t_0) = u_0, \tag{2.2}$$

where $u \in D \subset R^n, t \in R^+$. D is an open subset of R^n. In most cases we have $D = R^n$. A system of differential equations of the form (2.2), in which the independent variable t does not occur explicitly is called autonomous system. Its order is considerate to be equal n.

Consider the following differential equation:

$$\dot{u} = f\ (u, t), \qquad u\ (t_0) = u_0, \qquad u \in D \subset R^n, \qquad t \in R^+. \tag{2.3}$$

If the right-hand side depends explicitly on time Eqn (2.3) is called nonautonomous system. If $T > 0$ such that

$$f\ (u, t) = f\ (u, t + T)$$

exist for all u and t, then Eqn (2.3) is said to be time periodic with period T.

An nth-order time periodic nonautonomous system with period T can always be converted into an $(n+1)$th-order autonomous system by appending an extra variable.

$$\theta = \frac{2\pi t}{T}.$$

The new autonomous system is given by

$$\begin{aligned} \mathbf{f}\ (\mathbf{u}, t) &= \mathbf{f}\ (\mathbf{u}, \theta), \qquad \mathbf{u}\ (t_0) = \mathbf{u}_0, \\ \dot{\theta} &= \frac{2\pi}{T}, \qquad \theta\ (t_0) = \frac{2\pi t_0}{T}. \end{aligned} \tag{2.4}$$

The function f on the right-hand side of Eqn (2.2) defined a mapping $f : R^n \to R^n$. Thus a mapping defined a vector field on R^n.

The phase space of a dynamical system is a mathematical space with ortogonal coordinated directions representing each of the variables needed to specific an isntantaneous state of the system. Generally, the dimension of the space of phase of Eqn (2.2) is n, (the number of first order scalar differential equations)

2.1.2 Fixed Point and Linearization

Definition 1 *The point* $u^* \in R^n$ *where*

$f\ (u^*) = 0$

is called a fixed point $\dot{u} = f\ (u)$.

Remark 1 *Sometimes the fixed point are called equilibrium point or critical point.*

Fixed point u^* of a differential equation $\dot{u} = f\ (u)$ in R^n is called attractor

if there exist a neighborhood $A \subset R^n$ of u^* such that $u(t) \in A$ implies $\lim_{t\to\infty} u(t) = u^*$.

If a fixed point $u^* = a$ has this property at $t \to -\infty$, then u^* is called a repeller.

Let us assume that f is analytic. The linearization of the differential equation $\dot{u} = f\ (u)$ in a neighborhood of the fixed point u^* consists in the expansion of the Taylor series of f around u^*. Linearizing means that we neglect higher order terms.

In the neighborhood of the fixed point u^* we can write

$$\frac{d\mathbf{u}}{dt} = \frac{\partial \mathbf{f}\ (\mathbf{u}^*)}{\partial \mathbf{u}}(u - u^*) + \text{higher order terms}$$

and study the linear differential equation

$$\frac{d\mathbf{u}}{dt} = \frac{\partial \mathbf{f}\ (\mathbf{u}^*)}{\partial \mathbf{u}}(u - u^*)$$

The $n\ x\ n$ matrix $\frac{\partial \mathbf{f}\ (\mathbf{u}^*)}{\partial \mathbf{u}}$ is called the Jacobian matrix or function matrix. To simplify the notation the fixed point is shifted to the origin of the space phase by $\bar{y} = u - u^*$. Thus,

$$\frac{d\bar{y}}{dt} = \frac{\partial \mathbf{f}\ (\mathbf{u}^*)}{\partial \mathbf{u}}\bar{y}$$

where $\frac{\partial \mathbf{f}\ (\mathbf{u}^*)}{\partial \mathbf{u}} = A$. It is an $n\ x\ n$ -dimensional matrix with constant coefficients. So the linearized system in the neighborhood of a fixed point u^* is of the form

$$\frac{d\bar{y}}{dt} = A\bar{y}. \tag{2.5}$$

Definition 2 *Suppose that the n x n dimensional matrix A has K negative eigenvalues* $\lambda_{1,...,}\lambda_k$ *and* $n-k$ *positive eigenvalues* $\lambda_{k+1,...,}\lambda_n$ *and that these eigenvalues are distinct. Let* $\{v_{1,}...v_{n,}\}$ *be a corresponding set of eigenvector. Then stable and unstable subspace of the linear system Eqn (2.5),* E^s *and* E^u*, are the linear subspace spanned by* $\{v_{1,}...v_k\}$ *and* $\{v_{k+1,}...v_n\}$ *, respectively*

$E^s = span\{v_{1,}...v_k\}$

$E^u = span\{v_{k+1,}...v_n\}$.

Let us considered a two dimensional case, i.e., A is of 2 x 2 dimensional matrix.

If the eigenvalues are real and have the same sign the critical point is called node. If $\lambda_1 < 0$ and $\lambda_2 < 0$ then the critical point is an attractor and $\lambda_1 > 0$ and $\lambda_2 > 0$ then it is a repeller Figs.(2.1),(2.2).

If the eigenvalues are still real but have different sign, the critical point is called saddle (Fig.2.3)

When the eigenvalues λ_1 and λ_2 are complex conjugates

$$\lambda_{1,2} = u \pm \omega\ i$$

with $u\omega \neq 0$, the critical point is called a focus (Figs. 2.4,2.5).

The last case is when the eigenvalues are purely imaginary. If

$$\lambda_{1,2} = \pm\omega\ i$$

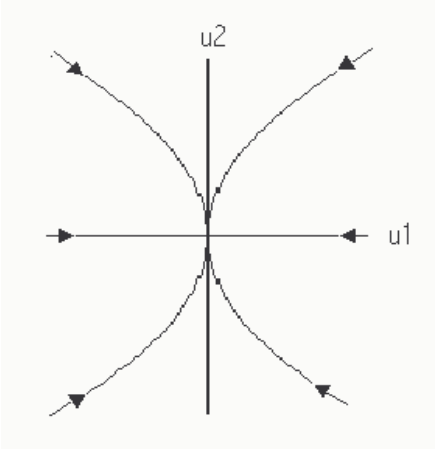

Figure 2.1: The Node attractor (sink)

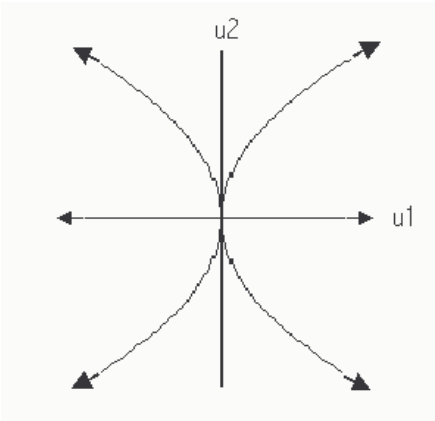

Figure 2.2: Node Repeller

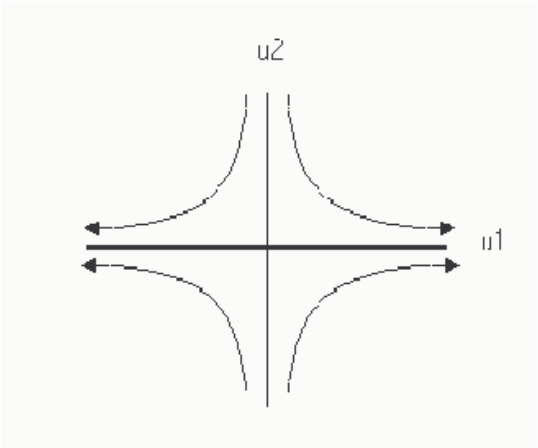

Figure 2.3: Saddle point

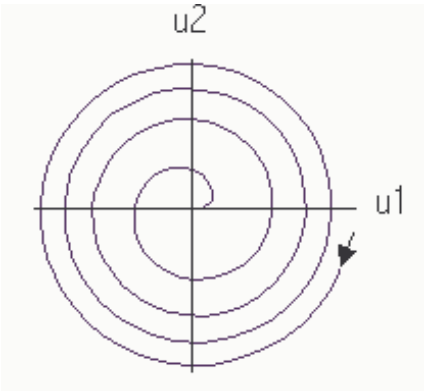

Figure 2.4: Focus Attractor

Figure 2.5: Focus Repeller

then the critical point is called centre (Fig. 2.6). It is clear that in this case a critical point is neither an attractor nor a repeller.

2.1.3 Periodic Solution

Let us consider the case differential equation $\dot{u} = f\ (u)$ which can be represented by a closed orbit in the phase space. The closed orbit is related to periodic solution. If $\Phi(t, u_0)$ is a solution of the differential equation $\dot{u} = f\ (u), u \in D \subset R^n$, and suppose that there exists a positive number T such that

$$\Phi(t + T) = \Phi(t) \tag{2.6}$$

for all $t \in R^+$, then $\Phi(t)$ is called periodic solution of period T. A periodic solution of autonomous equation $\dot{u} = f\ (u)$ corresponds to a closed orbit in phase space and a closed orbit corresponds to a periodic solution. A periodic

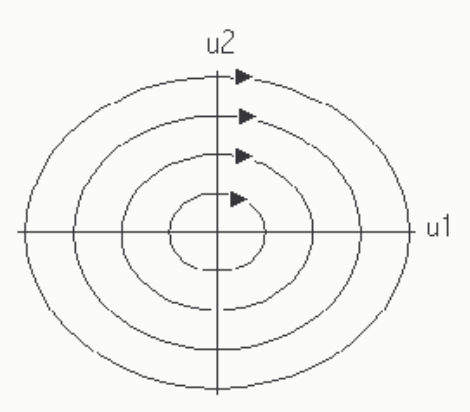

Figure 2.6: Center

solution can be a limit cycle. If a limit cycle is reached asymptotically for $t \to \infty$, it is stable, i.e., an attractor. If a limit cycle is reached asymptotically for $t \to -\infty$, it is unstable, i.e., a repeller.

Definition 3 *Specific subset A of a phase space R^n of differential equation $\dot{u} = f\ (u)$ which is reached asymptotically as $t \to \infty$ $(t \to -\infty)$ is called attractor (repeller).*

Theorem 1 *Suppose $\Phi(t, u_0)$ is a trajectory of the differential equation $\dot{u} = f\ (u)$, $u \in R^2$ which flow $\Phi(t, u_0)$ is contained in a bounded region D of the phase space for $t \geq 0$. Then the only possible attractor for $\Phi(t, u_0)$ are a critical point or limit cycle.*

For stability analysis of periodic solution we use Poincare map function to analyze the nature of a limit cycle. Two points are important to analyze the Poincare map function and its derivatives.

(i) The Poincare section reduces the original two-dimensional system problem to an one-dimensional problem.

(ii) Poincare map function states an iterative (finite-size time step) relation rather than a differential (infinitesimal time step) relation.

Let us consider the Poincare map function as

$$P_{n+1} = F(P_n)$$

where F gives P_{n+1} in terms of P_n and the linearize system is given as

$$d_{n+1} = M\ ^n d_n,$$

where $d_{n+1} = P_i - P^*$, and $M = \frac{dF}{dP}\ |_{P^*}$, (Floquer multiplier for analytic details see [1]).

The possible behavior of the limit cycle depend of the Floquer multiplier M : For $M < 1$,we observe a attractor limit cycle. For $M > 1$ a repeller limit cycle and $M = 1$,a saddle limit cycle.

2.1.4 Chaotic Solution

Chaos is a behavior of a system that fluctuates irregularly in time. This is an attractor, but not a fixed point and not a cycle. However, not any system that fluctuates irregularly in time represents chaotic behavior. Chaos as used in nonlinear dynamics, represents a behavior observed in deterministic dynamic equation. Chaotic dynamics has the additional property that the small differences in the initial value will grow over time, but the dynamic will

be finite, and not grows indefinitely. This property is often called sensitive dependence on initial conditions. Because of sensitive dependence on initial conditions, it is impossible to make accurate long term prediction about the state of the system without knowing exactly its initial state. Any minor uncertainty will be amplified so as to render actual knowledge of the state of the system is impossible. In a real system it is always impossible to know state of the system exactly, since there always exists some experimentally measured uncertainty.

Deterministic Chaos means that there is a definite rule with no random term governed the dynamics.

2.1.5 Bifurcation

A bifurcation describes the qualitative change in dynamics that can be observed while parameter in a system is varied. For example, under the variation in the parameter value, a fixed point may change from being stable to unstable, or a cycle might suddenly appear.

These terms can all be mathematically rigorously defined, and we will give some illustrative examples

2.1.6 Saddle Node Bifurcation

A saddle-node bifurcation results in the creation of two new fixed points, one stable and one unstable. This can be seen in the simple example

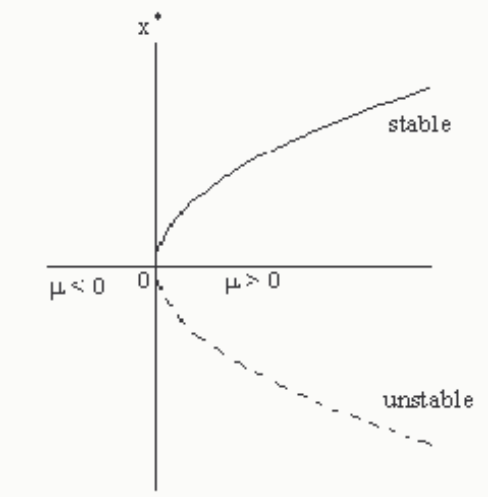

Figure 2.7: Bifurcation diagram demostrationg saddle-node bifurcation

$$\frac{dx}{dt} = \mu - x^2 \tag{2.7}$$

where μ is the control parameter. For $\mu < 0$ there are no fixed points in the system. For $\mu = 0$ (the bifurcation value) there is one fixed point (at the origin $x^* = 0$), which is semistable. For $\mu > 0$ there are two fixed points, one of which ($x^* = \sqrt{\mu}$) is stable, while the other ($x^* = -\sqrt{\mu}$) is unstable.

Figure 2.7 shows the corresponding bifurcation diagram, in which the equilibrium value (x^*) of the bifurcation variable is plotted as a function of the bifurcation parameter μ. The stable point are show as the solid line, while the unstable point are denotes the dashed line.

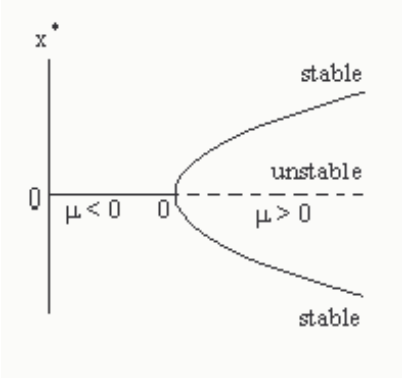

Figure 2.8: Bifurcation diagram for pitchfork bifurcation

2.1.7 Pitchfork Bifurcation

In a pitchfork bifurcation, a fixed point reverses its stability and two new fixed points are born. The pitchfork bifurcation occurs at $\mu = 0$ in the one-dimensional ordinary differential equation

$$\frac{dx}{dt} = x(\mu - x^2) \tag{2.8}$$

For $\mu < 0$ there is a fixed point at $x^* = 0$, for $\mu > 0$, there are three fixed points, but the original fixed point at zero now become unstable, and new symmetrically place stable point appear (see Fig 2.8).

Figure 2.8 shows the bifurcation diagram for the pitchfork bifurcation. The bifurcation in figure 2.8 is supercritical bifurcation, since there are stable fixed points to either side of the bifurcation point. Replacing the minus sign with plus in the Eqn(2.8) results in a subcritical pitchfork bifurcation.

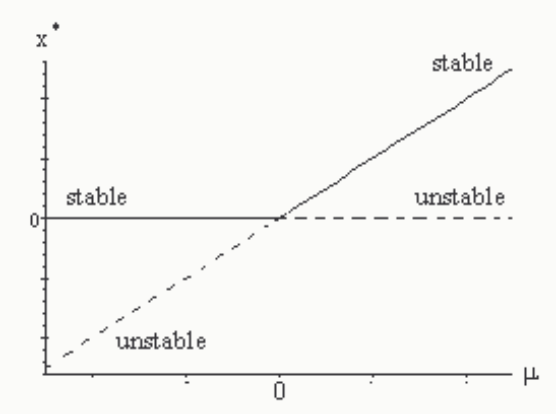

Figure 2.9: The bifurcation diagram for the transcritical bifurcation

2.1.8 Transcritical Bifurcation

In the transcritical bifurcation there is an exchange of stability between two fixed points. For the following ordinary differential equation

$$\frac{dx}{dt} = x(\mu - x) \tag{2.9}$$

there is a transcritical bifurcation at $\mu = 0$ (see Fig.2.9). The fixed point $x^* = 0$ stars out being stable for $\mu < 0$, becomes semistable at $\mu = 0$, and unstable for $\mu > 0$. The sequence of the changes is the opposite for the other point ($x^* = \mu$).

2.1.9 Hopf Bifurcation

The birth and death of a limit cycle are bifurcation events. The birth of the stable limit cycle is called Hopf bifurcation. We can use the Poincare method

to study a limit cycle bifurcation, since for two dimensional state space, the Poincare section is just a line segment.

To illustrate some of the important concept associated with a limit cycle, we considerate a two-dimensional equation differential in a polar coordinate system

$$\begin{aligned} \frac{dr}{dt} &= f\ (r,\mu) \\ \frac{d\phi}{dt} &= 2\pi \end{aligned} \tag{2.10}$$

where r is the distance from the origin and ϕ is the angular coordinate and $f\ (r,\mu)$ is a nonlinear function that depends on parameter μ. We can say that any fixed point of the function $f\ (r,\mu)$ would correspond to a limit cycle. A stable fixed point of $f\ (r,\mu)$ corresponds to a stable limit cycle of Eqn(2.10), and an unstable fixed point of $f\ (r,\mu)$ corresponds to an unstable limit cycle of Eqn (2.10). Consequently, changes in stability of the fixed point of $f\ (r,\mu)$ would lead to changes in the stability of the limit cycle in the Eqn (2.10).

Consider the following example

$$\begin{aligned} \frac{dr}{dt} &= f\ (r,\mu) = r(\mu - r^2) \\ \frac{d\phi}{dt} &= 2\pi \end{aligned} \tag{2.11}$$

Let us interpreter the geometric nature of trajectories Eqn (2.11). The solution of the angular part is simply

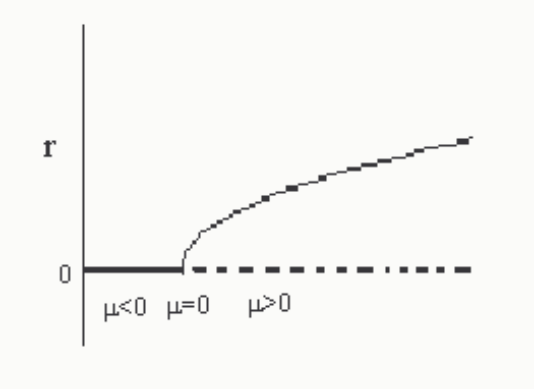

Figure 2.10: Supercritical Hopf bifurcation. The solid curve corresponds to stable solution and the dashed curve refer to the unstable solution.

$$\phi(t) = \phi_0 + 2\pi t \tag{2.12}$$

that is, the angle continues to increase with time as the trajectory spirals around the origin. If $\mu < 0$ there is one stable fixed point of $f\ (r, \mu)$ at $r = 0$, whereas for $\mu > 0$ there is an unstable fixed point of $f\ (r, \mu)$ at $r = 0$,and stable fixed point of $f\ (r, \mu)$ at $r = \sqrt{\mu}$ (remember that in a polar coordinate system the radial coordinate r corresponds to the distance of a point from the origin and is always taken to be positive).

If μ increase from negative to positive part, a stable limit cycle will be born as μ crosses 0. . This is called supercritical Hopf bifurcation. The amplitude of the limit cycle is show in Fig. 2.10

A different scenario for generate a limit cycle, albeit an unstable limit cycle, occurs when

$$\frac{dr}{dt} = f\ (r, \mu) = r(\mu + r^2) \tag{2.13}$$

For $\mu > 0$ there is a single stable fixed point at $r = 0$, and for $\mu < 0$ there is a single unstable fixed point at $r = 0$ and an unstable limit cycle with amplitude $r = \sqrt{-\mu}$. This scenario is called subcritical Hopf bifurcation.

2.1.10 Routes to Chaos

The mechanism of the transition to chaos is of fundamental importance for understanding any chaotic behavior. There are three main route to chaos which can be observed in nonlinear dynamic.

(i) A period doubling bifurcation is commonly observed in periodically forced nonlinear system, where the varying amplitude of the force signal (for instance a sinusoidal one) acts as a bifurcation parameter [2]. A typical diagram of phase space of one of such systems may look like in Figure 2.11. By increasing one of the bifurcation parameter we observed the transformation a closed orbit (Fig.2.11a), into two closed orbits (Fig.2.11b), four closed orbits (Fig.2.11c) and finally an infinite number of closed orbits (Fig.2.11d), which is the typical period-doubling route to chaos. The period T of the closed orbit is equal to a period of the excitation force, Two closed orbits indicate that the period of oscillations is twice as long.

Another possibility, not discussed here, is the transitions to chaos via global bifurcation; Chaotic transients and Crisis

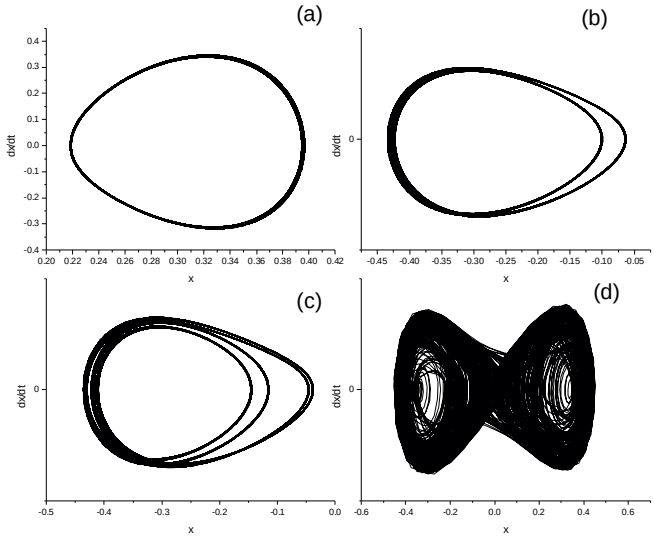

Figure 2.11: Phase space diagrams demostrating typical perid-double route to chaos. (a) T periodic solution, (b) 2T periodic solution, (c) 4T periodic solution and (d) chaotic solution

(ii) Quasiperiodic route the second route to chaos is associated with a Hopf bifurcation, which generates a limit cycle starting from a fixed point. In many system undergoing the Hopf bifurcation, a further increase of the control parameter makes possible to find the second Hopf bifurcation. After the bifurcation the response of the system is quasiperiodic with two independent frequencies, so that trajectories are drawn on a two-dimensional torus T^2.

If the ratio of the period of the second type of motion (second Hopf bifurcation) to the first period (first Hopf bifurcation) is not a rational number, then we say, the motion is quasiperiodic. Under some circumstances, if the control parameter is change further, the motion becomes chaotic. This is sometime called Ruelle-Takens scenario (D. Ruller and F. Takens were the first, who in 1970 suggested the theoretical possibility of this route [20]).

The intermittency route to chaos is characterized by dynamics with irregularly occurring bursts of chaotic behavior interspersed with intervals of apparently periodic behavior. A some control parameter of the system is changed, the chaotic bursts become longer and occur more frequently until, eventually, the time record is chaotic.

2.1.11 Control of Chaos

The problem of controlling of chaos attract attention of researchers and engineers since the early 1990's. Several thousand publications have appeared over the recent decade [21].They suggested that it may be possible to overcome the butterfly effect and control chaotic systems. The idea is to apply

appropriately designed minute perturbations to an accessible system parameter that forces it to follow a desired behavior rather than the erratic, noise-like behavior indicative of chaos.

In greater details, the key idea underlying most controlling-chaos schemes is to take advantage of the unstable steady states (USSs) and unstable periodic orbits (UPOs) of the system (infinite in number) that are embedded in the chaotic attractor characterizing the dynamics in phase space. Many of the control protocols attempt to stabilize one such UPO by making small adjustments to an accessible parameter when the system is in a neighborhood of the state.

Techniques for stabilizing unstable states in nonlinear dynamical systems using small perturbations fall into three general categories: open loop control (nonfeedback control), closed loop control (feedback control), and a combination of open loop control and closed loop control.

2.1.12 Open Loop Control

The principle of control by perturbation or "control by the program signal", that is, the generation of a control signal as a time function disregarding the values of the controlled process, is based on varying behavior of the nonlinear system under the action of a predetermined external input $u(t)$ which can be either a certain physical action on the system such as force or field or variation (modulation) of some parameter of the controlled system [21]. This approach has appeal owing to its simplicity because it does without any

measurements or sensors. This is specially important for control of superfast processes occurring, where the system state cannot be measured (at least in real time). Unfortunately, periodic modulation fails in many cases to entrain the UPO (its success or failure is highly dependent on the specific form of the dynamical system).

2.1.13 Closed Loop Control

Feedback of chaos suggested by Ott, Grebogi, and Yorke (OGY) in 1990 [22]. The basic building blocks of a generic feedback scheme consist of the chaotic system that is to be controlled, a device to sense the dynamical state of the system, a processor to generate the feedback signal, and an actuator that adjusts the accessible system parameter, as shown schematically in Fig. 2.12.

In their original conceptualization of the control scheme, OGY suggested the use of discrete proportional feedback because of its simplicity and because the control parameters can be determined straightforwardly from experimental observations. In this particular form of feedback control, the state of the system is sensed and adjustments are made to the accessible system parameter as the system passes through a surface of section. Figs. 2.13 [23] illustrates a portion of a trajectory in a three-dimensional phase space and one possible surface of section that is oriented so that all trajectories pass through it. The dots on the plane indicate the locations where the trajectory pierces the surface.

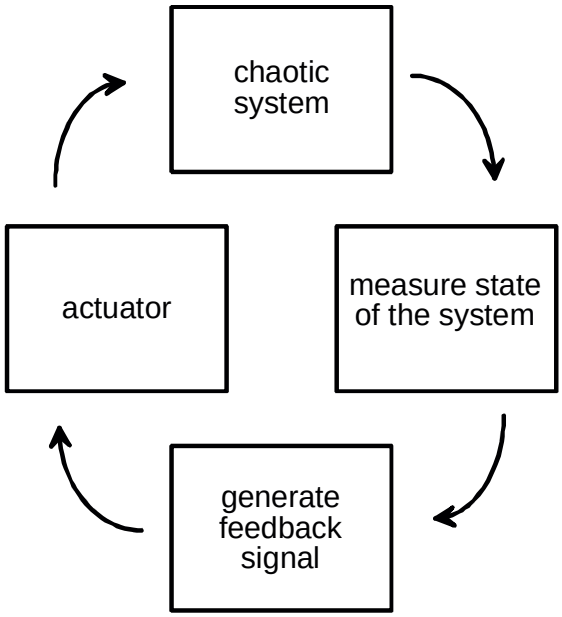

Figure 2.12: Closed loop feedback control scheme

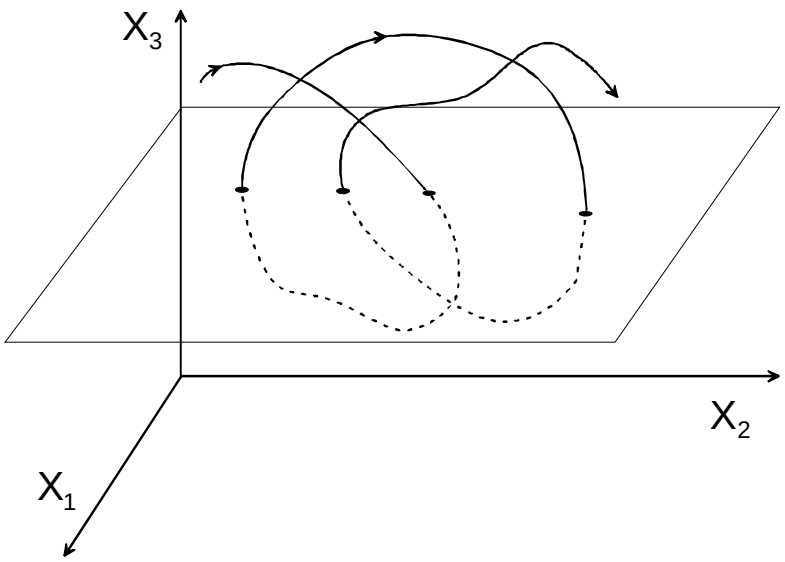

Figure 2.13: A segment of a trajectory in a three-dimensional phase space and a possible surface of section through which the trajectory passes. Some control algorithms only require knowledge of the coordinates where the trajectory pierces the surface, indicated by the dots

In the OGY control algorithm, the size of the adjustments is proportional to the difference between the current and desired states of the system. Specifically, consider a system whose dynamics on a surface of section is governed by the m-dimensional map $z_{i+1} = F(z_i, p_i)$, where z_i is its location on the ith piercing of the surface and p_i is the value of an externally accessible control parameter that can be adjusted about a nominal value p_0. The map F is a nonlinear vector function that transforms a point on the plane with position vector z_i to a new point with position vector z_{i+1}. Feedback control of the desired UPO (characterized by the location $z_*(p_0)$ of its piercing through the section) is achieved by adjusting the accessible parameter by an amount $\delta p_i = p_i - p_0 = -\gamma n \times [z_i - z_*(po)]$ on each piercing of the section when z_i is in a small neighborhood of $z_*(p_0)$, where γ is the feedback gain and n is a m-dimensional unit vector that is directed along the measurement direction. The location of the unstable fixed-point $z_*(po)$ must be determined before control is initiated; fortunately, it can be determined from experimental observations of z_i in the absence of control (a learning phase). The feedback gain γ and the measurement direction n necessary to obtain control is determined from the local linear dynamics of the system about $z_*(po)$ using the standard techniques of modern control engineering ([24, 1]), and it is chosen so that the adjustments δp_i force the system onto the local stable manifold of the fixed point on the next piercing of the section. Successive iterations of the map in the presence of control direct the system to $z_*(po)$. It is important to note that δp_i vanishes when the system is stabilized; the control only has to counteract the destabilizing effects of noise.

Chapter 3

Duffing Oscillators

The Duffing oscillator is one of the prototype systems of nonlinear dynamics and was successfully explored to model a variety of physical processes such as stiffening strings, beam buckling, nonlinear electronic circuits, superconducting Josephson parametric amplifiers, and ionization waves in plasmas, as well as biological processes [6, 7, 8, 9, 10, 11, 12, 13, 14, 15]. This model was first introduced to understand forced vibrations of industrial machinery by the German electrical engineer Duffing in 1918 [5].

The Duffing equation is

$\frac{d^2x}{dt^2} + \alpha\frac{dx}{dt} + \omega_0^2 x + \beta x^3 = f(t), \alpha > 0; f(t) = f\sin\omega t \ \ (\text{or } f\cos\omega t)$

can be thought of as the equation of motion for a particle of unit mass in the potential well

$V(x) = \frac{1}{2}\omega_0^2 x^2 + \frac{\beta}{4}x^4$

subjected to a viscous drag force of strength α and driven by an external periodic signal of period $T = (\frac{2\pi}{\omega})$ and strength f. However we can distinguish

three types of potential wells of physical relevance here:

(i) $\omega_0^2 < 0, \beta > 0$: A double-well with potential minima at $x = \pm\sqrt[2]{(\frac{|\omega_0^2|}{\beta})}$ and a local maximum at $x = 0$.

(ii) $\omega_0^2 > 0, \beta > 0$: A single-well with potential minima at the equilibrium point at $x = 0$.

(iii) $\omega_0^2 > 0, \beta < 0$: a double-hump potential well with a local minimum at and maxima at $x = \pm\sqrt[2]{(\frac{|\omega_0^2|}{\beta})}$.

Each one of the above three cases has become a classic model to describe inherently nonlinear phenomenon, exhibiting a rich and baffling variety of regular (periodic) and complex (chaotic) motions which can coexist or exist in neighboring parameter regimes. In this thesis we only have discussed the first case.

3.1 Synchronization of Coupled Oscillators System

In the last years, synchronization of coupled oscillatory systems is attracted a great attention in almost all areas of natural sciences, engineering and social life. The main reason of such interest is important practical applications which include communications, modelling brain and cardiac rhythm activity, earthquake dynamics, etc. (see, e.g., [4] and references therein). Different types of synchronization, complete [25], phase [26], lag [27], generalized [28], intermittent lag [27], and almost synchronization [29], have been identified.

Moreover, an intriguing synchronization phenomenon, known as oscillation death (or quenching), which deals with the absence of oscillations for the coupled system while each subsystem oscillates when isolated, has been obtained theoretically [30, 31, 32] and demonstrated experimentally in chemical [33] and optical systems [34].

Considering a system of two coupled subsystems: $\dot{\mathbf{x}} = f(x, y; A)$ and $\dot{\mathbf{y}} = g(x, y; B)$, where x and y are phase-space variables, A and B are sets of parameters, and f and g are the corresponding nonlinear velocity fields, one supposes that these subsystems are generally synchronized when $y(t) = h[\mathbf{x}(t)]$, where h represents a functional relation between x and y [28]. When $h = const$, one deals with the phenomenon of oscillation death, that can originate either from a strong coupling that creates a saddle-node pair of fixed points on the limit cycle [35] or from time delay in the coupling that initiates a Hopf bifurcation in which the oscillators pull each other off their limit cycles and collapse to a steady state [36]. Thus, the oscillation death is a particular case of synchronization when all variables become independent on time. It should be noted that the death effect has been discovered even in the middle of the 19th century by William Strutt [37], long before there was any theory to explain it. He observed that two organ-pipes of the same pitch, when they stand side by side, may almost reduce one another to silence. The same effect can appear in two electronic generators, like those used by Appleton [38], coupled via a resistor. The additional energy loss due to the current through this resistor may not be compensated by the supply of energy from the source, and as a result the oscillations die out. All previous studies

of autonomous (self-oscillatory) systems have demonstrated that oscillation death can occur only in two cases: (i) if the coupling between oscillators is sufficiently strong and when the natural frequencies of the oscillators are sufficiently separated or (ii) if there exists time delay in coupling even when the frequency mismatch between the oscillators is zero. However, a study of synchronization phenomena in nonautonomous (periodic forced) systems has received little attention. It was even thought that oscillation death has no analogy in the case of periodic forcing and direct coupling [4].

3.2 Dynamics Two Coupled Duffing Oscillators With Parametric Modulation

The purpose of this part of work is to study the change of dynamic behavior in a nonautonomous system. In which oscillations appear only either a system variable or a parameter in one of the coupled subsystems is modulated, while without modulation the system stays in a steady state. Coupled systems using strictly dissipative externally driven oscillators have been investigated in the literature less intensely than self-excited models. For example, Kapitaniak [39] studied the transition to hyperchaos for a system of coupled Duffing oscillators, and Landa and Rosenblum [40] investigated synchronization phenomena for different types of coupled systems. Furthermore, the structure of local bifurcations in the parameter space of two coupled periodically driven Duffing oscillators was studied by Kozłowski et al. [41], and later

Yin et al. [42] considered the effect of phase difference in mutually coupled chaotic oscillators. Recently, Raj et al. [43] investigated coexisting attractors and synchronization of chaos in two coupled Duffing oscillators with driving forces. However, in all above-mentioned works the external driving force was applied to the variable of one or both oscillators. Nevertheless, in many real experiments it is more convenient to modulate a system parameter rather than a variable. Parametrically modulated systems are commonly used in many practical applications, in particular, in communications.

The principal difference in studying dynamics of autonomous and nonautonomous systems is that in the latter system two additional parameters (in addition to coupling strength) can be controllable. These are the amplitude and frequency of the external modulation. By manipulating these two parameters one can control positions of critical points [44, 45, 46, 47, 48]. In the parametrically modulated system one of the parameters, say a ($a \in A$), is a function of time, i.e., $a = \varphi(t)$ while the other parameters can be constant, and therefore, the subsystems are not completely identical, i.e. $f \neq g$. Nevertheless, we may consider the subsystems to be almost identical when averaged in time parameters are the same, i.e., $\langle A \rangle = B$, where $\langle A \rangle$ is the averaged in time set of parameters. In this chapter we show that in such a system the oscillation death can exist even in the almost identical subsystems, when the amplitude and frequency of the parametric excitation are sufficiently large and that the above conditions for the death are not necessary to be fulfilled. We present detailed numerical estimates of the parameter space in the coupling strength, modulation amplitude and frequency where

the death occurs. The boundary values of the modulation parameters for the death are very important characteristics of a parametrically modulated system because these values indicate the dead region for information transmission by such a system.

The analysis is carried out on an example of two coupled Duffing oscillators. First, we search analytically for steady-state solutions of the system without modulation. Then we find numerically all solutions of the whole system with parametric excitation for different coupling strengths, modulation amplitudes and frequencies. This allows us to reveal the relation with the coupling effects on the Hopf bifurcation of the whole system and on crisis of coexisting attractors.

3.2.1 Analytical Solutions.

3.2.2 General Equations.

Dynamics of two identical nonlinear oscillators is governed by the equation,

$$\ddot{\mathbf{x}}+\boldsymbol{\gamma}\dot{\mathbf{x}} = -\frac{dV(\mathbf{x})}{d\mathbf{x}}, \tag{3.1}$$

where $x \equiv (x, y)$, γ is a damping factor, and $V(x)$ is a two-dimensional nonharmonic potential function of coupled oscillators. The potential functions for symmetric Duffing oscillators can be expressed as follows:

$$V(x,y) = \frac{a}{2}x^2 + \frac{b}{4}x^4 + \frac{\delta}{2}x^2y^2, \tag{3.2}$$

$$V(y,x) = \frac{a_0}{2}y^2 + \frac{b}{4}y^4 + \frac{\delta}{2}x^2y^2, \tag{3.3}$$

where a, a_0 and b are parameters and δ is a coupling coefficient. The system of Eqs. (3.1-3.3) has only steady state solutions. To observe oscillation, we make the system adding the external modulation in the following form

$$a = a_0[1 - m\sin(2\pi ft)], \tag{3.4}$$

where m and f are the modulation depth and frequency. Here we consider only the case of a double-well potential, i.e. $a_0 < 0$, with positive b ($b > 0$). This case is more interesting for modelling a real experiment for signal transmission, because the oscillators have nonzero stable equilibrium points as distinct from a single-well case.

Equation (3.1) with parametric modulation Eq. (3.4) has steady state and oscillatory solutions. Since the equilibrium becomes stable at the onset of oscillation death, conditions for this phenomenon can usually be obtained by a linear stability analysis of equilibrium points. On the other hand, nonlinear techniques are better suited for obtaining more global results and details of dynamical behavior. First, we find steady state solutions analytically in linear approximation for nonmodulated case.

3.2.3 Nonmodulated Case.

Consider first the system Eqs. (3.1-3.4) without parametric excitation ($m = 0$ and $a = a_0$). It is convenient to replace Eqs. (3.1-3.3) by a system of first-order differential equations by introducing four new variables: $x_1 = x$, $x_2 = \dot{x}$, $x_3 = y$, $x_4 = \dot{y}$. Then Eqs. (3.1-3.3) become

$$\dot{x_1} = x_2, \tag{3.5}$$

$$\dot{x_2} = -\gamma x_2 - a x_1 - b x_1^3 - \delta x_1 x_3^2, \tag{3.6}$$

$$\dot{x_3} = x_4, \tag{3.7}$$

$$\dot{x_4} = -\gamma x_4 - a x_3 - b x_3^3 - \delta x_1^2 x_3. \tag{3.8}$$

In the system Eqs. (3.5-3.8) when $\dot{x}_1 = \dot{x}_2 = \dot{x}_3 = \dot{x}_4 = 0$, We found nine fixed points, which are $Q_i = (\overline{x_1}, \overline{x_2}, \overline{x_3}, \overline{x_4})$, $(i = 1, ..., 9)$: $Q_1(0, 0, 0, 0)$, $Q_{2,3}(0, 0, \pm\sqrt{-\frac{a}{b}}, 0)$, $Q_{4,5}(\pm\sqrt{-\frac{a}{b}}, 0, 0, 0)$,

$Q_{6-9}(\pm\sqrt{-\frac{a}{b+\delta}}, 0, \pm\sqrt{-\frac{a}{b+\delta}}, 0)$.

The stability of the fixed points (steady states) in given by eigenvalues of the Jacobian matrix,

$$J = \begin{bmatrix} 0 & 1 & 0 & 0 \\ -a - 3b\overline{x}_1^2 - \delta\overline{x}_3^2 & -\gamma & -2\delta\overline{x}_1\overline{x}_3 & 0 \\ 0 & 0 & 0 & 1 \\ -2\delta\overline{x}_1\overline{x}_3 & 0 & -a - 3b\overline{x}_1^2 - \delta\overline{x}_3^2 & -\gamma \end{bmatrix}$$

For simplicity we consider the case of $\gamma = 0.4$, $a = a_0 = -0.25$, and $b = 0.5$. The three-dimensional potential function $V(x, y)$ at fixed coupling

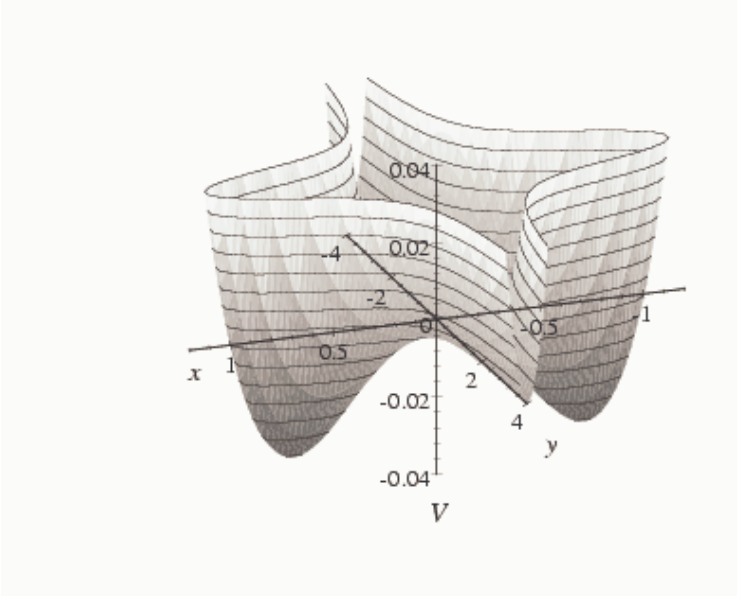

Figure 3.1: Double-Well potential function Eqn (3.2)

strength $\delta = 0.5$ is shown in Fig. 3.1. For two-dimensional double-well potential of the subsystem described by Eq. (3.2) there exist a saddle equilibrium point at $x^u = 0$ and a conjugate pair of stable equilibrium points at $x^s = \pm\sqrt{0.5 - \delta y^2}$. The positions of stable points x^s depend on the coupling strength as shown in Fig. 3.2. For the potential function Eq. (3.3) of another subsystem, the equilibrium points are at $y^u = 0$ and $y^s = \pm\sqrt{0.5 - \delta x^2}$ (super indices u and s denote, respectively, to unstable and stable solution). For our parameters, point Q_1 is a saddle and points Q_{2-5} are sinks for any value of $\delta \geq 0$, while the stability of the other four solutions, Q_{6-9}, depends on δ: they are sinks for $\delta < 0.5$ and saddles for $\delta \geq 0.5$.

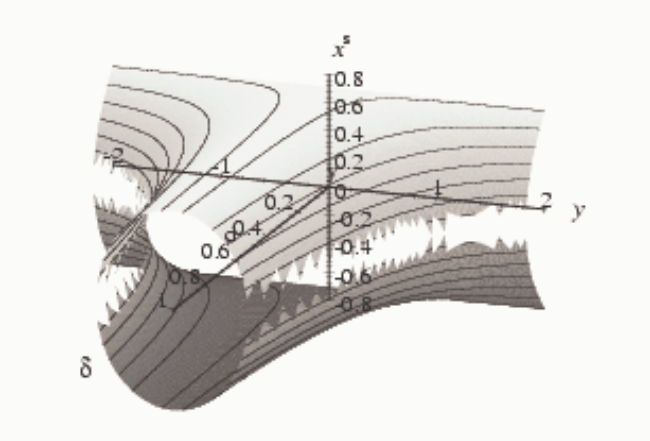

Figure 3.2: Position of stable points x^s versus coupled strenth δ and variable y.

3.2.4 Nonautonomous System.

In the presence of the parametric excitation Eq. (3.4) in one of the oscillators (master oscillator Eq. (3.6), the system of Eqs. (3.5-3.8) becomes

$$\dot{x_1} = x_2, \tag{3.9}$$

$$\dot{x_2} = -\gamma x_2 - a_0[1 - m\sin(2\pi f t)]x_1 - bx_1^3 - \delta x_1 x_3^2, \tag{3.10}$$

$$\dot{x_3} = x_4, \tag{3.11}$$

$$\dot{x_4} = -\gamma x_4 - a_0 x_3 - bx_3^3 - \delta x_1^2 x_3. \tag{3.12}$$

The system Eqs. (3.9-3.12) exhibits a wide range of dynamical regimes ranging from steady states to periodic and chaotic oscillations and represents different types of synchronization

3.2.5 Codimensional-one Bifurcation Diagrams.

The typical bifurcation diagrams of peak amplitudes of the master (X_1) and slave (Y_3) oscillators with f as a control parameter for different δ and m are shown respectively in Figs. 3.3 and 3.4. The general information analysis of the results performed on the basis of the consideration of the bifurcation diagrams and time series allows us to reveal the following possible situations which can be awaited from a system of two coupled oscillators with parametric driving.

(i) When the coupling and modulation frequency are sufficiently small ($\delta \lesssim 0.1$ and $m \lesssim 0.1$), the bifurcation diagram of each subsystem has a standard shape of a linear response (Fig. 3.3(a)). As known, a system of two coupled oscillators has two resonance (natural) frequencies and at small δ these resonances are almost coincide.

(ii) With increasing δ the response becomes nonlinear and the resonances are shifted to the high-frequency region and finally disappear at $\delta \approx 0.5$ (Figs. 3.3(b) and (c)). However, for $\delta \leq 0.5$ both subsystems oscillate in a periodic regime with the period equal to the period of the modulation (period one) over all frequency range.

(iii) A further increase in δ leads to the appearance of multiple periodic attractors and death states, i.e., steady state solutions, which does not depend on either f or δ (Figs. 3.3(d) and 3.4). These steady state solutions correspond to the stable equilibrium points in the three-dimensional double-well potential (Fig. 3.1). At certain parameters the death state coexists

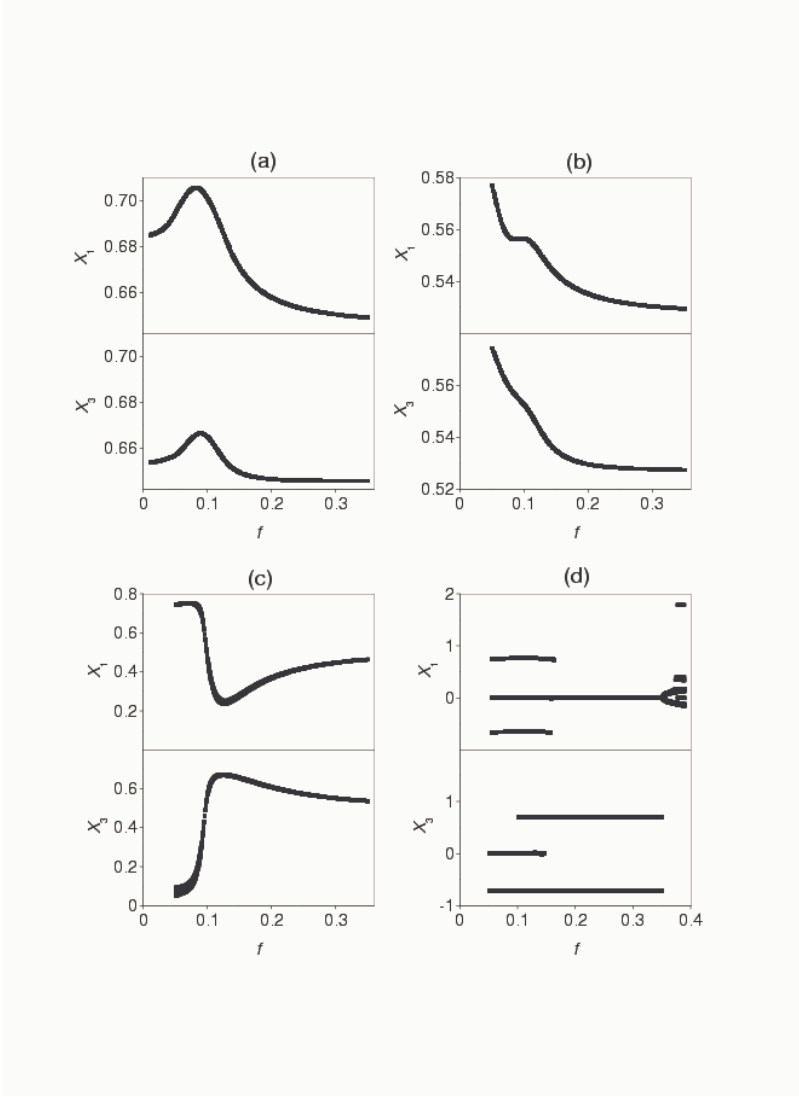

Figure 3.3: Bifurcation diagram for the master (X_1) and slave (X_3) oscillator for $m = 0.1$and different coupling strengths (a) $\delta = 0.1$, (b) $\delta = 0.4$,(c) $\delta = 0.5$,(d) $\delta = 0.51$

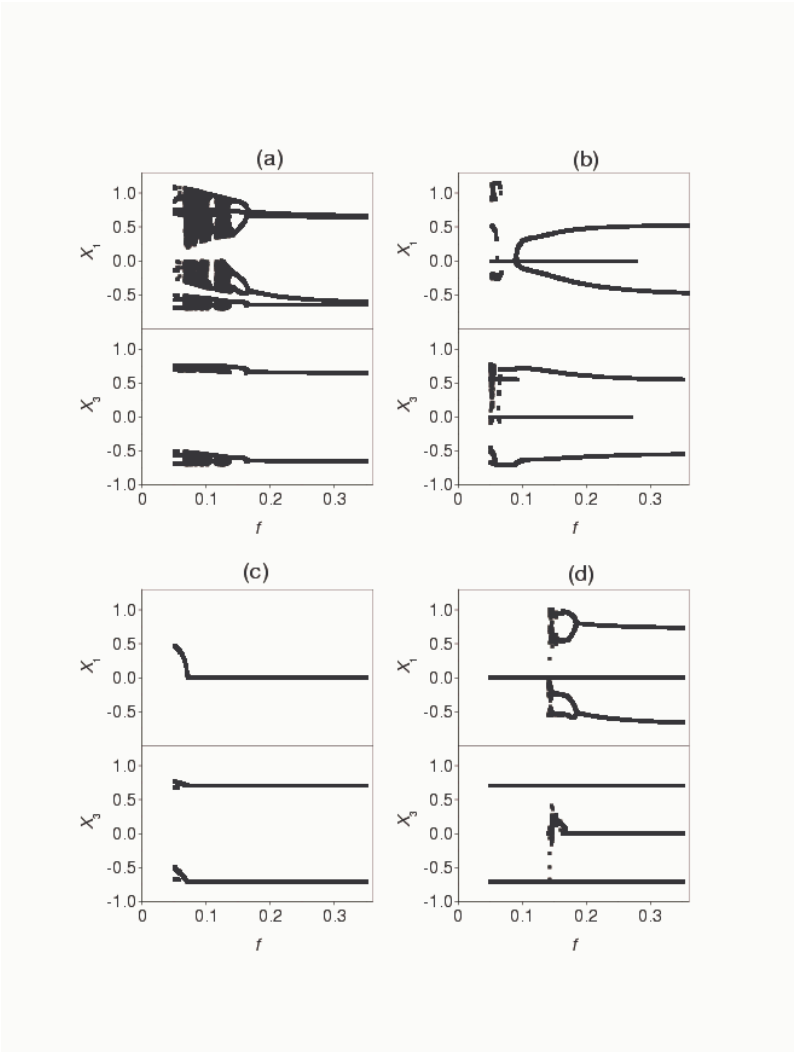

Figure 3.4: The same as in Fig 3 but for $m = 0.9$

with periodic or chaotic regimes. Thus, the whole system may be either oscillating or dead depending on its previous history. The coexistence of states in the death phenomena has been also detected in coupled autonomous oscillators (self-modulated) [30, 31, 34]. One can see that, as distinct from autonomous systems, where oscillation death is possible only for strong couplings, in the parametrically modulated system this effect may occur also for relatively weak couplings, when m and f are relatively high (see Fig. 3.4(a)). The death state appears in the Hopf bifurcation (HB) (at $f \approx 0.17$ in Fig. 3.4(a)) where the oscillators pull each other off their limit cycles and collapse to steady states. In Fig. 3.4(a) the periodic attractors coexist with the steady state for $f > 0.17$ (partial death).

(iv) At high δ all periodic and chaotic attractors undergo boundary crisis and disappear and only the death state remains (pure death). This situation is illustrated in Figs. 3.4(b)-(d). The frequency range for the pure death is located between the HB and crisis points. For example, in Fig. 3.4(b) this regime is observed between the crisis point at $f \approx 0.06$ and the HB point at $f \approx 0.09$, in Fig. 3.4(c) for $f > 0.07$ (after the HB), and in Fig. 3.4(d) for $f < 0.15$ (before crisis).

3.2.6 Codimensional-two Bifurcation Diagrams.

The codimensional-two bifurcation diagrams in (m, δ) parameter space for different modulation frequencies are shown in Fig. 3.5(a). For low modulation frequencies ($f \longrightarrow 0$) the HB line (H) approaches to a straight line

going from $\delta = 0.5$ at $m = 0$ to $\delta = 0$ at $m = 1$. This line coincides with a saddle-node bifurcation line for steady state solutions of Eqs. (3.9-3.12) in linear approximation [49]. A faster modulation changes the stability of periodic solutions by shifting the critical points [44, 45, 46]. With increasing f from 0 to ∞, the H line grows to $\delta = 0.5$. Above this line the steady state solutions, responsible for the death state, coexist for certain parameters with the periodic solutions. We should note that for some frequencies ($f < 0.1$) the second HB line appears where the steady state solutions change their stability (for example, $H_2(f = 0.05)$ in Fig. 3.5(a)). Thus, there exists the parameter range bounded by this HB line (dashed region) where the death state is absent.

It is known that coexisting attractors can be destroyed in boundary crisis. Crisis phenomena in a single two-well forced Duffing oscillator were studied by Kao et al. [10]. Recently, is was shown that coexisting attractors can undergo crisis and be annihilated in a parametrically modulated system when the modulation frequency is close to the frequency of relaxation oscillations (imaginary part of corresponding eigenvalues) of the associated attractor [50, 51]. This means that only the steady state solutions remain stable, while the other (periodic) solutions become unstable. In Fig. 3.5 we plot the crisis lines for two modulation frequencies, $C(f = 0.05)$ and $C(f = 0.1)$. Two crisis lines for the same frequency, $C_1(f = 0.1)$ and $C_2(f = 0.1)$, correspond to different coexisting attractors, each of which has its own relaxation oscillation frequency. Between C and H lines only the steady state solutions

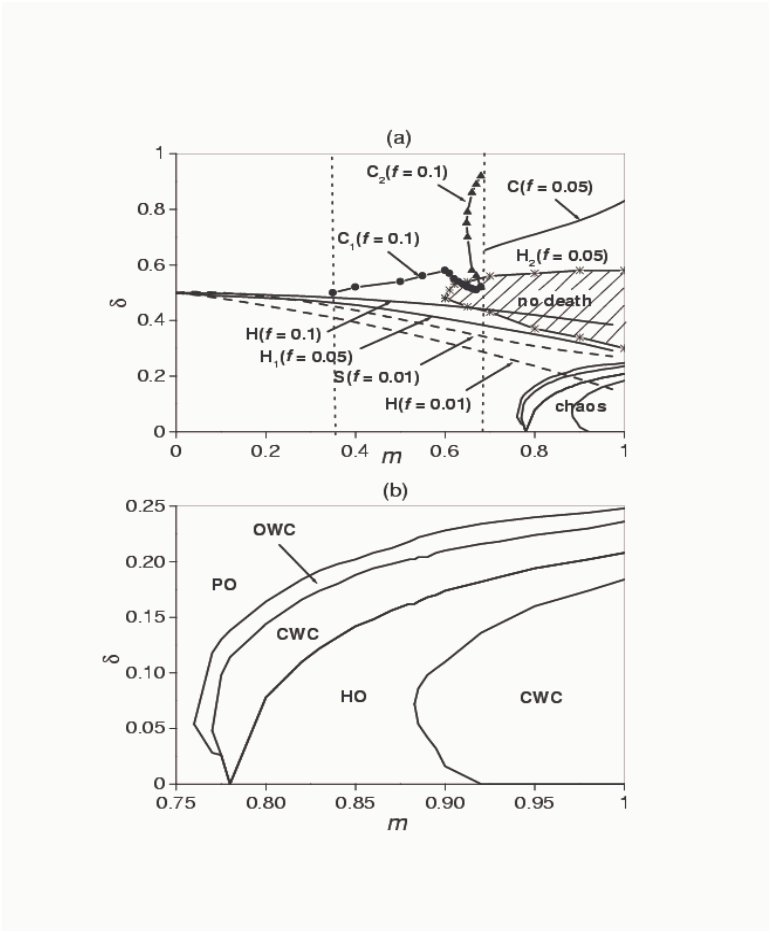

Figure 3.5: Codimentional-two bifurcation diagrams in (m, δ) parameter space for different modulation frequencied f (a) H indicated the Hopf bifurcation lines,S is the Saddle node bifurcation, and C is crisis lines. No deth occurs inside the deshed region bounded by line H_2. The dotted vertical lines indicate the minimal modulation amplitude for crisis of attractor for correspondig frequencies. (b) Enlarge region of Fig. 5(a) demostranding different types of chaos at $f = 0.1$. OWC is one well chaos, HO is hopping oscillation (perioding windows), and PO is periodic orbits.

are stable, i.e., no oscillatory solutions can be found at any initial conditions (pure death). Thus, the HB and crisis points indicate the boundaries of the pure death state in the parameter space. These boundaries are of fundamental importance in communications with parametrically modulated coupled systems because they indicate the dead region for information transmission by such systems.

Chaotic oscillations are observed for high modulation amplitudes ($m > 0.75$). The bifurcation lines bounded different chaotic regimes are shown in Figs. 3.5(b) in (m, δ) parameter spaces. The regions of one-well chaos (OWC), cross-well chaos (CWC), and hopping oscillations (periodic windows) can be distinguished.

3.2.7 Chaos Synchronization

In the coupled oscillators with modulated parameter all periodical regimes are completely synchronized with the frequency of the external modulation. The lag in pulses of the master and slave oscillators depends on δ, m, and f. In this section we pay our attention on the most interesting case: synchronization of chaos.

3.2.8 Phase Synchronization

Figures 3.6 and 3.7 show time series (a,b), amplitude (c), and phase correlations (d) for two types of chaos: one-well chaos (Fig. 3.6) and cross-well chaos (Fig. 3.7). To examine the phase correlation, the time of the nth peak (τ_1)

for the master oscillator x_1 is plotted against that (τ_2) for the slave oscillator x_3. As seen from the figures in both cases the phases are locked (straight lines in Figs. 3.6(d) and 3.7(d)), while the amplitudes remain noncorrelated and sustain an irregular motion of their own (Figs. 3.6(c) and 3.7(c)). Thus, the chaotic oscillations in the coupled oscillators with parametric modulation are always synchronized with the phase of the external driving force.

3.3 Intermittent Lag Synchronization in a Two Coupled Duffing Oscillators with Parametric Modulation.

It is known, that in chaotic autonomous nonidentical oscillators, a symmetric coupling can lead to phase synchronization [26]. This regime is characterized by a perfect locking of the phases of the two signals, whereas the two chaotic amplitudes remain uncorrelated. Lag synchronization consists of hooking one system to the output of the other shifted in time of a lag time τ_{lag} $[s_1(t) = s_2(t - \tau_{lag})]$ [27]. Recently, Boccaletti and Valladares [52] characterized intermittent lag synchronization of two nonidentical symmetrically coupled Rösler systems. They observed intermittent bursts away from the lag synchronization and described this phenomenon in terms of the existence of a set of lag times $\tau^n_{lag}(n = 1, 2, ...)$, such that the system always verifies $s_1(t) \simeq s_2(t-\tau^n_{lag})$ for a given n. In this work we study a similar phenomenon

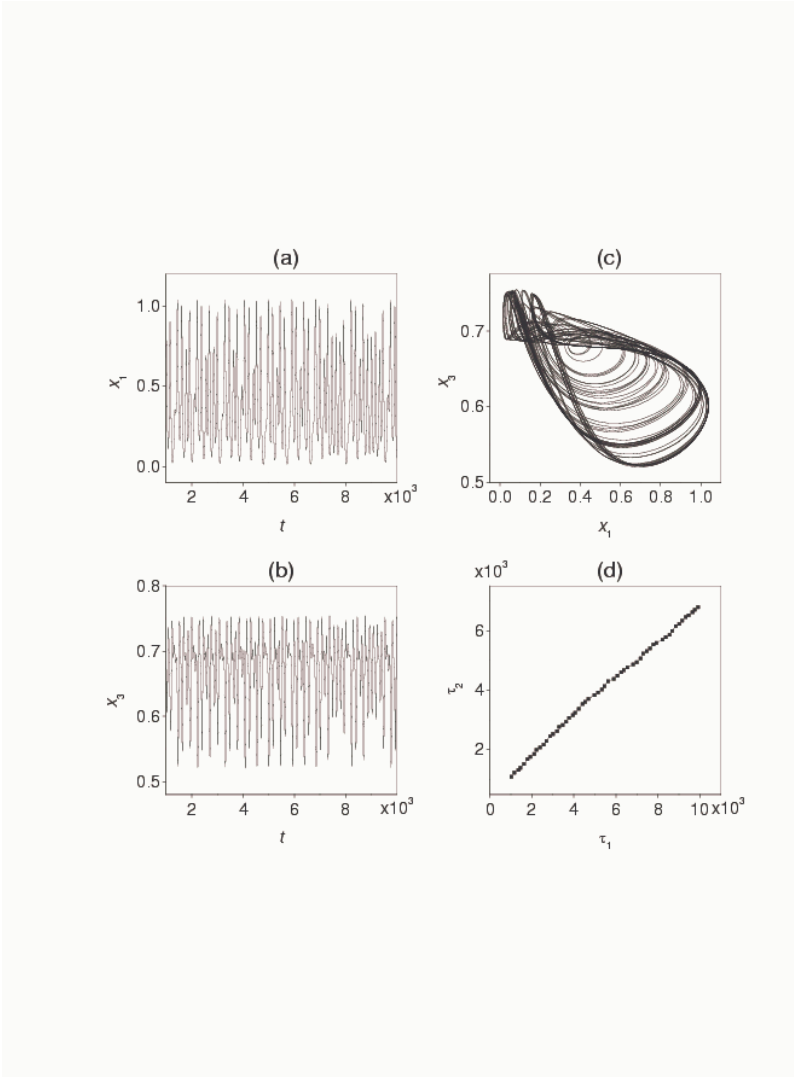

Figure 3.6: Phase synchonization of one-well chaos. (a,b) Time serien master (x_1) and slave (x_3) oscillators, (c) $x_1 - x_3$ plot showing that the amplitude are noncorrelated, and (d) phase correlation. $\delta = 0.1, f = 0.065, m = 0.8$

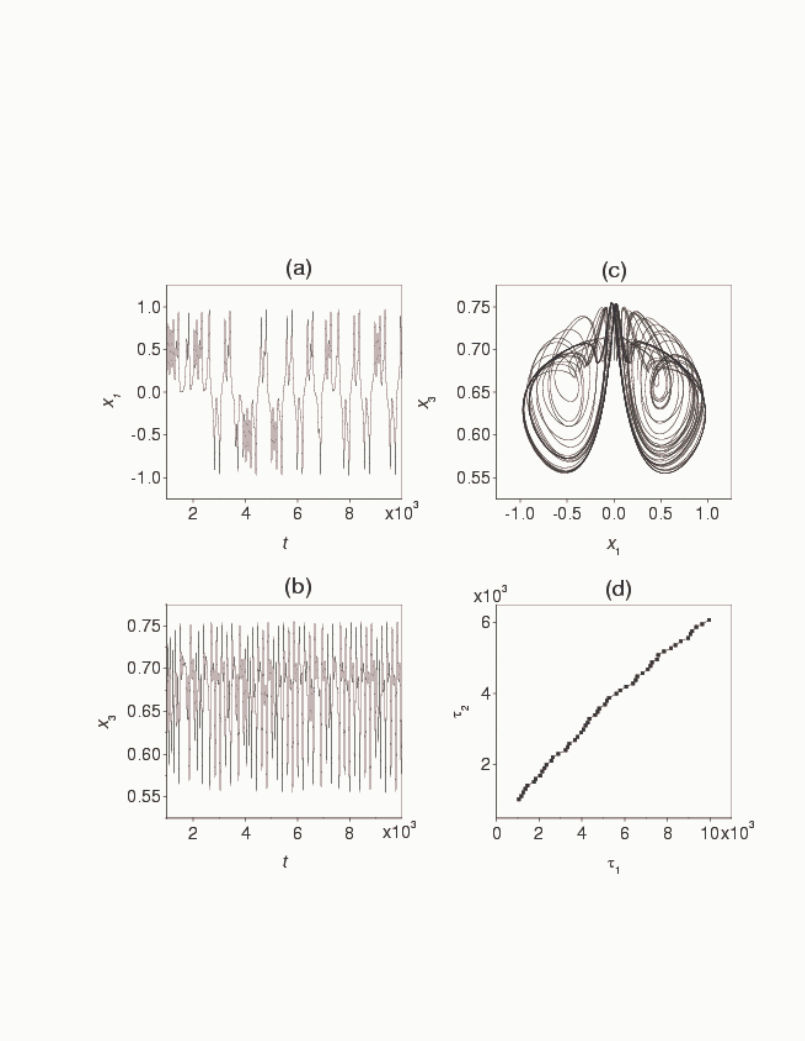

Figure 3.7: Phase synchronization of cross-well chaos $\delta = 0.1, f = 0.101, m = 0.8$

in a nonautonomous system with parametric modulation. As distinct from a self-oscillatory system, all oscillations in a parametrically modulated system are the forced oscillations induced and driven by an external periodic forcing and hence they are always phase-locked with the forcing, even when the oscillators are identical (see, for example, [53]). In this work we will show that at certain conditions the regime of *intermittent lag synchronization* appears in the nonautonomous system of the coupled oscillators. Similarly to [52], this regime can be considered as the intermittent behavior between phase synchronization and lag synchronization.

For stability analysis, it is convenient to transform the nonautonomous systems Eqs. (3.9-3.12) to the autonomous one by adding one degree of freedom

$$\dot{x_1} = x_2, \tag{3.13}$$

$$\dot{x_2} = -\gamma x_2 - a_0[1 - m\sin x_5]x_1 - bx_1^3 - \delta x_1 x_3^2, \tag{3.14}$$

$$\dot{x_3} = x_4, \tag{3.15}$$

$$\dot{x_4} = -\gamma x_4 - a_0 x_3 - bx_3^3 - \delta x_1^2 x_3, \tag{3.16}$$

$$\dot{x_5} = \omega. \tag{3.17}$$

The system Eqs. (3.13-3.17) in vector notation can be written in the form

$$\dot{X} = \Psi(\ X; p), \tag{3.18}$$

where $X = [x_1, x_2, x_3, x_4, x_5]^t$ is the state-space vector ($[...]^t$ being transpose), $\Psi = [\psi_1, \psi_2, \psi_3, \psi_4, \psi_5]^t$ is the function space, and $p = (\gamma, a_0, b, \delta, m, \omega)$ is an

element of the parameter space. This system generates a flow $\Phi = \left\{\Phi^T\right\}$ on the phase space $\mathbf{R}^4 \times \mathbf{S}^1$ and $\mathbf{S}^1 = \mathbf{R}/T$ is the circle of length $T = 2\pi/\omega$.

The frequency $f = \omega/2\pi$ and the amplitude m of the parametric modulation are used as control parameters in the bifurcation diagrams that will be presented in the following. Due to the symmetric potential of both oscillators, the coupled system Eqs. (3.13-3.17) possesses the same symmetry properties as a single Duffing oscillator [54], i.e., it is symmetric since the transformation $S : (x_1, x_2, x_3, x_4, x_5) \rightarrow (-x_1, -x_2, -x_3, -x_4, x_5 + \pi)$ leaves Eqs. (3.13-3.17) invariant. Therefore, this system can support symmetric orbits and also asymmetric ones which are not invariant with the transformation S. Saddle-node, period-doubling, Hopf, and symmetry-breaking bifurcations occur in the coupled system Eqs. (3.13-3.17). We use a perturbation analysis to analyze solution stability in the Poincaré section defined by $\Sigma = \{(x_1, x_2, x_3, x_4, x_5) \in \mathbf{R}^4 \times \mathbf{S}^1 : x_5 = \text{const}\}$.

The equations for small deviation δX from the trajectory $X(t)$ are

$$\dot{\delta X} = L_{ij}\left(X(t)\right)\delta X, \qquad i, j = 1, 2, ..., 5, \tag{3.19}$$

where $L_{ij} = \partial\Psi_i/\partial x_j$ is the Jacobian 5×5 matrix of derivatives. Equation (3.19) for system Eqs. (3.13-3.17) becomes:

$$\begin{bmatrix} \dot{\delta x_1} \\ \dot{\delta x_2} \\ \dot{\delta x_3} \\ \dot{\delta x_4} \\ \dot{\delta x_5} \end{bmatrix} = \begin{bmatrix} 0 & 1 & 0 & 0 & 0 \\ A_{21} & -\gamma & A_{23} & 0 & A_{25} \\ 0 & 0 & 0 & 1 & 0 \\ A_{41} & 0 & A_{43} & -\gamma & 0 \\ 0 & 0 & 0 & 0 & 0 \end{bmatrix} \begin{bmatrix} \delta x_1 \\ \delta x_2 \\ \delta x_3 \\ \delta x_4 \\ \delta x_5 \end{bmatrix} \tag{3.20}$$

where $A_{21} = -a_0 + a_0 m \sin x_5 - 3b{x_1}^2 - \delta {x_3}^2$, $A_{23} = -2cx_1x_3$, $A_{25} = a_0 m x_1 \cos x_5$, $A_{41} = -2cx_1x_3$, $A_{43} = -a_0 - 3b{x_3}^2 - \delta {x_1}^2$

When using the unit matrix I as the initial condition $X_0 = I$, the resulting solution $X(T)$ after one period T of the oscillation represents the linearized Poincaré map P. The solution of Eq. (3.19) can be found in the form

$$X(t) = X_0 \exp[tL_{ij}(X(0))], \tag{3.21}$$

where the time-independent matrix $L_{ij}(X(0))$ and the matrix X_0 contains the initial conditions. Let $\mu_k = \lambda_k + i\Omega_k$ $(k = 1, 2, 3, 4)$ be the eigenvalues of the matrix $L_{ij}(X(0))$. Then the eigenvalues of the linearized Poincaré map P may be written as

$$\rho_k = e^{T\mu_k} = e^{T\lambda_k}[\cos(T\Omega_k) + i\sin(T\Omega_k)]. \tag{3.22}$$

Globally, if all $\lambda_k < 0$, then these eigenvalues spiral into the origin of the complex plane when the modulation frequency ω is decreased, i.e., all sufficiently small perturbations tend towards zero as $t \to \infty$ and the steady state

(nodes, saddle nodes, spiral) is stable. For larger values of the modulation amplitude m, the influence of the nonlinearity becomes more important and the eigenvalues move towards the critical value +1 (saddle-node bifurcation) or -1 (period-doubling bifurcation). In the case of the coupled Duffing oscillators Eqs. (3.13-3.17) the symmetry of their potentials (Fig. 3.1) implies the existence of a root $\overline{P} = -H$ of the Poincaré map $P = \overline{P}_0\overline{P} = (-H)^2$, where the map H is obtained by integrating the variables of the Poincaré map over half a period of the oscillation [41].

Although the two oscillators are almost identical, the origin of the lag in their oscillations is the same as in the case of nonidentical autonomous oscillators [27, 52], namely, a mismatch of their nonlinear resonance frequencies, that appears due to the nonlinear coupling and because the modulation is applied only to the master oscillator.

In this paper we are interested in chaotic regimes. Chaotic oscillations are observed for relatively high modulation amplitudes ($m > 0.75$) and low couplings ($\delta < 0.25$). In Fig. 3.8 we present the codimensional-two bifurcation diagrams in the (m, f) parameter space. In the figure we plot the saddle-node bifurcation lines which bound different dynamical regimes: periodic orbits (PO), one-well chaos (OWC), cross-well chaos (CWC), and hopping oscillations (HO) (periodic windows).

In our system all oscillations are excited by external periodic modulation and hence they are always phase-locked with the forcing. When the system oscillates in a periodic regime, the state variables of the two subsystems

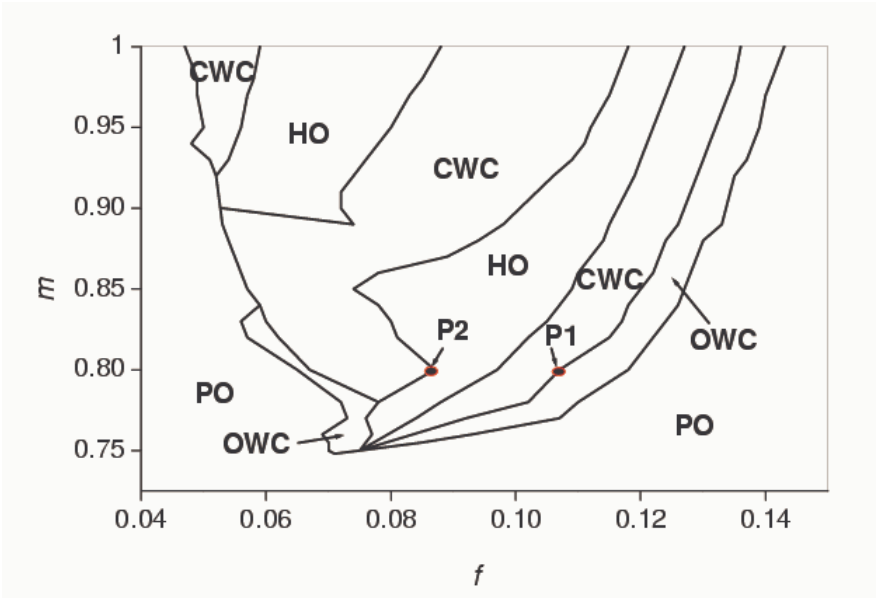

Figure 3.8: Codimentional-two bifurcation diagram in parameter space of modulation frequency f and depth for $\delta = 0.1$.Intermittent lag synchronization occurs in the vecinity of the saddle-node bifurcation lines which bound different dynamic regimen: one-well chaon (0WC), cross-well chaos (CWC), hopping oscillations (HO), and periodic orbits (PO). The dots indicated the parameter for which the regimen of period-1 ILS (P1) and period-2 ILS (P2) are observed (see Figs 3.9 and 3.10)

are shifted in time, i.e. lag synchronization takes place. Within very narrow parameter range, close to the saddle-node bifurcations, short periodic windows are observed in time, where system jumps from chaos to local periodicity (Figs. 3.9 and 3.10). During these jumps, the chaotic trajectory visits closely a periodic orbit. We identify this phenomenon with *intermittent lag synchronization* (ILS). Two kinds of ILS are seen in Figs. 3.9 and 3.10: one-state period-1 (P1) ILS (Fig. 3.9) and cross-state period-2 (P2) ILS (Fig. 3.10). In the former case, the x_1-trajectory jumps intermittently from cross-well chaos to the small P1 orbit around each of the potential wells and back, whereas in the latter case, the trajectory jumps from cross-well chaos to the large P2 orbit oscillating between the two wells. Figures 3.9(b) and 3.10(b) display the enlarged parts of the time series where lag synchronization is observed. The modulation parameters for the regimes shown in Figs. 3.9 and 3.10 are indicated in Fig. 3.8 by the dots. These dots lie on the saddle-node bifurcation lines which bound respectively the one-well and cross-well chaotic regimes and the regimes of hopping oscillations and cross-well chaos.

Rosenblum *et al.* [27] proposed to describe the occurrence of ILS as a situation where during some periods of time the system verifies $\Delta \equiv |x_3(t) - x_1(t-\tau)| \ll 1$ (τ being a lag time), but where bursts of local non-synchronous behavior may occur. This phenomenon was identified with on-off intermittency [55] and the bursts from lag synchronization was found to result from the small, but negative value of the second global Lyapunov exponent of the system, so that the trajectory visits attractor regions where the

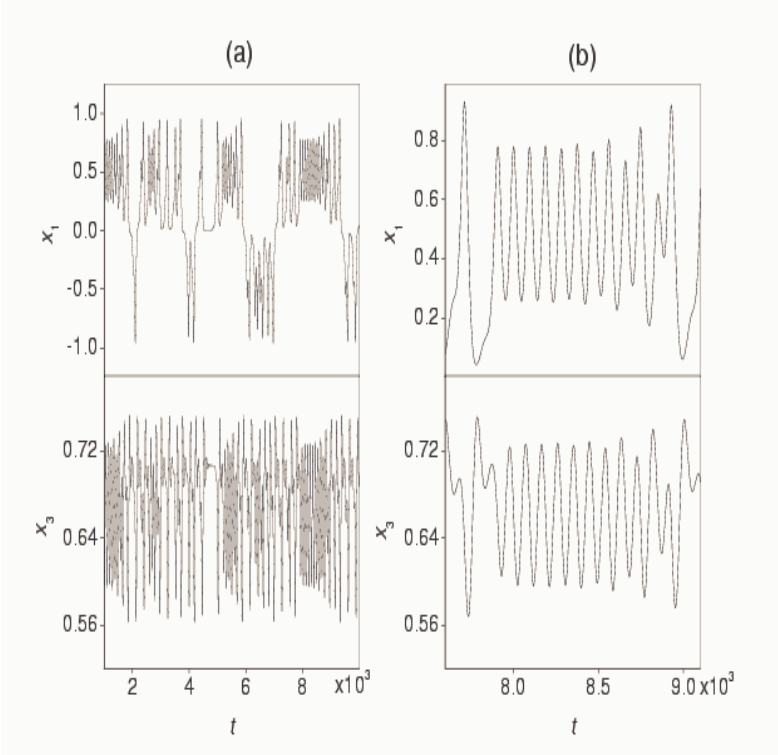

Figure 3.9: One-state period-1 intermittent lag synchronization of cross-well chaos (small orbit synchronization). (a) Time series of master (x_1) and slave (x_3) oscillators, (b) enlarged part of (a) demostrating synchronous windows of periodicity in one states. $\delta = 0.1, f = 0.107, m = 0.8$

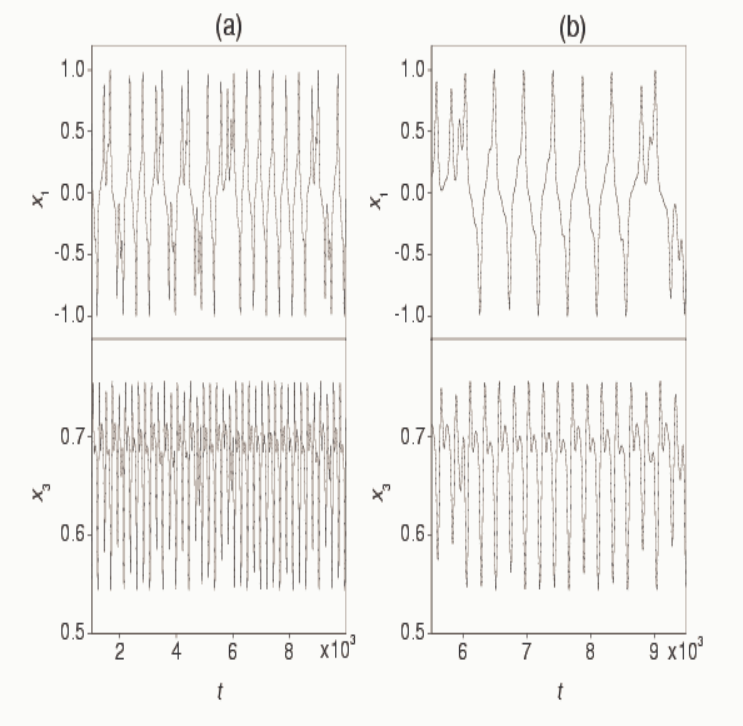

Figure 3.10: Two state period-2 of intermittent lag synchronization of cross-well chaos (large orbit synchronization). (a) Time series of master (x_1) and slave (x_3) oscillators, (b) enlarged part of (a) demostranting synchronous windows of periodicity in one of the states. $\delta = 0.1, f = 0.087, m = 0.8$

local Lyapunov exponent is still positive. In the case of periodically driven systems, this condition should be modified to be

$$\Delta \equiv |x_3(t) - < x_3(t) > -\eta\left[x_1(t-\tau) - \langle x_1(t)\rangle\right]| \ll 1, \tag{3.23}$$

where η is a proportional coefficient between the alternative amplitudes of the variables in the synchronous regime, $\eta = \left(x_3^{\max} - x_3^{\min}\right) / \left(x_1^{\max} - x_1^{\min}\right)$. The proportionality coefficient η is introduced because the modulation is applied only to the master oscillator (X_1), and hence the response of the slave oscillator (X_3) is smaller than that master system. Due to the above reason the averages of the two signals are different and hence they also should be normalized. As distinct from a (self-oscillatory) system, in our system the chaotic oscillations of the two variables $x_1(t)$ and $x_3(t)$ are always phase synchronized. Therefore, the intermittent jumps from chaos to the windows of periodicity can be considered as the intermittent behavior from phase to lag synchronous regimes. Of course, the criterion Eq. (3.23) can be used only for characterization of the simplest case of P1 ILS (Fig. 3.9). For higher periodic regimes (P2, P3,...) of ILS, the shapes of the oscillations in the periodic windows are different for two oscillators, and hence more complex relation is required. The temporal behavior of $\Delta_0(\tau_0 = 116)$ for the case of P1 ILS is shown in Fig. 3.11(a).

Similarly to Rosenblum *et al.* [27], we may characterize lag synchronization by the similarity function $S(\tau)$, defined as the time averaged difference Δ, conveniently normalized to the geometrical average of the two mean sig-

nals

$$S^2(\tau) = \frac{\langle \Delta^2 \rangle}{\left[\langle x_1^2(t)\rangle \langle x_3^2(t)\rangle\right]^{1/2}}, \tag{3.24}$$

and search for its global minimum $\sigma = \min_\tau S(\tau)$, for $\tau_0 \neq 0$. The dependence of the similarity function on the lag time shown in Fig. 3.11(b) resembles the similar dependence reported previously by Boccaletti and Valladares [52] for Rössler systems. Looking at Fig. 3.11(b), one can see that, besides a global minimum at $\tau_0 = 116$, $S(\tau)$ displays many other local minima at smaller and larger lag times τ_n ($n = 1, 2, 3, ...$). This means that the system Eqs. (3.13-3.16), besides being lag synchronized during some periods of time with respect to the global minimum τ_0, occasionally visits closely other lag configurations corresponding to the condition Eq. (3.23). The deep of the nth local minimum is closely related to the fraction of time that the corresponding lag configuration is closely visited by the system. The different lag times τ_n can be expressed by the relation $\tau_n \approx \tau_0 + nT$, where T is the period of external modulation or the return time of the limit cycle onto the Poincaré section. The nonharmonicity in function $S(\tau)$ results from the nonharmonicity of the periodic oscillations due to the high nonlinearity of the system.

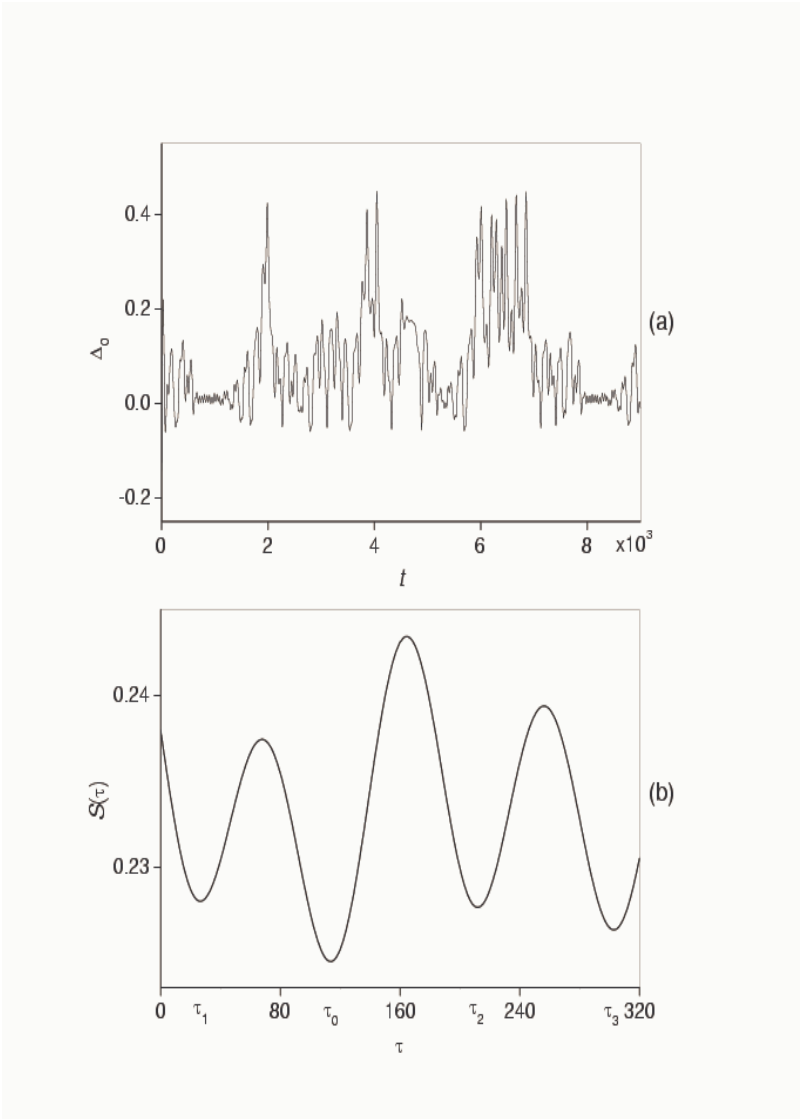

Figure 3.11: (a) Times series of $\Delta_0(\tau = 116)$ in period-1 intermittent lag synchronization regime. The windows with $\Delta \approx 0$ are see as the low-dimensional " lag synchronization" attractor. (b) Similarity function $S(\tau)$ vs lag time τ. There exists a global minimun at $\tau_0 = 116$ and local minima for smaller and larger times $\tau_n (n = 1, 2, 3)$

3.4 Conclusions

We have studied synchronization properties of two mutually coupled oscillators with parametric modulation in one of them. Chaos in such a system is always synchronized in phase with the external modulation. We have demonstrated the oscillation death phenomenon in this system. As distinct from a (self-oscillatory) system, the death can occur in almost identical oscillators without any delay in coupling. Detailed numerical estimates of the parameter space in the coupling strength, modulation amplitude, and frequency where the death occurs have been presented. The death can be either partial or pure. In the partial death state, oscillatory (periodic or chaotic) solutions coexist with the death state, whereas in the pure death state there are no oscillations at all and both subsystems have stable steady state solutions which are independent on the modulation parameters (amplitude and frequency) nor on the coupling strength. In this regime there exit only zero solution for the master oscillator and two nonzero solutions (fixed points) corresponding to the potential wells for the slave oscillator.

The conditions for oscillation death have been revealed. There are three important mechanisms responsible for the pure death state: (i) the Hopf bifurcation in which the death state appears, (ii) the shift of the bifurcation points due to parametric modulation, and (iii) attractor annihilation in boundary crisis. The Hopf bifurcation of the whole system indicates the low boundary in coupling for the death state. This boundary is shifted to larger coupling strengths when the modulation frequency is increased. At relatively

large couplings ($\delta > 0.5$) the chaotic solutions can undergo crisis and disappear when the modulation frequency approaches the frequency of relaxation oscillations of the associated attractor. The crisis point indicates the upper boundary in coupling for the pure death state. The knowledge of boundary conditions for the death of oscillations is very important in communications with parametrically modulated systems because these boundaries indicate the region in the parameter space where information can be lost while transmitting. Recently, oscillation death has been found out numerically in a loss-modulated CO_2 laser with two coupled cavities [56].

We have found synchronous states, which we identified with intermittent lag synchronization in two coupled parametrically driven chaotic oscillators. In the intermittent states, the system during its temporal evolution occasionally changes the behavior from phase synchronization to lag synchronization. The regime of intermittent lag synchronization appear in the narrow parameter range in the vicinity of saddle-node bifurcations. We believe that the main features of the synchronization phenomena observed in the coupled Duffing oscillators have to be expected for a wide class of coupled dissipative driven system and may be found in experiments.

Chapter 4

On-Off Intermittence

4.1 On-Off Intermittency in Two Coupled Duffing Oscillators With Parametric and Stochastic Driving

Intermittency occurs when the behavior of the system switches back and forth intermittently between apparently regular behavior and chaotic behavior. The intermittency appears to occur randomly even though the system is described by deterministic equations. In the intermittency regime, the behavior of the system is periodic or steady state for some control parameter value with occasional bursts to chaotic. As the control parameter is changed, the time spent the system being chaotic increases and the time spent being periodic decreases until, eventually, the behavior is chaotic all time. As the control parameter is changed in the other direction, the time spent being pe-

riodic increases until at some value critical, call it A_c the behavior is periodic all the time.

Coexisting attractors and intermittency are common complex phenomena observed in many nonlinear dynamical systems. The intermittency route to chaos may be observed in a dynamical system when a control parameter passes through a critical value. The intermittent behavior is characterized by irregular bursts (turbulent phases) interrupting the nearly regular (laminar) phases. Different types of intermittency have been observed and classified into type I, type II, and type III of Pomeau-Manneville intermittency [57], on-off [55], and crisis-induced intermittency [58]. The type of intermittency can be distinguished by the behavior of the Floquet multiplier for a Poincare map, depends on the type of bifurcation at the critical point.

Type I intermittency. The Floquet multiplier crosses the unit circle along the real axis at $+1$. This leads to irregular by occurring bursts of periodic and chaotic behavior. However, during these bursts, the amplitude of the motion are stable. This intermittency is called stable intermittency or tangent bifurcation intermittency since the bifurcation event is a tangent bifurcation or saddle node bifurcation.

Type II intermittency. If the Floquet multiplier forms a complex conjugate pair, then the imaginary part indicates the presence of the second frequency in the behavior of the system (the first frequency corresponds to the original limit cycle, which disappears at the bifurcation event). At the bifurcation event, the limit cycle associated with the second frequency becomes unstable and we observe bursts of two-frequency behavior mixed

with intervals of chaotic behavior. Thus, type II intermittence is a type of Hopf bifurcation.

Type III intermittency. If the Floquet multiplier is negative and become more negative than -1, then a type of period-doubling bifurcation take place. The amplitude of the subharmonic behavior created at the bifurcation point grows, while the amplitude of motion associated with the original period decreases. This periodic behavior, however, is interrupted by bursts of chaotic behavior. Hence, this is period-doubling intermittency since the Floquet multipliers change as they do for period doubling, but after the bifurcation event, the period-double behavior is unstable.

On-off intermittency is associated with saddle-node bifurcations, and **the crisis-induced intermittency** is associated with crisis of chaotic attractors when two (or more) chaotic attractors simultaneously collide with a periodic orbit (or orbits) [59].

On-off intermittency differs from other types of intermittency because it requires a dynamical time-dependent forcing of a bifurcation parameter through a bifurcation point [60], whereas for other types of intermittency the parameters are fixed. Therefore, this type of intermittency is often called modulational intermittency [61]. In on-off intermittency one or more dynamical variables of the system exhibit two distinct states as the system evolves in time. In the "off" state the variables remain approximately constant in various time intervals. These periods are called laminar phases. The "on" states are characterized by irregular bursts (turbulent phase) of the variables away from their constant values.

The effect of on-off intermittency has been investigated in one-dimensional maps coupled to either random or chaotic signals [60, 62], in a forced logistic map whose control parameter fluctuates either chaotically or stochastically [63] and in periodically forced coupled Duffing oscillators [64, 65]. Like the other types, on-off intermittency is characterized by fundamental statistical properties with typical power-law scalings near the onset of intermittency: (i) for the mean laminar phase as a function of the coupling parameter with a critical exponent of -1 [62], and (ii) for the probability distribution of the laminar phase versus the laminar length with exponent -3/2 [62]. The on-off intermittency has been also detected experimentally in electronic circuits [66], in a gas discharge plasma [67], in a spin wave system [68], in nematic liquid crystals [69], and in a laser [70]. In the case of periodically driven systems, the same critical exponent of -1 for the mean laminar phase has been found in laser experiments as a function of both the amplitude and frequency of the parametric modulation near the onset of intermittency [70]

4.2 Coexisting Attractors and On-Off Intermittency in Duffing Oscillators.

In this chapter we study on-off intermittency in a modulated system. On-off intermittence in such a system appear when either a system variable or a parameter of the coupled subsystem is driven either randomly or chaotically [71], or it requires a dynamical-time dependent forcing of a bifurcation

parameter through a bifurcation point[72], while without modulation, the system stays in a steady state or periodic state. In a system with externally of driven dynamic time-dependent forcing has been investigated by Yoshihiko *et al* [71], they reported two-stated on-off intermittency. They also studied two-dimensional map with randomly driven variable, and found one -stated on-off intermittency. Experimental observation of on-off intermittence was reported by Philip W., Hammer *et al* who observed one-state on off intermittence in a tuned nonlinear electronic circuit [72].The noise effects also was taken into account. Recently A. Pisarchik and V. Pinto [73] have observed experimentally on-off intermittence in a diode laser with an external cavity experimentally. The control parameter was the length of the external cavity that was periodically modulated.

In all above works mentioned , the system has been driven randomly or chaotically or the external modulation was applied to one of the system variable [71, 72]. Moreover, in an experimental position it is more convenient to modulate a system parameter. Parametrically modulated systems are commonly used in many practical applications, and in particular, in communication.

In this chapter we show that in such systems multiple attractors may coexist: one-state, two-state on off intermittence and limit cycles. When the system is not modulated only steady state are observed . We also investigate the influence of noise.

The analysis is carried out two coupled Duffing oscillators with additional external noise. First we find numerically all solutions of the whole system

with parametrical excitation for different amplitudes and frequencies of modulation. This allows us to identify the location of different attractors. Then we build the basin of attraction of coexisting attractors for fixed values of the modulation amplitude and frequency. Finally, we investigate to the system without noise.

4.2.1 General Equations

Dynamics of two identical nonlinear oscillators with random driving can be governed by the equation,

$$\ddot{\mathbf{x}}+\gamma\dot{\mathbf{x}}-q\boldsymbol{\xi}x = -\boldsymbol{\nabla}V(\mathbf{x}), \tag{4.1}$$

where $\mathbf{x} \equiv (x, y)$, γ is a damping factor, ξ is uniformly distributed noise with level of q in the unit interval $[0, 1]$,and $V(\mathbf{x})$ is a two-dimensional nonharmonic potential function of coupled oscillators that for symmetric Duffing oscillators can be expressed as follows [65]

$$V(x, y) = (1 - x^2)^2 + (y^2 - a^2)^2(x - d) + b(y^2 - a^2)^4, \tag{4.2}$$

where a, d and $b(> 0)$ are parameters. We assume that one of the coupled subsystems (in the x direction) is randomly driven, i.e. noisy. The solution of Eqn. (4.1) represents on-off intermittency and limit cycle.

4.2.2 Time Series

The system Eqs. (4.1,4.2) can be written as four first-order differential equations in terms of dynamical variables $x_1 = x$, $x_2 = \dot{x}$, $x_3 = y$, and $x_4 = \dot{y}$,

$$\dot{x}_1 = x_2, \tag{4.3}$$

$$\dot{x}_2 = -\gamma x_2 + 4x_1(1 - x_1^2) - (x_3^2 - a^2)^2 + q\xi x_1, \tag{4.4}$$

$$\dot{x}_3 = x_4, \tag{4.5}$$

$$\dot{x}_4 = -\gamma x_4 - 4x_3(x_3^2 - a^2)(x_1 - d) - 8bx_3(x_3^2 - a^2)^3. \tag{4.6}$$

The system Eqs. (4.3-4.6) exhibits different dynamical regimes from regular states to on-off intermittency in a wide range of parameter values [64]. For simplicity we consider the case $\gamma = 0.04$, $a = 0.73$, $b = 0.008$, and $d = -1.8$. Due to the presence of two invariant subspaces at $x_3 = \pm a$ and $x_4 = 0$, there are two "off" states, i.e., the phenomenon referred to as *two-state on-off intermittency* [65]. The two "off" states arise from two wells in the potential $V(x, y)$ on the y direction. The potential function $V(x, y)$ Eq. (4.2) at $x = 1$ is shown in Fig.4.1, which indicates two potential wells at $y = \pm 0.73$.

We choose a to be the parameter to which the control modulation is applied in the following form:

$$a = a_0[1 - m\sin(2\pi f t)], \tag{4.7}$$

where m and f are the modulation depth and frequency and a_0 is the initial value of the parameter ($a_0 = 0.73$).

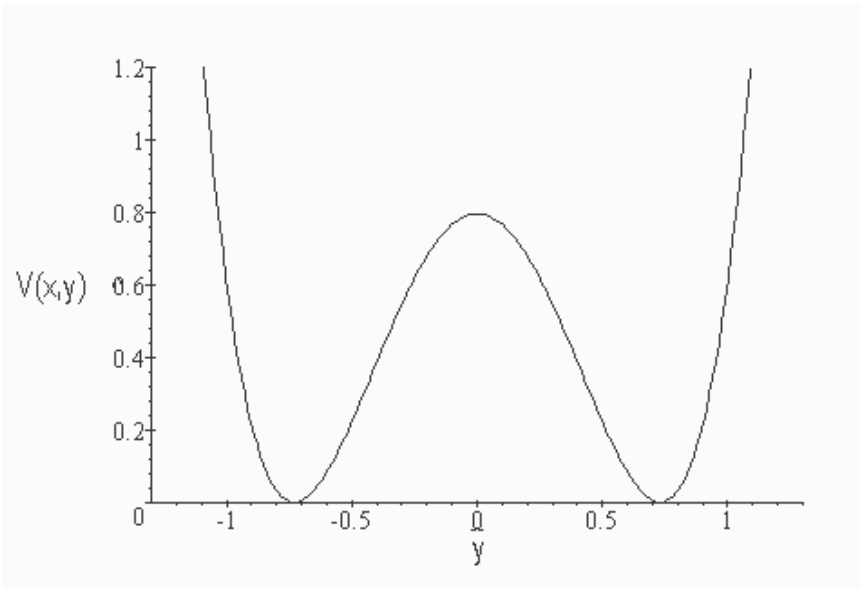

Figure 4.1: The potential function $V(x, y)$ Eq. 4.2 at $x = 1$, indicating two wells at $y = \pm a$

With Noise Without Modulation

The Figure. 4.2 shows the solution of the system Eqs. (4.3-4.7) with noise amplitude $q = 2.5$ without modulation . In this figure we observe that trajectory $x_3(t)$ is attracted to steady states in the vicinity of the invariant subspace in $x_3 = \pm a_0$. one state and two state on off intermittency are only in transients, Figs 4.2 (a)-4.2 (d).

With Noise and Modulation

The Fig.4.3 show the solutions of the system Eqs. (4.3-4.7) with noise amplitude $q = 2.5$ and parametric modulation which frequency $f = 0.001$, and m as control parameter. The time series display typical behavior of on-off intermittency and periodic orbits. General information analysis of the results performed on the basis of the time series allows us to reveal the following possible situations which can be awaited from the system of Eqs. (4.3-4.7) with parametric and random driving.

(i) two-state on off intermittence Fig 4.3(a). This behavior appears due to the presence of two invariants subspaces, which occurs when the variable x_3 complies with condition $x_3 = a_0[1 - m\sin(2\pi ft)]$ and $x_4 = 0$, and therefore the equations of motion Eqs. (4.3-4.7) become a set of equations that describe a random (stochastic)-damped Duffing Oscillators [71, 74], in which chaos occurs commonly.

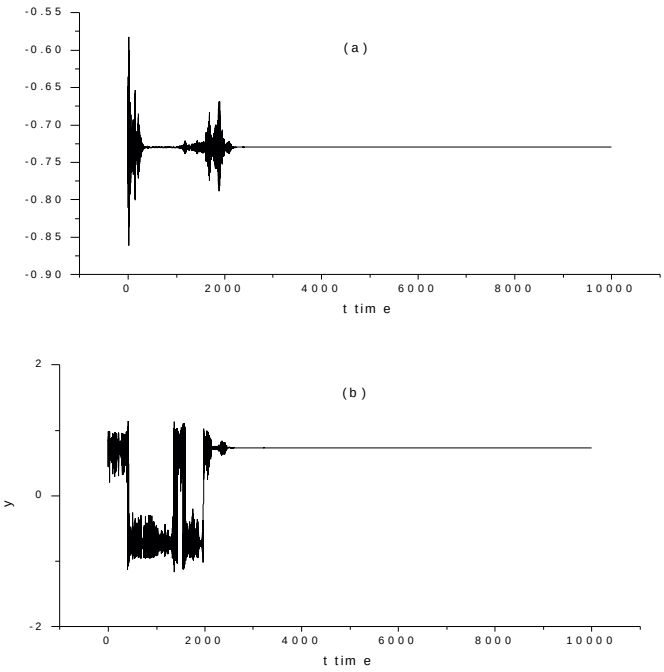

Figure 4.2: Steady states in the vecinity of the invariant subspace in; (a) $x_3 = -a_0$. (b) $x_3 = a_0$. Noise $q = 2.5$. One state and two state on-off intermitency are observed only in transients.

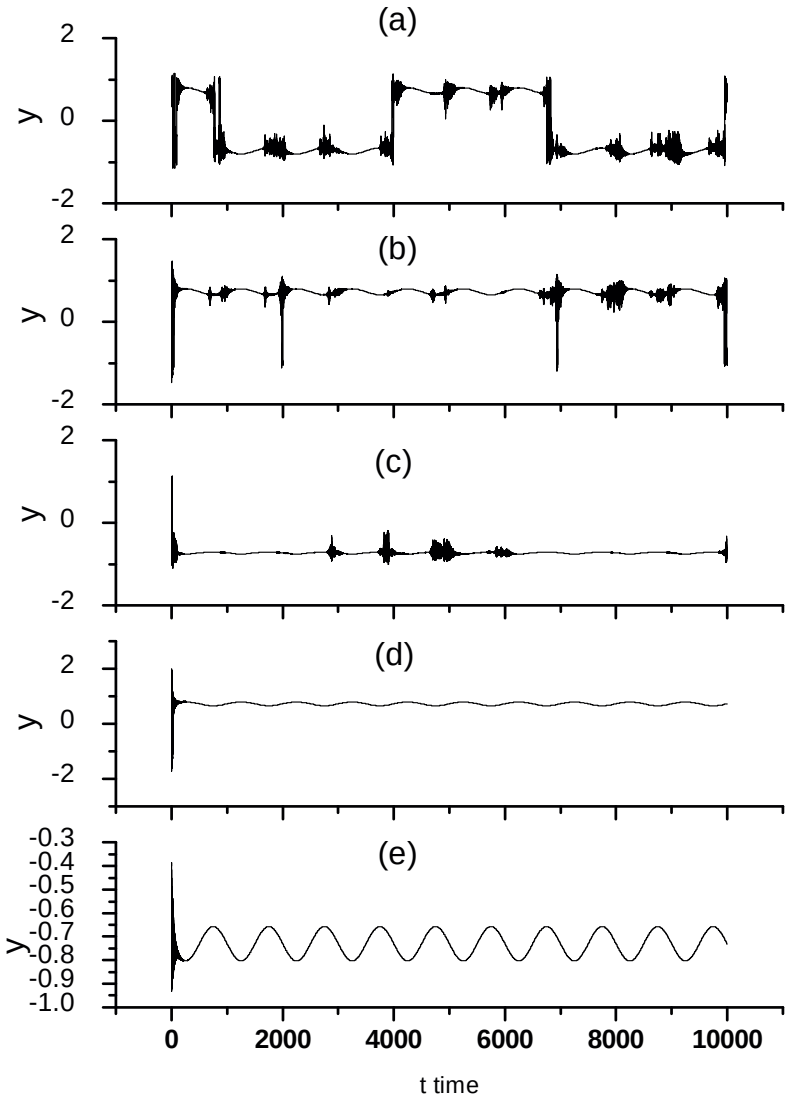

Figure 4.3: Coexisting chaotic and periodic attractors at small modulation (a) Two-state on-off intermittency. (b) and (c) One-state on-off intermittency. around each fixed point(d) and (e) Peiodic orbits. $q = 2.1$,and $f = 0.001$

The phenomenon of two-stated on-off intermittency can be understood in the context of two invariants subspaces. In randomly driven damped Duffing oscillators, which possesses two invariants subspaces, a typical trajectory spends a long time near one invariant subspace, is repelled away from this subspace, then is possibly attracted to the other invariant subspace or the same subspace, temporally spending a long stretch of time there, is repelled away again, etc.

(ii) One-state on off intermittency Fig 4.3(b). Regular phase (laminar phase) is interrupted by an irregular burst (turbulent phase), that is characteristic of on off intermittency. This behavior result from the presence of the invariant subspace. In our case the system of Eqs. (4.3-4.7) has an invariant subspace in $x_3 = a_0$, in which there is a chaotic attractor. The trajectory $x_3(t)$ spends a long time in the vicinity of the invariant subspace (off state), is repelled away from the invariant subspace towards irregular burst or on intermittence, then is attracted to the invariant subspace and spends a long stretch of time there, is repelled away again,etc.

One-state on off intermittence, in the invariant subspace $x_3 = -a_0$ is shown Fig 4.3(c).

(iii) The Figs 4.3 (d-e) shows limit cycle, situated each one in the invariants subspaces. In this case the control maintains to the trajectory $x_3(t)$ in the vicinity of one of the invariant subspace.

The manipulation of the control parameters (modulation depth and frequency) permits us to determine the location of different coexisting attractors. The Fig 4.4 we show the existence of two-state on-off intermittency,

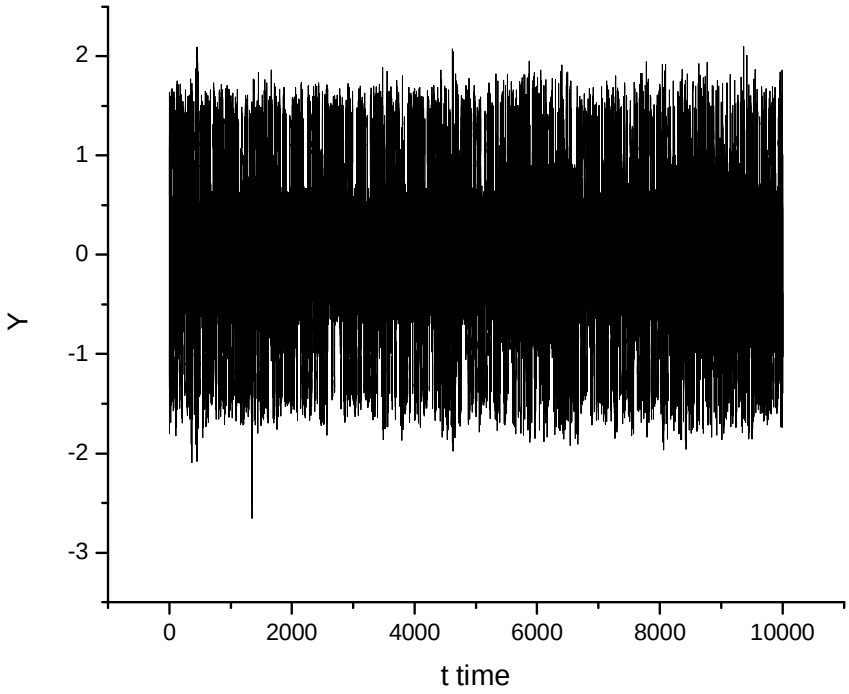

Figure 4.4: Two state on-off intermittency at $f = 0.12$ and $m = 0.6$.

and in Fig. 4.5 we demonstrate the coexistence of four attractors; two-state on-off intermittence, one-state and two-state limit cycle.

These figures have been obtained when we fixed the parameter m and f and changing the initial condition to find the solution of the system Eqs. (4.3-4.7).

(iv) For low modulation frequencies f and large amplitude m only the

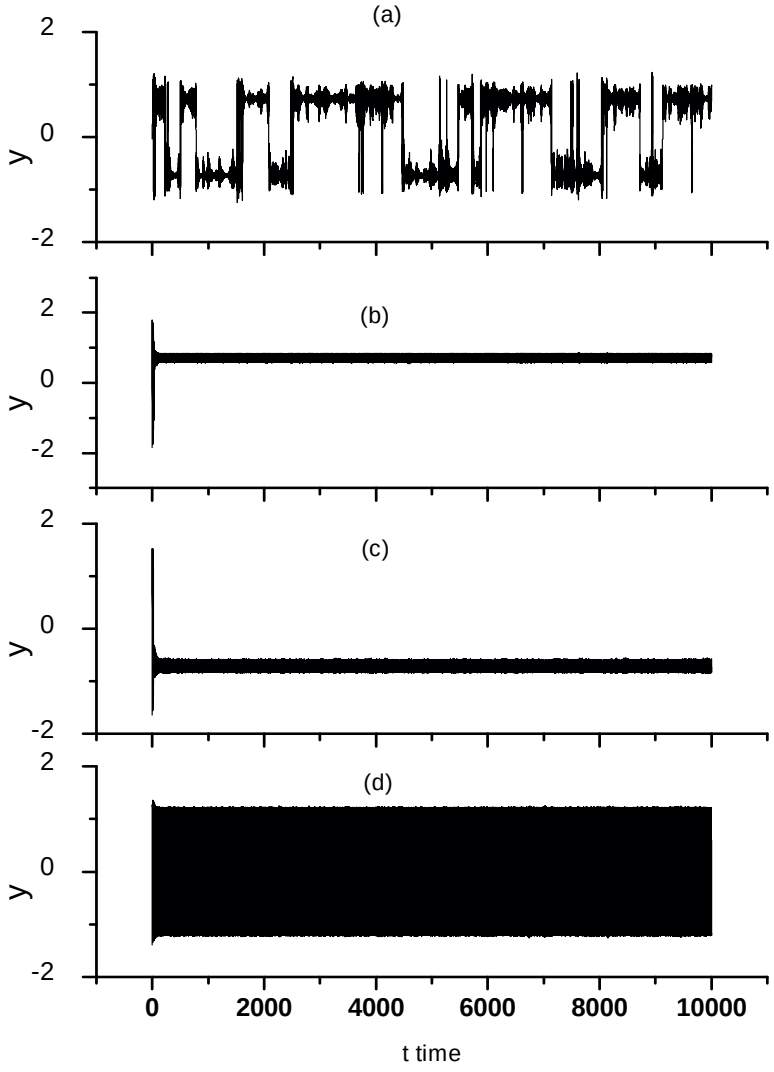

Figure 4.5: (a) Two state on-off intermittency. (b)-(c) One state periodic orbit. (d) Two state periodic orbit. $f = 0.7$ and $m = 0.099$.

regime of Two-state on off intermittency is observed in Fig.4.4. With increasing of f and m, the duration of the laminar phase decreases and finally the laminar phase disappears as a result the trajectory $x_3(t)$ oscillating between of two invariant subspace in $x_3 = \pm a_0[1 - m\sin(2\pi f t)]$.

(v) For large f and small m we observe coexistence of four attractors; two-state on off intermittence and one-well, cross-well periodic orbit Fig 4.5

.

4.2.3 Codimensional-Two Bifurcation Diagrams

The codimensional-two bifurcation diagram in (m, f) is shown in Fig.4.6. For low modulation frequencies and amplitude we find the coexistence of five attractors: two one-state on-off intermittence, two-state on-off intermittence and two one-well period attractors. For very low values of m and f, the duration of the laminar phase is large. The temporary series in this region is shown in Fig. 4.3. For large m and low frequencies of modulation we find the existence of only one-well period attractor.

For high m and f we find coexistence of three attractors: two one-well, orbits and two-state on off intermittence, coexistence of two attractors: two-state on off intermittency and cross-well periodic orbits and single attractor: two-state on off intermittency. For others values of m and f, we find also the coexistence two, three and four attractors.

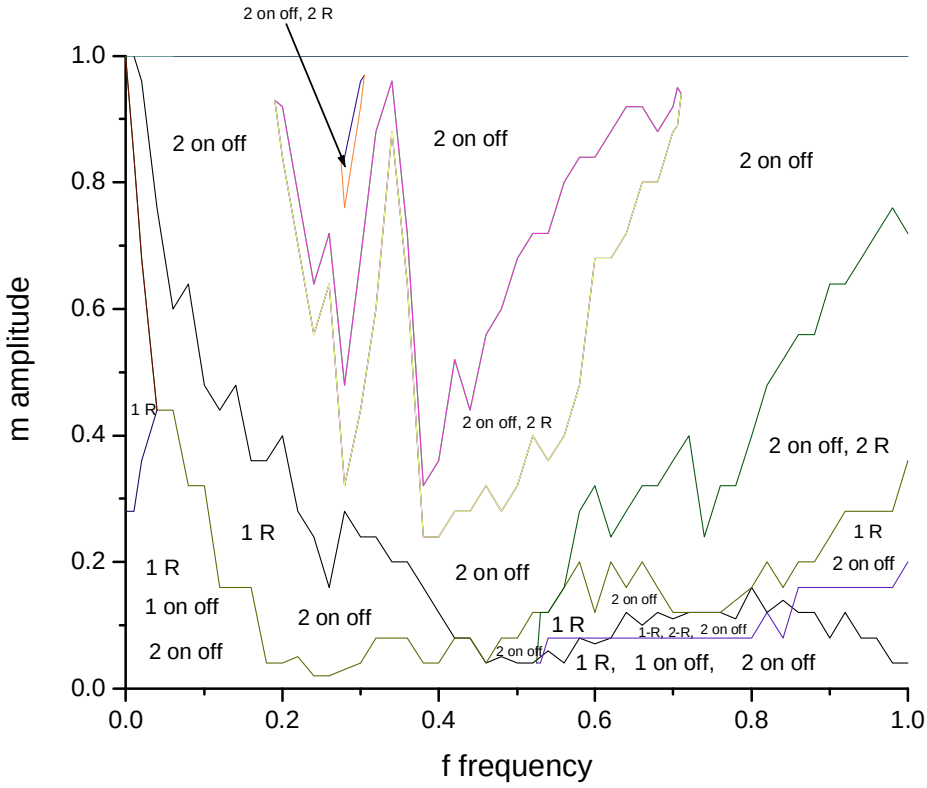

Figure 4.6: Codimentional-two bifurcation diagram in $(m.f)$ parameter space of the system Eqs.(4.3-4.7) with noise $q = 2.5$. Where one-state on-off intermitency, 2 0n-0ff is two-state on-off intermittency, 1 R is the one-well period orbit, and 2 R is cross-well period orbit

Basin of Attraction

The diagram of Fig 4.7 show the basin attractions for $m = 0.09$ and $f = 0.7$, in which four attractors coexist: two one-well period orbits, cross-well period orbit and two-state on off intermittence. The black, blue and green dots represent respectively two-state on off intermittency, one-well periodic orbit and cross-well periodic orbit. We can observe a light symmetry in y direction in the basin, because the close orbits are located in the vicinity of invariant subspaces in $x_3 = \pm a_0$.

Without Noise

The codimensional-two bifurcation diagram in parameter space (m, f) without noise ($q = 0$), are shown in Fig. 4.8. The dynamic of the systems without noise is much poor that with it. One can see that without noise at small m only period state exist. We should note that one-state on-off intermittency never appears without noise.

4.3 Control of On-Off Intermittency by Slow Parametric Modulation

The possibility for controlling on-off intermittent dynamics was investigated first by Nagai, Hua, and Lai [65]. Their control method is based on Ott,

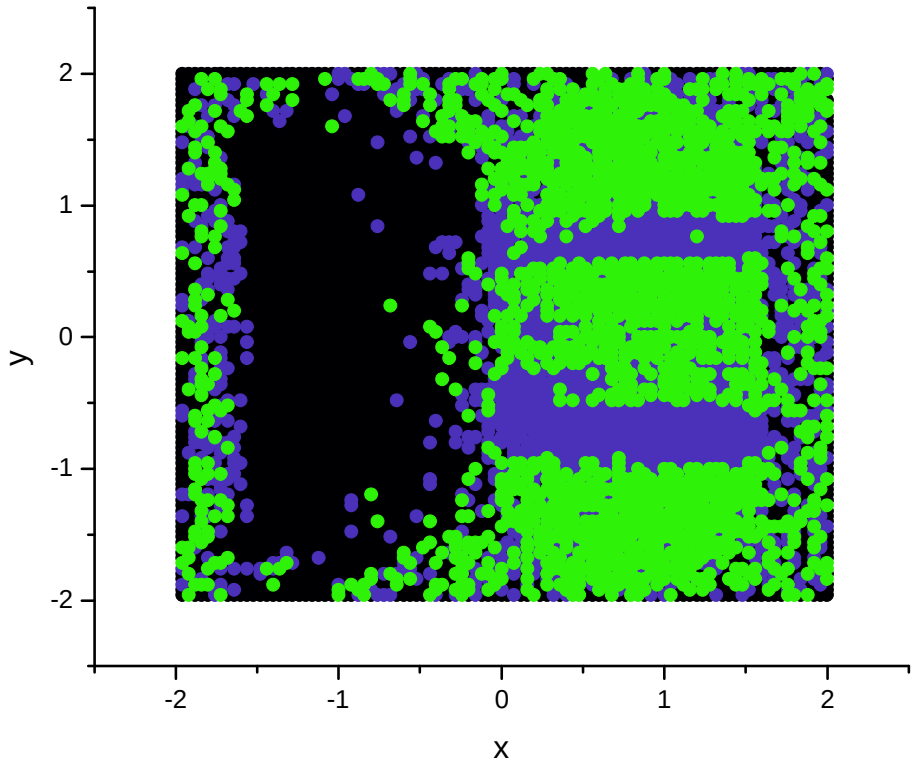

Figure 4.7: Basins of attraction of coexisting attractors for $m = 0.099, f = 0.7$. The black, blue and green dots represent respectively two-state on-off intermittency and one-well and cross-well periodics orbits.

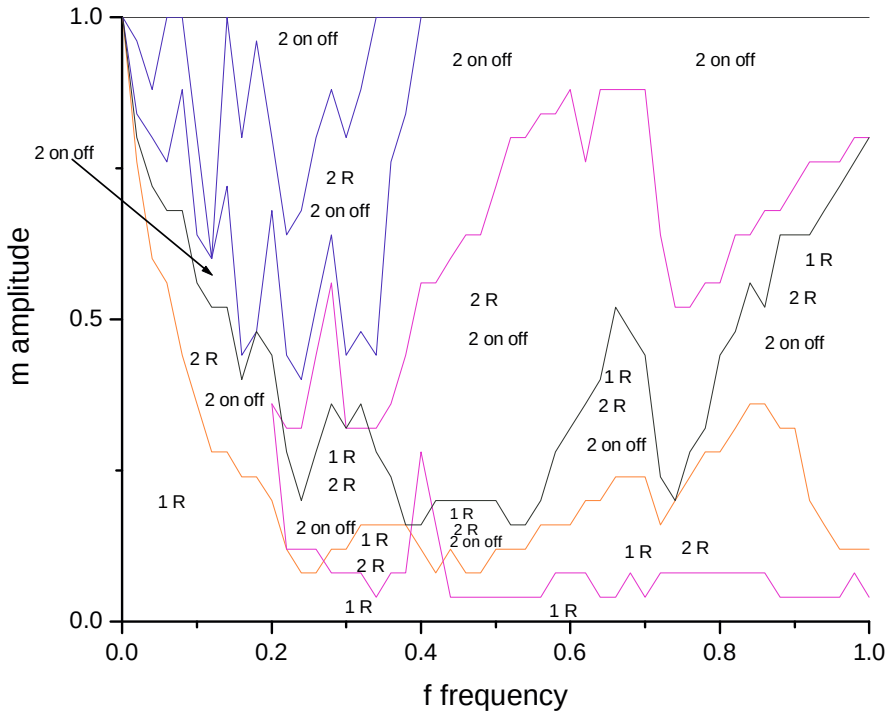

Figure 4.8: Codimentional-two bifurcation diagram in (m, f)parameter. Where 2 0n-0ff is two-state on-off intermittency, 1 R is the one-well period orbit, and 2 R is cross-well period orbit

Grebogi, and Yorke (OGY) idea of controlling chaos [75]. Specifically, they devised an algorithm for stabilizing a trajectory in the vicinity of a desirable ("off") state by using arbitrarily small feedback perturbations to a system parameter. Their close-loop control algorithm requires the knowledge of system equations. However, in many practical situations the detailed system equations are not available. For such a case, an open-loop control algorithm might be more realistic. Before OGY method, Lima and Pettini [76] proposed a nonfeedback perturbation technique for stabilizing a chaotic system towards a periodic state. This technique was applied experimentally for eliminating chaotic oscillations in a bistable magnetoelastic system [77] and for stabilizing periodic orbits in a laser [78].

In this work we study the possibility for controlling on-off intermittency by harmonic modulation applied to an accessible system parameter. Our method to confine a trajectory in the "off" state is base on Lima and Pettini's idea of the open-loop control of chaos. Similarly to Nagai, Hua, and Lai [65], we assume that the desirable operational state of the system is the "off" state and the "on" state is undesirable. That is, we wish to avoid temporal bursts ("on" states) of dynamical variables. As distinct from the closed-loop control, the open-loop control is not restricted to small perturbations. The modulation amplitude may be an arbitrarily large to achieve the control goal. However, the main advantage of this type of the control is that it does not require a prior knowledge of system equations and thus it may be useful for some kinds of practical applications. We also show how the control works at the presence of external noise of different levels.

4.3.1 System of Equations

The analysis is carried out on an example of two coupled double-well Duffing oscillators with random driving. Along with many other complex systems, the coupled Duffing oscillators exhibit coexistence of several attractors, some of them may be chaotic (intermittent), while the others are steady states. In such a situation, the control of intermittency may be manifested as annihilation of the intermittent attractors so that all trajectories are driven to the steady states. In our recent works [50] we showed that coexisting fixed points and limit cycles in multistable systems can be annihilated by harmonic parametric modulation. In this work we demonstrate how the annihilation effect is achieved with intermittent states in randomly driven Duffing oscillators.

We consider two identical oscillators modelled by Eqs.4.1-4.7

4.3.2 Control

A glimpse of the results is presented in Fig. 4.9 where we demonstrate the control effect on some of the coexisting attractors. The system, prior to the control, is in the chaotic state. When the control is switched on (at $t = 5000$), the intermittent attractors disappear and the trajectory is attracted to one of the remaining steady states. Note, that the external harmonic modulation creates a limit cycle around each fixed point so that the final state is a periodic orbit. When the modulation amplitude is applied but it is not sufficiently large to eliminate an intermittent attractor, the system exhibits the coexistence of five attractors. In addition to two limit cycles in the

vicinity of each potential well, two one-state and one two-state intermittency regimes coexist. In Figs. 4.9(b,c) we demonstrate how a sudden increase in m annihilates the intermittent states resulting in the periodic bistability.

The required modulation amplitude for the control depends on both the noise level and modulation frequency as shown in Fig. 4.10. In the presence of the parametric modulation Eq. (4.7), the intermittent attractors appear at the certain level of noise ($q > 1.9$ for $f = 0.01$) [Fig. 4.10(a)]. To eliminate these attractors, we need to apply the control modulation with m to be above some critical value m_c, i.e., above the bifurcation lines marked in Fig. 4.10. Note, that for relatively low noise ($1.9 < q < 3$), there are two critical values for the modulation amplitude, which correspond to the onset and offset of on-off intermittency. The two bifurcation lines in Fig. 4.10(a) are the good fits of the data to the exponential growth and decay with critical exponents of 1 and 0.25, respectively. As seen from Fig. 4.10(b), the intermittency attractors can be destroyed only by slow parametric modulation ($f < 0.05$) and when $m > m_c$. In the regime of on-off intermittency, a typical trajectory spends a long time near one invariant subspace (laminar phase) and when the modulation is fast, the system has no time to respond to the control. In the other words, the period of the modulation should be of the same order of magnitude as the characteristic time for which the trajectory spends near one invariant subspace before being repelled away. Of course, the duration of the laminar phase depends on the noise level. This suggests that the reason for the control effect is a resonant interaction of the modulation frequency

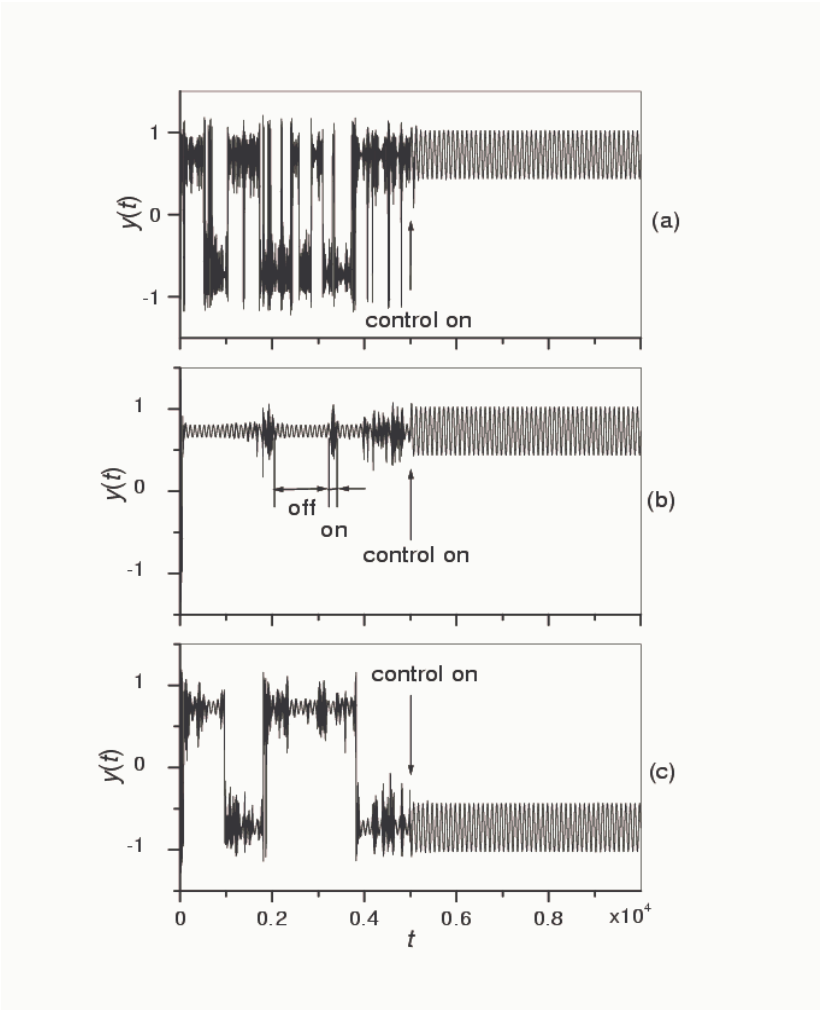

Figure 4.9: A slow parametric modulation leads to the disappearence of intermittency attractor. The initial system are (a) two-state on-off intermitency without modulation ($m = 0$), (b) one-state and (c) two-state on-off intermitency with small modulation ($m = 0.1$). The arrows indicate the moments when the control with $m = 0.4$ and $f = 0.01$ is applied. The trayectory is attract to the limit cycle in the vicinity of one of the potential wells.This demostrates the flexibility of the control to select different "off" states

with the frequency at which the trajectory repelled away from one of the invariant subspaces.

Taking into account the above speculations, the mean duration of the laminar phase is one of the important characteristics as for achieving the control goal as for characterization of the observed intermittent behavior in general. In Fig. 4.11 we plot in the log-log scale the mean duration of the laminar phase, $< \tau >$, as a function of both the relative difference of the modulation depth from its critical value $(m_c - m)/m_c$ [Fig. 4.11(a)] and the modulation frequency f. We find that in both cases these dependences obey the -1 scaling law that characterizes on-off intermittency. This result agrees well with other theoretical works where the control parameter was driven randomly [62] and with laser experiments where the parameter was modulated periodically [70].

4.4 Conclusion

The coexistence of multiple attractors has been observed in four dimensional flow subjected to parametric and/ or stochastic driving. Different coexisting attractors (one-wel and cross-well periodic orbits, one-state and two-state on-off intermittency) appear in different regions of the parameters space of the modulation frequency and amplitude. One-state on-off intermittency exists only in the presence of noise. With increasing the control parameter, the

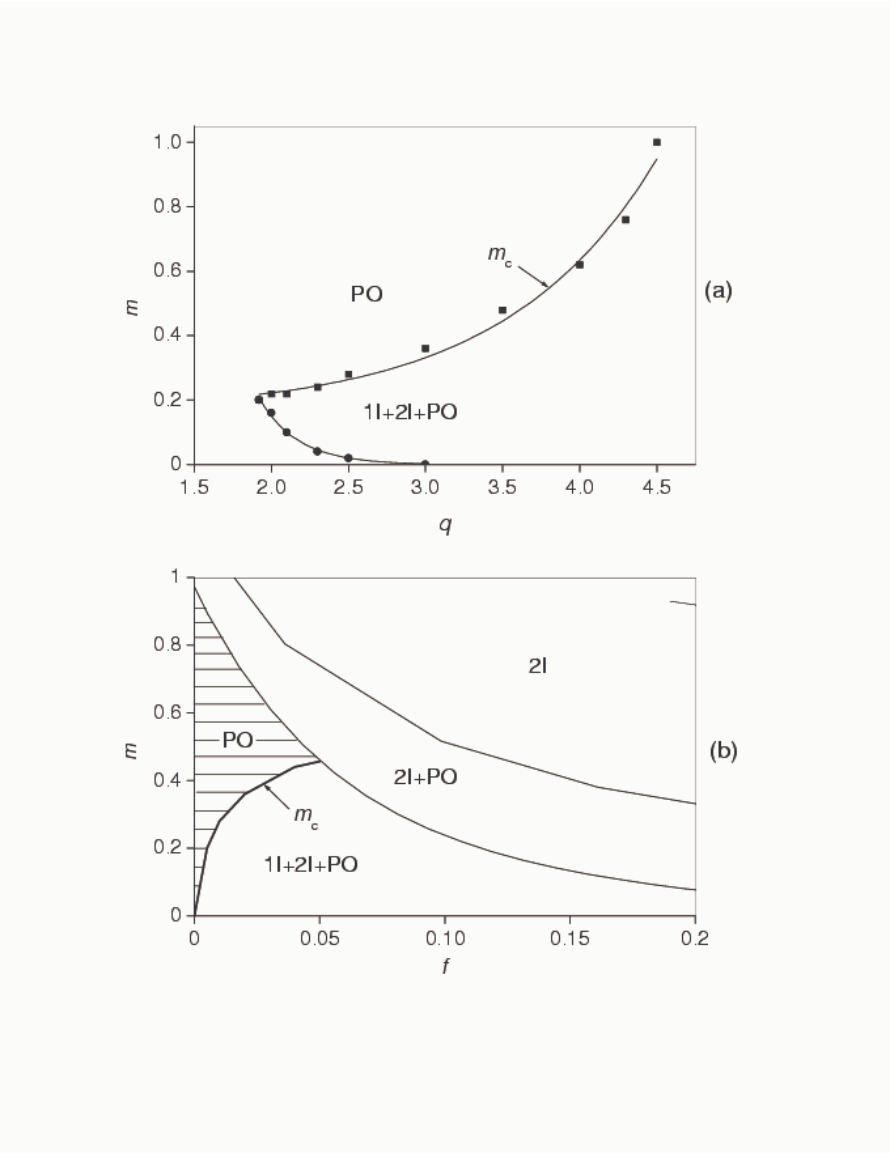

Figure 4.10: Codimentional-two bifurcation diagram in space of (a) noise level and modulation depth at $f = 0.01$ and (b) modulation frequency and depth at $q = 3$. The boundaries betwen different dynamic regimen, one-state (1I) and two-state (2I) intermittentency and peridic orbit (PO) are shown. The bifurcation lines for the onset of intermittency are indicated by the arrows. Only periodical regimes exist in the dashed region.

Figure 4.11: Avarege laminar length (a) versus relative difference of modulation depth from its critical value at $f = 0.01$, and (b) versus modulation frequency at $m = 0.14$ in log-log scales. $q = 2.5$. The fits of the data to straight lines are good, the slopes of which are -1.

duration of laminar phase for both one-state and two-state on-off intermittency decreases.

The possibility of the open-loop control of a chaotic dynamical system that exhibits on-off intermittency has been demonstrated. We have shown that a trajectory can be stabilized in the vicinity of a desired state ("off" state) by slow harmonic modulation applied to an available system parameter. We have derived the conditions for the modulation amplitude and frequency to achieve the control goal in the presence of noise of different levels. The scaling law with a critical exponent of -1 for the mean duration of the laminar phase versus both the modulation amplitude and frequency has been found. The coincidence of this scaling relation with other works verifies a universal character of this scaling relation for different types of driving and different types of on-off intermittency. The control can be easily realized in practice, because in the experimental situation the driving signal is well defined and hence the appropriate modulation parameters can be computed and applied to the system to eliminate intermittent attractors even without the knowledge of an adequate theoretical model.

Chapter 5

Laser Dynamic

Laser are usually classified according to the material that provides the optical amplification. This material determines largely the properties of laser: the mode of operation (pulse or continuous), the emission wavelength, the output power/ energy and the coherence properties. Gases, liquid , solid and doped fiber can provide optical amplification when properly excited.

The laser transition of the amplifying material may be homogeneously broadened, i.e. light of a certain optical frequency can interact with all atom/molecules, all of them having the same resonance frequency. The homogeneous line width $\Delta\nu_H$, is given by the medium relaxation rates:

$\gamma_\perp + \gamma_\parallel = \pi\Delta\nu_H$

where $\gamma_\perp$ and $\gamma_\parallel$ are the relaxation rates for inversion and polarization, respectively. In the inhomogeneous broadening case, the material consists of atoms/molecules of different resonance frequencies. Light of a particular optical frequency can then only interact with a fraction of the total number

atoms / molecules.

Lasers may be classified in still another way. Lasers operating in a single emission mode are described by the three equation for the three relevant variables: field, population and polarization. Usually decay on very different time scale, which is given by the relaxation rates κ (damping rate of the laser resonator), $\gamma_\perp$ and $\gamma_\parallel$. If one of theses is large compared with the others, the corresponding variable relax fast and consequently adiabatically adjusts to the other variables. The number of equations describing the laser is then reduced.

Those lasers for which the population and the polarization decay fast in comparison with the field have been name class A lasers, those for which only the polarization relaxes fast, class B lasers, and those for which all three relaxation rates are of same magnitude, class C lasers.

Laser equations for class A laser reduce to one. Therefore, only constant output solution exist. For the class B laser, oscillation of energy between field and inversion population is possible and the equations yield relaxation oscillations. Class C laser with their coupled dynamics of field, inversion and polarization can display undamped periodic or non-periodic (chaotic) pulsing.

Class B lasers can, however, show chaotic dynamic when they are external influenced (modulation of a parameter, injection of external light , feedback).

5.1 Dynamics of an Erbium-Doped Fiber Laser With Pump Modulation: Theory and Experiment

From the viewpoint of nonlinear dynamics, rare-doped fiber lasers with external modulation among with solid-state, semiconductor, and gas lasers with electric discharge (like CO_2 and CO lasers) belong to class-B lasers [79]. These are systems in which polarization is adiabatically eliminated and the dynamics can be ruled by two rate equations for field and population inversion. In spite of an impressive array of research on complex dynamics in lasers, nonlinear dynamics of Erbium Doper Fiber Lasers (EDFLs) was started to study only recently. The main features of the dynamical behavior of these lasers are very similar to those of other class-B lasers. Different scenario for development of a chaotic motion have been found in EDFLs. First, a period-doubling route to chaos has been observed by Lacot *et al.* [80] in a bipolarized two-mode EDFL with harmonic pump modulation of the krypton laser. The authors also developed a model based on two coherently pumped coupled lasers. Then, a quasi-periodic route to chaos has been found by Sanzhez *et al.* [81] in a dual-wavelength EDFL. Eventually, Luo *et al.* [82] have revealed the coexistent scenario of the period doubling and intermittency routes to chaos in a pump-modulated ring EDFL. They also reported on bistability (coexistence of two periodic attractors) in this laser [82, 83]. More recently, optical bistability (coexistence of a limit cycle and a

fixed point) has been detected by Mao and Lit [84] in the vicinity of the first laser threshold in a dual-wavelength EDFL with overlapping cavities. In our previous works, we have reported on coexistence of multiple periodic attractors (generalized multistability) found both theoretically and experimentally in EDFL subjected to loss [85] or pump modulation [18, 19]. There are also many works devoted to a study of a self-pulsation behavior of EDFL (see, for example, [86] and references therein). Such a behavior has been suggested to be due to the presence of a saturable absorber in the fiber in the form of ion pairs [87] or pump depletion [88], although these mechanisms are not necessary for explanation of this behavior. Small quasi-sinusoidal modulation of the laser intensity with a broaden frequency of relaxation oscillations appears in the power spectrum due to the presence of noise in a diode pump laser [89] and large self-pulsations can be explained by accounting for a thermo-lensing effect due to the excited state absorption [90]. These theoretical speculations describe well all experimentally observed self-pulsing features of EDFLs.

Only few works are devoted to a study of the nonlinear response of EDFL on parametric modulation. The dynamics of this laser were reported recently in the work of Sola *et al.* [86] and in our works [85, 18, 19]. Sola *et al.* studied the dynamics of a ring 1533-nm EDFL with sinusoidally modulated 1470-nm pump diode laser. They developed a rather complicated model [87] which describes well their experimental results. In our previous works we studied a linear 1560-nm EDFL pumped by a 967-nm laser diode. Such a laser is commonly used in many laboratories and serves for various applications. However, the spectroscopy of this laser is quite different from that of the

laser studied by Sola *et al.*, and hence their model cannot be used for our laser.

In this chapter, we study the dynamics of a 1560-nm EDFL with Fabry-Perot cavity subjected to harmonic pump modulation of the diode laser. We develop a novel simple model which can be used to describe such a laser and, as we will show below, perfectly addresses all laser peculiarities observed experimentally. We investigate theoretically the laser dynamics over a wide range of frequencies of pump modulation. Our model does not account for a saturable absorber phenomenon in a fiber and hence the self-pulsing behavior does not appear. This is stipulated by the following reasons. First, the pump power used in our experiments is too small to induce a thermo lens in the fiber, and second, the pump modulation amplitude is much larger than noise.

The chapter is organized as follows. In Section 5.1.1 we describe our model. In order to test the model, in Section 5.1.2 we simulate numerically the experiments reported in our previous works [18, 19] for the case when the modulation frequency is higher than the relaxation oscillation frequency of the laser. Then, in Section 5.1.3 we study numerically the laser dynamics in the low-frequency range, i.e. when the modulation frequency is smaller than the relaxation oscillation frequency. We demonstrate that the low-frequency range exhibits a rather interesting insight to EDFL dynamics with external modulation because of the appearance of many "fine" dynamical phenomena that become latent at higher modulation frequencies. In Sections 5.1.4, 5.1.5and 5.1.6 we describe the experimental setup of the diode-pumped EDFL with pump modulation and compare the results of simulations with exper-

iments. In the course of experiments, we determine directly the structure of frequency- and phase-locked states (with respect to pump modulation) through bifurcation diagrams in space of the modulation parameters. Finally, the main conclusions are given in Section 5.2

5.1.1 Laser Model

The model is based on the rate equations in which we use a power-balance approach applied to a longitudinally pumped EDFL, where the excited state absorption (ESA) in erbium at the 1.5- μm wavelength and the averaging of the population inversion along the pumped active fiber are accounted for. Such a model would address the two most evident factors, i.e., ESA at the laser wavelength (see Fig. 5.1) and the depleting of the pump wave at propagation along the active fiber. This model does not include mechanisms for a self-pulsing behavior of the laser because in our experiments the amplitude of self-pulsations is small (in 2-3 orders of magnitude) as compared with the amplitude of the laser response due to pump modulation, and hence this effect has no influence of the laser dynamics. The possible mechanisms for the self-pulsing behavior of EDFL (i.e., thermo-lensing effects and noisy pumping) are considered in other works [88, 89] where some modifications are made in the model.

The balance equations for the intra-cavity laser power P (being a sum of the powers of the contra-propagating waves inside the cavity, in s^{-1}) and the averaged (over the active fiber length) population y of the upper ("2")

level (being a dimensionless variable, $0 \leq y \leq 1$) have been derived to be as follows:

$$\frac{dP}{dt} = \frac{2L}{T_r} P \left\{ r_w \alpha_0 \left[y \left(\xi - \eta \right) - 1 \right] - \alpha_{th} \right\} + P_{sp}, \tag{5.1}$$

$$\frac{dy}{dt} = -\frac{\sigma_{12} r_w P}{\pi r_0^2} (y\xi - 1) - \frac{y}{\tau} + P_{pump}, \tag{5.2}$$

where $y = \frac{1}{n_0 L} \int\limits_0^L N_2(z) dz$, where N_2 is the population of the upper laser level "2", n_0 is the refractive index of a "cold" erbium-doped fiber core, and L is the active fiber length, σ_{12} is the cross-section of the absorption transition from the ground state "1" to the upper state "2". Here we suppose that the cross-section of the return stimulated transition is practically the same in magnitude [90] that yields $\xi = \frac{\sigma_{12} + \sigma_{21}}{\sigma_{12}} = 2$. $\eta = \frac{\sigma_{23}}{\sigma_{12}} = 0.4$ is the coefficient that stands for the ratio between ESA (σ_{23}) and ground-state absorption cross-sections at the laser wavelength, $T_r = \frac{2n_0}{c}(L + l_0)$ transition time around trip of a photon in the cavity, (l_0 being the intra-cavity tails of the fiber Bragg grating (FBG) couplers), $\alpha_0 = N_0 \sigma_{12}$ is the small-signal absorption of the erbium fiber at the laser wavelength ($N_0 = N_1 + N_2$ being the total concentration of erbium ions in the active fiber), $\alpha_{th} = \gamma_0 + \frac{1}{2L} \ln\left(\frac{1}{R}\right)$ is the intra-cavity losses on the threshold (γ_0 being the non-resonant fiber loss and R is the total reflection coefficient of the FBG couplers), τ is the lifetime of erbium ions in the excited state "2", r_0 is the fiber core radius, w_0 is the radius of the fundamental fiber mode, and $r_w = 1 - \exp\left[-2\left(\frac{r_0}{w_0}\right)^2\right]$ is the factor indicating a match between the laser fundamental mode and erbium-doped core volumes inside the active fiber. In Eq. (5.1), $P_{sp} =$

$\frac{10^{-3}y}{\tau T_r}\left(\frac{\lambda_g}{w_0}\right)^2 \frac{r_0^2\alpha_0 L}{4\pi^2\sigma_{12}}$ is the spontaneous emission into the fundamental laser mode. We assume here that the laser spectrum width is 10^{-3} of the erbium luminescence spectral bandwidth (λ_g being the laser wavelength). In Eq. (5.2), $P_{pump} = P_p \frac{1-\exp[-\beta\alpha_0 L(1-y)]}{N_0 \pi r_0^2 L}$ is the pump power, where P_p is the pump power at the fiber entrance (left-hand side in Fig. 5.5) and $\beta = \frac{\alpha_p}{\alpha_0}$ is the dimensionless coefficient that accounts for the ratio of absorption coefficients of the erbium fiber at pump wavelength λ_p (α_p) to that at laser wavelength λ_g (α_0). The system of Eqs. (5.1,5.2) describes the laser dynamics without an external modulation. In order to account for the harmonic pump modulation, one needs to write the pump power at the active fiber facet as

$$P_p^m = P_p \left[1 + m_0 \sin\left(2\pi F_m t\right)\right], \tag{5.3}$$

where m_0 and F_m are the modulation depth and frequency.

The calculations were performed for the experimental conditions described in Refs. [18, 19] and in Section 5. The following main parameters are used

L	n_0	l_0	T_r	r_0	w_0	$\sigma_{12} = \sigma_{21}$	σ_{23}	τ	γ_0	R
cm		cm	ns	cm	cm	cm^2	cm^2	s		
70	1.45	20	8.7	1.5×10^{-4}	3.5×10^{-4}	3×10^{-21}	0.9×10^{-21}	10^{-2}	0.038	0.8

The value of w_0 has been measured experimentally and it is a bit higher than the value 2.5×10^{-4} cm given by the formula for a step-index single-mode fiber $w_0 = r_0\left(0.65 + \frac{1.619}{V^{1.5}} + \frac{2.879}{V^6}\right)$, where the V- parameter is connected with numerical aperture NA and r_0 as $V = \frac{2\pi r_0}{\lambda_g} NA$; the values r_0 and w_0 result in $r_w = 0.308$. The coefficients characterizing the resonant-absorption properties of the erbium fiber at the laser and pump wavelengths are $\alpha_0 = 0.4$ cm^{-1}

and $\beta = 0.5$. These values correspond to direct measurements for the heavily doped fiber with erbium concentration of 2300 ppm. The values γ_0 and R yield $\alpha_{th} = 3.92 \times 10^{-2}$. The lasing wavelength is taken to be $\lambda_g = 1.56 \times 10^{-4}$ cm ($h\nu_g = 1.274 \times 10^{-19} J$), corresponding to the experiment, where the maximum reflection coefficients of both FBGs are centered on this wavelength. The parameters can be varied in the simulations: (1) the excess over the first laser threshold is defined as $\varepsilon = \frac{P_p}{P_{th}}$, where the threshold pump power $P_{th} = y_{th} \frac{N_0 L \pi w_p^2}{\tau} \left\{1 - \exp\left[-\alpha_0 L \beta \left(1 - y_{th}\right)\right]\right\}^{-1}$ and the threshold population of level "2" $y_{th} = \frac{1}{(\xi - \eta)} \left(1 + \frac{\alpha_{th}}{r_w \alpha_0}\right)$ with the radius of the pump beam being taken, for simplicity, the same as the radius of the lasing beam, i.e., $w_p = w_0$, and (2) the control parameters, i.e., the modulation frequency F_m and depth m_0.

The numerical calculations employing the system of Eqs. (5.1)-(5.3) allow us to obtain time series and bifurcation diagrams, characterizing the dynamics of the pump-modulated EDFL. The dynamics of a parametrically modulated EDFL [85, 18, 19], as well as other class-B lasers (see, for example, [79, 91] and references therein), is related to the main laser resonance which appears close to the relaxation oscillation frequency, f_0. The typical modeling results are presented in the next subsections. A rich variety of attractors arise in primary saddle-node bifurcations (SNBs). Depending on the modulation frequency, the laser response can contain either subharmonic or harmonic components of F_m. The laser dynamic depends on the modulation frequency. For the convenience, we consider two different ranges of F_m. At the high-frequency range ($F_m > f_0$), various SNBs give rise to subhar-

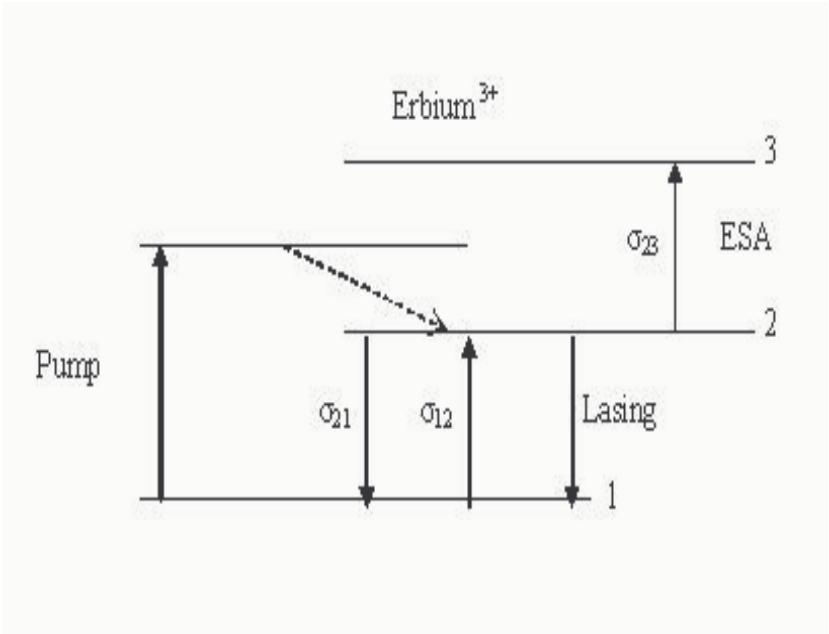

Figure 5.1: Energy level diagram of Erbium

monic laser oscillations, whereas at the relatively low modulation frequencies ($F_m < f_0$), the higher harmonics of F_m are involved in the laser dynamics. Recently, the dynamics of the pump-modulated EDFL in the high-frequency range has been investigated experimentally in Refs. [18, 19]. Therefore, in this work (see Section 5.1.2, 5.1.3) we present only theoretical results for this frequency range and compare with our previous experiments. The laser dynamics in the low-frequency range are studied in details both numerically and experimentally.

.

5.1.2 High-Frequency Range

In order to simulate the laser dynamics in the high-frequency range ($F_m > f_0$), we use the parameters close to the experimental ones taken from Refs. [18, 19]. The pump power is estimated as $P_p = 7.4 \times 10^{19}$ s^{-1}. For these parameters, we find the relaxation oscillation frequency of the laser $f_0 \approx 30$ kHz. The bifurcation diagrams of the peak-to-peak laser power with F_m as a control parameter for modulation depth $m_0 = 0.5(50\%)$ is shown in Fig. 5.2. These diagrams are constructed by taking different initial conditions for P and N that allows us to plot all coexisting stable solutions in the same diagram. It is seen from the figure, at high m_0 different subharmonic attractors, period 1 (P1), period 2 (P2), and period 3 (P3) born in the primary SNBs coexists within certain frequency range. The comparison of this diagram with the experimental one reported in Refs. [18, 19] gives a good agreement, even in details, between the experiment and the developed theoretical model. Note, that other models of EDFL, which do not address the contributions in laser dynamics stemming from the two mentioned features (ESA at the laser wavelength and the depleting of a pump wave within the active fiber) are not able to arrive such a perfect match with the experiment.

5.1.3 Low-Frequency Range

To study the laser dynamics in the low-frequency range ($F_m < f_0$) the pump power is chosen to be $P_p = 2.4 \times 10^{20}$ s^{-1}. This yields $f_0 \approx 50$ kHz. Depending

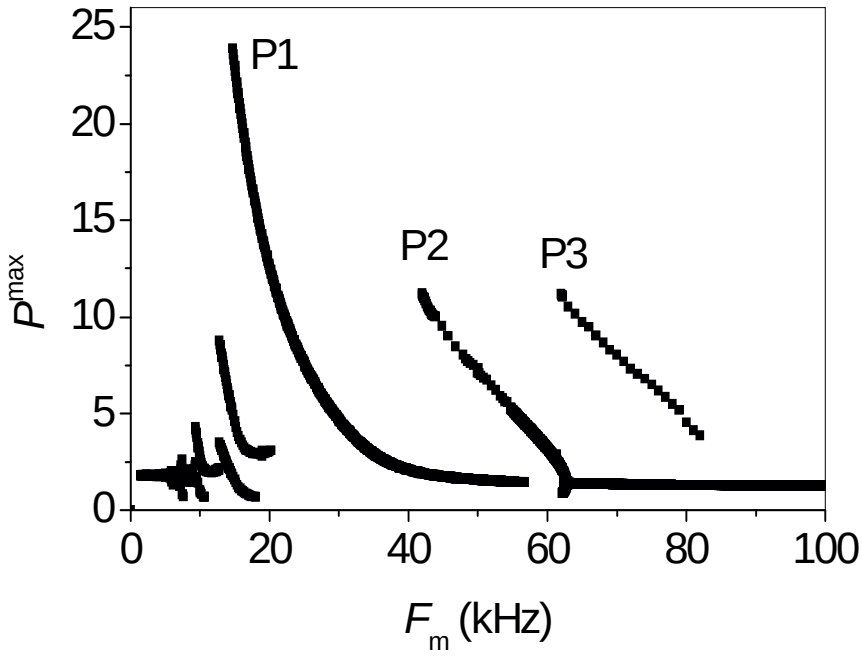

Figure 5.2: Numerical calculate bifurcation diagram of Peak-to-peak laser intensity with modulation frequency as a control parameter at 50% -depth modulation of pump laser diode current. The fundamental laser frequency f_0 is shown by the dotted line.

on initial conditions, the laser can oscillate in different periodic regimes with different number of pulses in the laser output with respect to the period of the pump modulation, e.g., 1:1, 2:1, 3:1, and so on. Within certain ranges of the modulation parameters, the laser displays generalized bistability, i.e., coexistence of two attractors.

Fig.5.3 shows the bifurcation diagram of the peak-to-peak laser intensity and phase difference $\Delta\phi$ between the pulses of the fiber laser and the diode pump laser versus the modulation frequency at the modulation depth = 50%. In Fig.5.3(a), some subdivisions of the coexisting attractors are marked (compare the regimes labeled with and without "star"). For instance, the subattractor (labeled as 2:1) is born as a continuous "degenerization" of the subattractor 1:1* via the appearance of its subharmonics. We plot, near each attractor branch, the corresponding time series which display the temporal dynamics in the chosen point of the parameter space. The labels (i runs from 1 to 6) indicate the associated saddle-node bifurcation points, where an attractor is born or dead. In Fig. 5.3(b) we shown the phase difference between the modulation signal from the pump laser and the output of fiber laser . One can see that the ranges of the phase and frequency locking are different for different branches of the bifurcation diagram; while for one of the coexisting periodic regimens the phase is locked to $\Delta\phi = 0$ for the other $\Delta\phi$ changes with F_m.

In Fig.5.4, we show the regions of different number of spikes in the laser response with codimensional two bifurcation diagram in the space of the

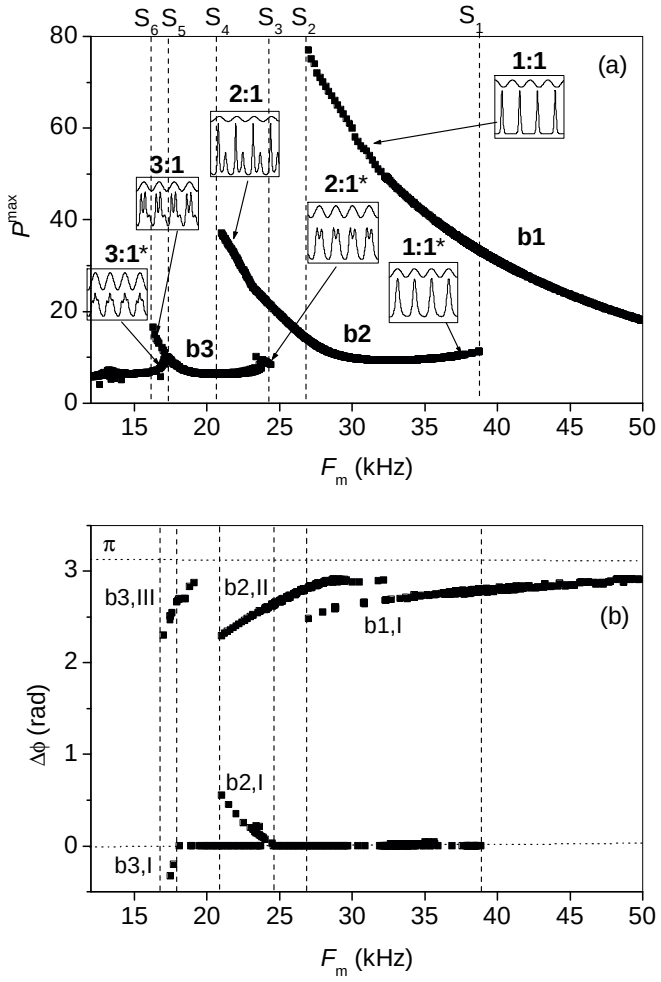

Figure 5.3: Peak-to-peak laser intensity and phase difference versus modulation frequency for $m = 0.5(50\%)$ b_1,b_2 and b_3 are the branches corresponding to diffenrent attractos. I, II and III denotte the first, second, and third spike in the laser reponse.

modulation amplitude and modulation frequency. The ration of the number of spikier *n:m* (winding number are always locked to the external modulation); P1 and P2 are the boundaries of the different frequency-locked regions. The cross-hatched regions indicate the bistable ranges with the same winding numbers, similar to Arnold' tongues [10], and the lines S1 - S6 are the saddle-node bifurcation lines where the attractors corresponding to different limit cycles are born and dead. Inside these regions, the two different regimes with the same periodicity coexist. In order to distinguish these regimes we make one of them by "stars".

5.1.4 Experimental setup

In our experiments, the erbium-doped fiber laser is pumped by a commercial laser diode (wavelength 976 nm, maximum pump power 300 mW) through a polarization controller (PC) (Fig. 5.5, [92]). The laser cavity of a 1.5-m length is formed by a piece of heavily doped erbium fiber of a 70-cm length and a core diameter of 2.7 μm, and two fiber Bragg gratings (FBG1 and FBG2) with a 2-nm FWHM (full width on half-magnitude) bandwidth and reflectivity of 91% and 95% at a 1560-nm wavelength. Output power of the pumping laser diode and fiber laser are recorded through a wavelength-division multiplexing coupler (WDM) and two photodetectors D1 and D2 and analyzed with an oscilloscope and a Fourier spectrum analyzer. The output power of the diode laser depends linearly on the laser diode current.

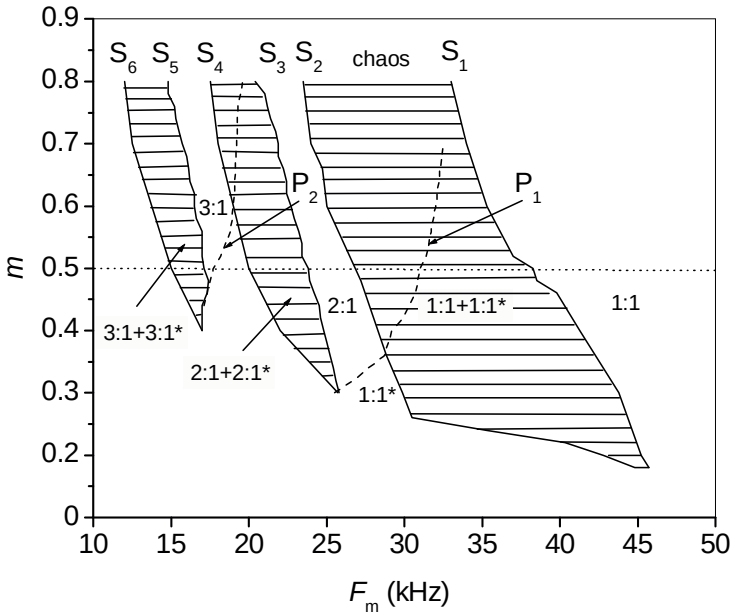

Figure 5.4: numerical codimentional-two bifurcation diagram in parameter space of modulation frequency and depth.

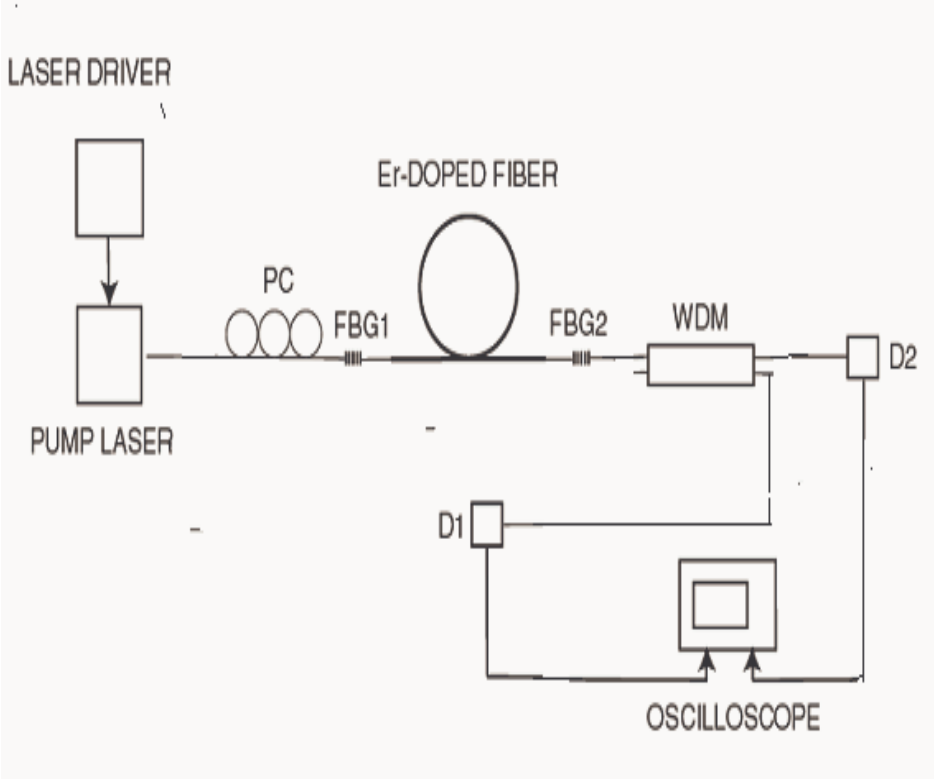

Figure 5.5: Experimental setup. WDM is the wavelength-divisor multiplexing coupler, PC is the polarization controler, FBG1 and FBG2 are the Bragg grating, and D1 and D2 are the photo-detector.

5.1.5 Experimental Results

Without any external modulation, the output power of the erbium-doped fiber laser represents self-oscillations at fundamental laser frequency f_0 (in our case $f_0 = 50$ kHz). Such a self-pulsing behavior is usually attributed to the presence of a saturable loss due to erbium ion pairs, excited state absorption, or pump depletion in the heavily doped fiber. The harmonic signal, $A_d \sin(2\pi f_d t)$ (where A_d and f_d are the driving amplitude and frequency), applied from a signal generator to the laser driver causes harmonic modulation of the diode current with f_d. In our experiments, the signal with $A_d = 800$ mV results in 50% modulation depth of the pump power, while the average diode current is fixed at 40 mA.

Without external modulation, the output of the laser represents self-spiking oscillations - either in the form of quasi-sinusoidal modulation (at the pump powers less than 40 mW), where a signal measured by the photodetector is weakly modulated (2-3% of the magnitude) at the relaxation frequency , or in the form of short pulses of sub-microsecond duration [92]. Note that such a self-pulsing behavior of the heavily doped Erbium fiber laser is usually attributed to some saturable losses inevitably presented in the fiber (ESA, pump depleting, etc.).

In this part we study only the case of low average pump powers, when the self-modulation of the laser output is observed, and of relatively low frequencies F_m of the pump modulation, when $F_m < f_0$. The relaxation oscillation frequency of our laser $f_0 = 50$ kHz (at the pump diode current of

40 mA).

The experimental bifurcation diagram of the peak-to-peak laser intensity versus the modulation depth at the modulation frequency $F_m = 30kHz$ is shown in Fig.5.6. One can see that bistability and even multistability (with an account of the central short branch 3:2) are observed in the laser under the pump modulation, i.e., two or three attractors (or limit cycles) may coexist in the system (like it occurs for a similar laser when the modulation frequency is higher than the fundamental laser frequency [6]). The insets of the experimental time series for each attractor clear up the different pulsed regimes of the laser (1:1, 3:2, and 2:1, from bottom to top).

Figure 5.7 shows the experimental bifurcation diagram of the peak-to-peak laser intensity versus the modulation frequency at the modulation depth = 50%. Within certain ranges of the modulation frequency, the laser displays generalized bistability, i.e., coexistence of two attractors. Depending on the initial conditions, the laser can oscillate in different periodic regimes with the same ratio of the number of pulses in the laser output and modulation signal (winding number), e.g., 1:1, 2:1 (compare with Fig.5.3), and 3:1, 4:1, and so on. In Fig.5.7, some subdivisions of the coexisting attractors are marked (compare the regimes labeled with and without "star"). For instance, the subattractor (labeled as 2:1) is born as a continuous "degenerization" of the subattractor 1:1* via the appearance of its subharmonics. Again, like in Fig.5.3, we plot, near each attractor branch, the corresponding time series which display the temporal dynamics in the chosen point of the parameter

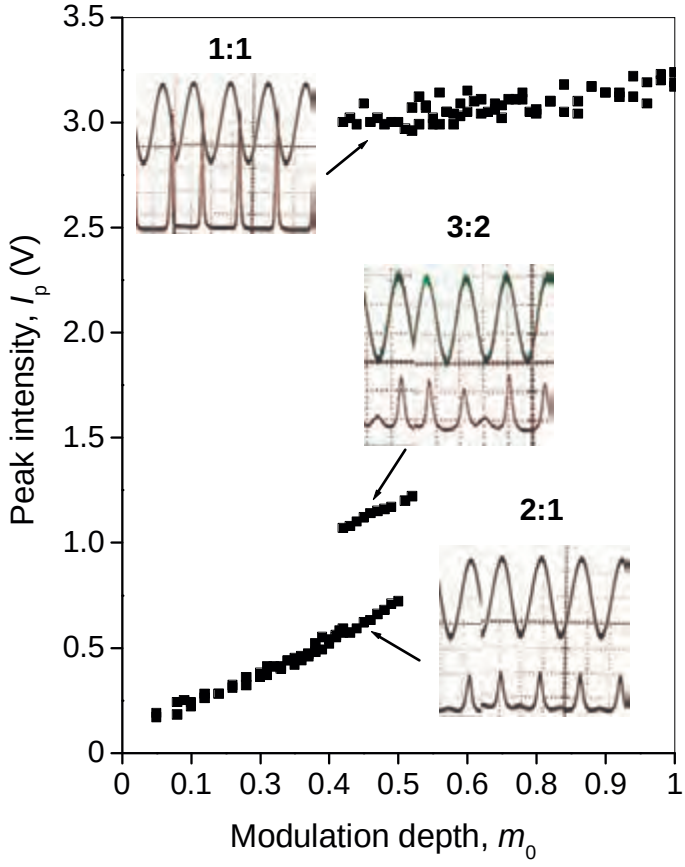

Figure 5.6: Experimental bifurcation diagram of laser peak intensity with modulation depth as a control parameter at $F_m = 30KHz$

space. The labels (i runs from 1 to 6) indicate the associated saddle-node bifurcation points, where an attractor is born or dead. In the Fig. 5.7 we also plot the phase difference between the modulation signal from the pump laser and the output of fiber laser . One can see that the ranges of the phase and frequency locking are different for different branches of the bifurcation diagram; while for one of the coexisting periodic regimens the phase is locked to $\Delta\phi = 0$ or π for other $\Delta\phi$ changes with f.

The experimentally measured frequency-locked regions are clearly seen from Fig.5.8(a) that is the codimensional-two bifurcation diagram in the space of the modulation amplitude and modulation frequency. Note that the horizontal and vertical dashed lines indicate, respectively, the values of modulation amplitude and modulation depth for which the diagrams in Fig.5.6 and Fig.5.7(a) are obtained. It is seen that frequency locking occurs everywhere at certain non-zero modulation depth because the Erbium fiber laser without external force acts as an autonomous oscillator; P1 and P2 are the boundaries of the different frequency-locked regions. The cross-hatched regions indicate the bistable ranges with the same winding numbers, i.e., the tongues like Arnold [10], and the lines S1 - S6 are the saddle-node bifurcation lines where the attractors corresponding to different limit cycles are born and dead. Inside these regions, the two different regimes with the same periodicity coexist. In order to distinguish these regimes they are marked (as in Fig.5.3,a) by "stars". Within the tongues, a period-doubling route to chaos occurs, whereas between the tongues a quasi-periodic route to chaos is

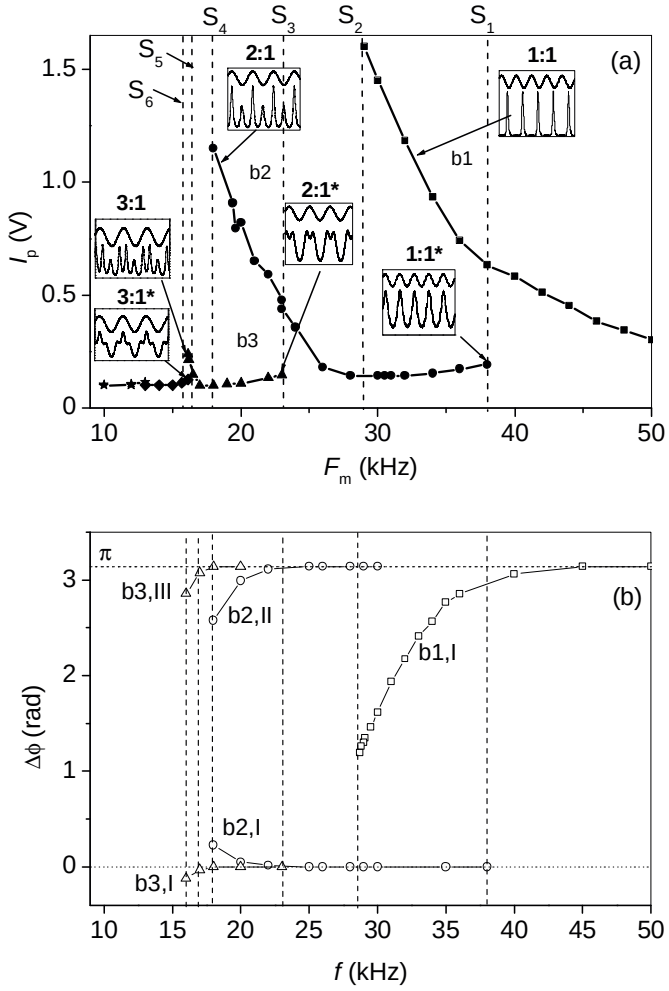

Figure 5.7: Peak-to-peak laser intensity and phase difference versus modulation frequency for $m = 0.5(50\%)$ b_1,b_2 and b_3 are the branches corresponding to different attractos. I, II and III denotte the first, second, and third spike in the laser response.

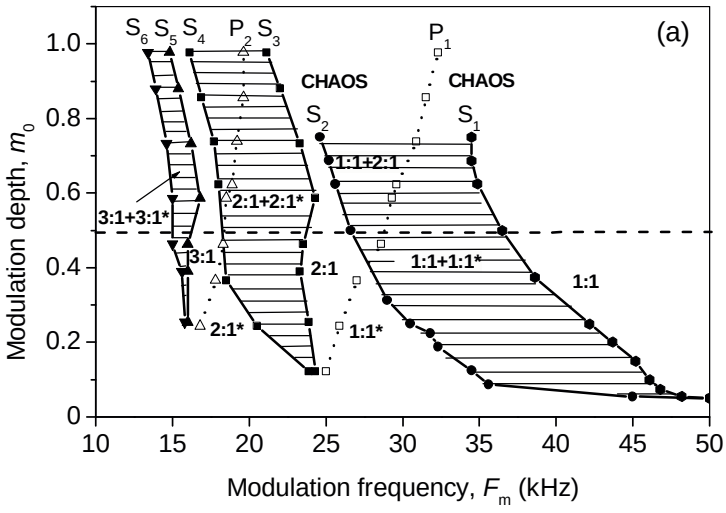

Figure 5.8: Experimental codimentional-two bifurcation diagram in parameter space of modulation frequency and depth.

registered.

5.2 Conclusions

In this chapter we have investigated in details nonlinear dynamics of a fiber laser subjected to harmonic modulation of a diode pump laser. Global analysis of bifurcation structure of phase space has been performed with the use of a simple theoretical model for an erbium-doped fiber laser. We also have demonstrated a rich variety of bifurcations and coexistence of multiple attractors that appear in the primary saddle-node bifurcations and discussed

their relation to main laser resonances.

We have analyzed, both experimentally and theoretically, the structure dynamic of the laser in the space of modulation parameters at frequencies lower and higher than the fundamental laser frequency. We have demonstrated that generalized bistability results in doubling the saddle-node bifurcation lines in the parameter space of the modulation frequency and amplitude. The laser modeling results have been shown to perfectly describe all the experimentally observed features. Therefore, we believe that our novel model of the Erbium laser may have a definite impact on future studies of more complicated rare-earth-doped fiber laser systems with essentially nonlinear dynamics.

Chapter 6

GENERAL CONCLUSION

In this word we have studied:

(i) Synchronization effects in nonautonomous systems and showed that at certain conditions, the regimes of *intermittent lag synchronization and oscillation death* appear in coupled oscillators with parametric modulation. Specifically, we considered two coupled double-well Duffing oscillators with harmonic modulation of a parameter in one of the oscillators.

(ii) We have developed the method of open-loop control of on-off intermittency in a stochastically driven system.

(iii) Dynamics of a 1560-nm erbium-doped fiber laser with Fabry-Perot cavity subjected to harmonic pump modulation of the diode laser. We developed a novel simple model of this laser, that describes perfectly all experimental features.

Chapter 7

APPENDIX

7.1 NORMALIZE THE SYSTEM OF EQUATIONS 5.1 and 5.2

$$\frac{dP}{dt} = \frac{2L}{T_r} P \left\{ r_w \alpha_0 \left[y \left(\xi - \eta \right) - 1 \right] - \alpha_{th} \right\} + P_{sp}, \tag{7.1}$$

$$\frac{dy}{dt} = -\frac{\sigma_{12} r_w P}{\pi r_0^2} (y\xi - 1) - \frac{y}{\tau} + P_{pump}, \tag{7.2}$$

where $P_{sp} = \frac{10^{-3} y}{\tau T_r} \left(\frac{\lambda_g}{w_0} \right)^2 \frac{r_0^2 \alpha_0 L}{4\pi^2 \sigma_{12}}$ and $P_{pump} = P_p \frac{1 - \exp[-\beta \alpha_0 L (1-y)]}{N_0 \pi r_0^2 L}$

Doing the following changes of variables

$P_{sp} = \frac{10^{-3} y}{\tau T_r} \left(\frac{\lambda_g}{w_0} \right)^2 \frac{r_0^2 \alpha_0 L}{4\pi^2 \sigma_{12}} = y\gamma$, where $\gamma = \frac{10^{-3}}{\tau T_r} \left(\frac{\lambda_g}{w_0} \right)^2 \frac{r_0^2 \alpha_0 L}{4\pi^2 \sigma_{12}}$

$(\xi - \eta) = \xi_1$, $\xi = \xi_2$ and $\tau = \tau_{sp}$

the system of equations 7.1 and 7.2 become

$$\frac{dP}{dt} = \frac{2L}{T_r} P r_w \alpha_0 \left[y\xi_1 - 1 \right] - \frac{2L}{T_r} \alpha_{th} P + y\gamma, \tag{7.3}$$

$$\frac{dy}{dt} = -\frac{\sigma_{12} r_w P}{\pi r_0^2} (y\xi_2 - 1) - \frac{y}{\tau_{sp}} + P_p \frac{1 - \exp\left[-\beta\alpha_0 L \left(1 - y\right)\right]}{N_0 \pi r_0^2 L}, \tag{7.4}$$

7.1.1 First Normalize

Doing the following in the eqn 7.3

$N_1 = r_w \left[y\xi_1 - 1 \right], \quad y = \frac{N_1 + r_w}{\xi_1 r_w}, \quad \frac{dy}{dt} = \frac{1}{\xi_1 r_w} \frac{dN_1}{dt}$

$\frac{dP}{dt} = \frac{2L}{T_r} \alpha_0 P N_1 - \frac{2L}{T_r} \alpha_{th} P + \frac{N_1 + r_w}{\xi_1 r_w} \gamma,$

doing $I = \frac{P}{\gamma}$ and $\theta = \frac{t}{\tau_{sp}}$

We have the following equation

$$\frac{dI}{d\theta} = 2L \left(\frac{\tau_{sp}}{T_r} \right) \alpha_0 I N_1 - 2L \left(\frac{\tau_{sp}}{T_r} \right) \alpha_{th} I + \left(\frac{\tau_{sp}}{\xi_1 r_w} \right) (N_1 + r_w). \tag{7.5}$$

For the eqn 7.4 with following change

$N_2 = r_w \left[y\xi_2 - 1 \right], \quad y = \frac{N_2 + r_w}{\xi_2 r_w}, \quad \frac{dy}{dt} = \frac{1}{\xi_2 r_w} \frac{dN_2}{dt}$

$\frac{dN_2}{dt} = -\left(\frac{\xi_2 r_w \sigma_{12}}{\pi r_0^2} \right) P N_2 - \frac{N_2 + r_w}{\tau_{sp}} + P_p \left(\frac{\xi_2 r_w}{N_0 \pi r_0^2 L} \right) \left\{ 1 - \exp\left[-\beta\alpha_0 L \left(1 - \frac{N_2 + r_w}{\xi_2 r_w} \right) \right] \right\}$

doing $I = \frac{P}{\gamma}$ and $\theta = \frac{t}{\tau_{sp}}$

We have the that equation 7.4 becomes

$$\frac{dN_2}{d\theta} = -\left(\frac{\tau_{sp}\xi_2 r_w \sigma_{12}}{\pi r_0^2}\gamma\right) IN_2 - (N_2 + r_w) + P_p\left(\frac{\tau_{sp}\xi_2 r_w}{N_0 \pi r_0^2 L}\right)\left\{1 - \exp\left[-\beta\alpha_0 L\left(1 - \frac{N_2 + r_w}{\xi_2 r_w}\right)\right]\right. \tag{7.6}$$

as $\frac{N_1 + r_w}{\xi_1 r_w} = \frac{N_2 + r_w}{\xi_2 r_w}$, $N_1 = \frac{\xi_1 N_2 + (\xi_1 - \xi_2) r_w}{\xi_2}$

for which the equation 7.5 becomes

$$\frac{dI}{d\theta} = 2L\left(\frac{\tau_{sp}}{T_r}\right)\left(\frac{\xi_1}{\xi_2}\right)\alpha_0 I N_2 - \left\{2L\left(\frac{\tau_{sp}}{T_r}\right)\left[\alpha_{th} - \frac{\alpha_0(\xi_1 - \xi_2)}{\xi_2} r_w\right]\right\} I + \left(\frac{\tau_{sp}}{\xi_2 r_w}\right)(N_2 + r_w) \tag{7.7}$$

The equations 7.6 and 7.7 can be write the following way

$$\frac{dI}{d\theta} = aIN_2 - bI + c(N_2 + r_w) \tag{7.8}$$

$$\frac{dN_2}{d\theta} = -dIN_2 - (N_2 + r_w) + e\left\{1 - \exp\left[-\beta\alpha_0 L\left(1 - \frac{N_2 + r_w}{\xi_2 r_w}\right)\right]\right\} \tag{7.9}$$

where

$a = 2L\left(\frac{\tau_{sp}}{T_r}\right)\left(\frac{\xi_1}{\xi_2}\right)\alpha_0 = 6.6207e + 007$

$b = \left\{2L\left(\frac{\tau_{sp}}{T_r}\right)\left[\alpha_{th} - \frac{\alpha_0(\xi_1-\xi_2)}{\xi_2}r_w\right]\right\} = 7.4151e+006$

$c = \left(\frac{\tau_{sp}}{\xi_2 r_w}\right) = 0.0163$

$d = \left(\frac{\tau_{sp}\xi_2 r_w \sigma_{12}}{\pi r_0^2}\gamma\right) = 4.0763e+003$

$e = P_p\left(\frac{\tau_{sp}\xi_2 r_w}{N_0 \pi r_0^2 L}\right) = 550$ for $F_m > f_0$

$e = 1750$ for $F_m < f_0$.

7.1.2 Second Normalize

We can write the Eqn. 7.8 the following way

$$\frac{dI}{d\theta} = aIN_2 - bI + cN_2 + cr_w \tag{7.10}$$

with $y_1 = aN_2$, $N_2 = \frac{y_1}{a}$ we have

$$\frac{dI}{d\theta} = Iy_1 - bI + \frac{c}{a}y_1 + cr_w \tag{7.11}$$

.

We can write the Eqn. 7.9 the following way

$$\frac{dN_2}{d\theta} = -dIN_2 - N_2 - r_w + e\left\{1 - e^{\left[-\beta\alpha_0 L\left(1-\frac{1}{\xi_2}\right)\right]}.e^{\left[\beta\alpha_0 L\frac{N_2}{\xi_2 r_w}\right]}\right\} \tag{7.12}$$

.

with $y_1 = aN_2$, $N_2 = \frac{y_1}{a}$ we have

$$\frac{dy_1}{d\theta} = -dIy_1 - y_1 - ar_w + ae\left\{1 - \exp\left[-\beta\alpha_0 L\left(1 - \frac{1}{\xi_2}\right)\right].\exp\left[\beta\alpha_0 L\frac{y_1}{a\xi_2 r_w}\right]\right\} \tag{7.13}$$

.

with $x = -dI$, $I = \frac{x}{-d}$ we have

$$\frac{dy_1}{d\theta} = xy_1 + (-1)y_1 + (-ar_w) + ae\left\{1 - \exp\left[-\beta\alpha_0 L\left(1 - \frac{1}{\xi_2}\right)\right].\exp\left[\beta\alpha_0 L\frac{y_1}{a\xi_2 r_w}\right]\right\} \tag{7.14}$$

Using $x = -dI$ and $I = \frac{x}{-d}$ in the Eqn 7.11 we have

$$\frac{dx}{d\theta} = xy_1 + (-b)x + \left(\frac{-dc}{a}\right)y_1 + (-dc)r_w \tag{7.15}$$

.

Doing the following

$a_1 = -b = -\left\{2L\left(\frac{\tau_{sp}}{T_r}\right)\left[\alpha_{th} - \frac{\alpha_0(\xi_1 - \xi_2)}{\xi_2}r_w\right]\right\} = -7.4151e + 006$

$a_2 = -\frac{dc}{a} = -\frac{\left(\frac{\tau_{sp}\xi_2 r_w \sigma_{12}}{\pi r_0^2}\gamma\right)\left(\frac{\tau_{sp}}{\xi_2 r_w}\right)}{2L\left(\frac{\tau_{sp}}{T_r}\right)\left(\frac{\xi_1}{\xi_2}\right)\alpha_0} = -1.0011e - 006$

$a_3 = -dcr_w = -\left(\frac{\tau_{sp}\xi_2 r_w \sigma_{12}}{\pi r_0^2}\gamma\right)\left(\frac{\tau_{sp}}{\xi_2 r_w}\right)r_w = -20.3813$

$b_1 = -1$

$b_2 = -ar_w = -2L\left(\frac{\tau_{sp}}{T_r}\right)\left(\frac{\xi_1}{\xi_2}\right)\alpha_0 r_w = -2.0359e + 007$

$b_3 = -\exp\left[-\beta\alpha_0 L\left(1 - \frac{1}{\xi_2}\right)\right] = -1.2341e - 004$

$b_4 = \frac{\beta\alpha_0 L}{a\xi_2 r_w} = -4.4207e - 007$

$P_m = ae = 2L\left(\frac{\tau_{sp}}{T_r}\right)\left(\frac{\xi_1}{\xi_2}\right)\alpha_0\left(\frac{\tau_{sp}\xi_2 r_w}{N_0\pi r_0^2 L}\right)P_p$, where $P_p = P_0(1 - m\sin 2\pi ft)$

for $F_m > f_0 \quad P_m = (3.6414e + 010) * (1 - m\sin 2\pi ft)$

for $F_m < f_0$. $P_m = (1.1586e + 011) \ *(1 - m \sin 2\pi ft)$

Then we can write the Eqs. 7.15 and 7.14 the following way

$$\frac{dx}{d\theta} = xy_1 + a_1x + a_2y_1 + a_3 \tag{7.16}$$

$$\frac{dy_1}{d\theta} = xy_1 + b_1y_1 + b_2 + P_m \left\{1 + b_3.e^{b_4y_1}\right\} \tag{7.17}$$

7.1.3 Third Normalize

Using the following $z = b_4y_1$, $y_1 = \frac{z}{b_4}$ in the Eqs. 7.16 and 7.17 we have

$$\frac{dx}{d\theta} = x\frac{z}{b_4} + a_1x + a_2\frac{z}{b_4} + a_3 \tag{7.18}$$

$$\frac{dz}{d\theta} = xz + b_1z + b_2b_4 + b_4P_m \left\{1 + b_3.e^z\right\} \tag{7.19}$$

Doing $x_1 = \frac{x}{b_4}$, $x = b_4x_1$ and $\theta_1 = \frac{\theta}{b_4}$, $\theta = b_4\theta_1$ in the Eqs. 7.18 and 7.19 we have

$$\frac{dx_1}{d\theta_1} = x_1z + a_1b_4x_1 + \frac{a_2}{b_4}z + a_3 \tag{7.20}$$

$$\frac{dz}{d\theta_1} = x_1z + \frac{b_1}{b_4}z + b_2 + P_m \left\{1 + b_3.e^z\right\} \tag{7.21}$$

using the following change

$A_1 = a_1b_4 = -\left\{2L\left(\frac{\tau_{sp}}{T_r}\right)\left[\alpha_{th} - \frac{\alpha_0(\xi_1 - \xi_2)}{\xi_2}r_w\right]\right\} * (\frac{\beta\alpha_0 L}{a\xi_2 r_w}) = -3.2780$

$$A_2 = \frac{a_2}{b_4} = \frac{-\frac{\left(\frac{\tau_{sp}\xi_2 r_w \sigma_{12}}{\pi r_0^2}\gamma\right)\left(\frac{\tau_{sp}}{\xi_2 r_w}\right)}{2L\left(\frac{\tau_{sp}}{T_r}\right)\left(\frac{\xi_1}{\xi_2}\right)\alpha_0}}{\left(\frac{\beta\alpha_0 L}{a\xi_2 r_w}\right)} = -2.2646$$

$$A_3 = a_3 = -\left(\frac{\tau_{sp}\xi_2 r_w \sigma_{12}}{\pi r_0^2}\gamma\right)\left(\frac{\tau_{sp}}{\xi_2 r_w}\right) r_w = -20.3813$$

$$B_1 = \frac{b_1}{b_4} = \frac{-1}{\left(\frac{\beta\alpha_0 L}{a\xi_2 r_w}\right)} = -2.2621e+006$$

$$B_2 = b_2 = -2L\left(\frac{\tau_{sp}}{T_r}\right)\left(\frac{\xi_1}{\xi_2}\right)\alpha_0 r_w = -2.0359e+007$$

$$B_3 = b_3 = -\exp\left[-\beta\alpha_0 L\left(1-\frac{1}{\xi_2}\right)\right] = -1.2341e-004$$

$P_m = ae = 2L\left(\frac{\tau_{sp}}{T_r}\right)\left(\frac{\xi_1}{\xi_2}\right)\alpha_0\left(\frac{\tau_{sp}\xi_2 r_w}{N_0\pi r_0^2 L}\right)P_p$, where $P_p = P_0(1 - m\sin 2\pi f t)$

for $F_m > f_0$ $\quad P_m = (3.6414e+010) * (1 - m\sin 2\pi f t)$

for $F_m < f_0$. $\quad P_m = (1.1586e+011) \ *(1 - m\sin 2\pi f t)$

$$\frac{dx_1}{d\theta_1} = x_1 z + A_1 x_1 + A_2 z + A_3 \tag{7.22}$$

$$\frac{dz}{d\theta_1} = x_1 z + B_1 z + B_2 + P_m\left\{1 + B_3.e^z\right\} \tag{7.23}$$

Remember that :

$x_1 = \frac{x}{b_4} = \frac{-dI}{b_4} = \frac{-d}{\gamma b_4}P = \frac{-\left(\frac{\tau_{sp}\xi_2 r_w \sigma_{12}}{\pi r_0^2}\gamma\right)}{\gamma b_4}P = \frac{-\left(\frac{\tau_{sp}\xi_2 r_w \sigma_{12}}{\pi r_0^2}\right)}{\frac{\beta\alpha_0 L}{a\xi_2 r_w}}P = A.P =$
$-(5.9044e-010) * P$

$z = b_4 y_1 = b_4 a N_2 = b_4 a r_w\left[y\xi_2 - 1\right] = \left(\frac{\beta\alpha_0 L}{a\xi_2 r_w}\right)\left\{2L\left(\frac{\tau_{sp}}{T_r}\right)\left(\frac{\xi_1}{\xi_2}\right)\alpha_0\right\} r_w\left[y\xi_2 - 1\right] =$

$z = B.\left[y\xi_2 - 1\right] = (8.9999) * [2y - 1]$

$\theta_1 = \frac{\theta}{b_4} = \frac{t}{b_4\tau_{sp}} = \frac{t}{\left(\frac{\beta\alpha_0 L}{a\xi_2 r_w}\right)\tau_{sp}}. = C.t = (2.2621e+008) * t$

where the coefficient are:

$A = -\frac{\left(\frac{\tau_{sp}\xi_2 r_w \sigma_{12}}{\pi r_0^2}\right)}{\frac{\beta\alpha_0 L}{a\xi_2 r_w}} = 5.9044e-010$

$$B = (\frac{\beta\alpha_0 L}{a\xi_2 r_w}) \left\{ 2L \left(\frac{\tau_{sp}}{T_r} \right) \left(\frac{\xi_1}{\xi_2} \right) \alpha_0 \right\} r_w = 8.9999$$

$$C = \frac{1}{(\frac{\beta\alpha_0 L}{a\xi_2 r_w})\tau_{sp}} = 2.2621e + 008$$

Bibliography

[1] Chaos and Nonlinear Dynamics, edited by R.C. Hilborn and N.B. Tufillaro (American Association of Physics Teachers, College Park, Maryland, 1999).

[2] Chaos for Engineers, Theory, 2nd ed., Tomas Kaptaniak (Springer-Verlag Berlin Heidelberg 2000, Printed in Germany).

[3] Nonlinear Dynamic in Physiology and Medicine, edited by Anne Beuter, Leon Glass, Michael C. Mackey, Michele S. Tit combe,(Springer-Verlag New York , Inc., 2003).

[4] A. Pikovsky, M. Rosenblum, J. Kurths, Synchronization: A Universal Concept in Nonlinear Science, Cambridge University Press, New York, 2001.

[5] G. Duffing, Erzwungene Schwingungen bei Veränderlicher Eigen Frequenz und ihre Techische Bedeutung (View, Brauschweig, 1918).

[6] J.M.T. Thompson and H.B. Steward, Nonlinear dynamic and Chaos (John-Wiley, Singapore,1988).

[7] F.C.Moon, Chaotic and Fractal Dynamic (John-Wiley, New York,1992).

[8] H.G. Schuster, Deterministic Chaos: An Introduction (Physik-Verlag, Weinheim, 1988).

[9] J. Guckenhimer and P. Holmes, Nonlinear Oscillations, Dynamic System and Bifurcations of Vector Fields , (Springer-Verlag, New York,1983)).

[10] Y.H. Kao, J.C. Huang, Y.S. Gou, Phys. Rev. A 35 (1987) 5228.

[11] Y. Ueda, Nonlinear Science 2, (1992) 1.

[12] F.C.Moon and P. J. Holmes, J. Sound & Vib. 65, (1979), 275.

[13] P.J.Holmes, Philos. Trans. R. Soc. London 292,419 (1979); F.C.Moon, Phys. Rev. Lett. **53** 962 (1984); F.C. Moon and G.-X. Li, ibid. **55,**1439,(1985).

[14] W. Szemplinska-Stupnicka and J. Rudowksi,Chaos 3 (1993) 375.

[15] E. Kreuzer, M. Kleczka and S. Schaub, Chaos Solitons & Fractals 1, (199).

[16] M. Digonnet, ed., *Rare Earth Doped Fiber Lasers and Amplifiers* (Marcel Dekker, New York, 1993).

[17] L. G. Luo and P. L. Chu, "Optical secure communications with chaotic erbium-doped fiber lasers," *J. Opt. Soc. Am. B*, vol. 15, pp. 2524-2530, 1998.

[18] A. N. Pisarchik, Yu. O. Barmenkov, and A. V. Kir'yanov, "Experimental characterization of bifurcation structure in an erbium-doped fiber laser with pump modulation," *IEEE J. Quantum. Electron.*, vol. 39, pp. 1567-1571, 2003.

[19] A. N. Pisarchik, Yu. O. Barmenkov, and A. V. Kir'yanov, "Experimental demonstration of attractor annihilation in a multistable fiber laser," *Phys. Rev. E*, vol. 68, pp. 066211-1/8, 2003.

[20] Newhouse, S., Ruller, D. and Takens, F. (1978), Occurence of strange axiom attractor near quasiperiodic on $T^m, m > 3$, Commun. Math. Phys., 64, 35-40.

[21] B. R. Andrievskii and A. L. Fradkov, Control Chaos: Methods Applicaations., Automation and Remote Control, Vol. 64, No. 5, 2003.

[22] Daniel J. Gautheir, Resouce Letter: CC-1 : Controlling Chaos, Am. J. Phys. 71 (8), August 2003.

[23] Controlling Chaos," E. Ott, C. Grebogi, and J.A. Yorke, Phys. Rev. Lett. 64, 1196-1199 (1990).

[24] Modern Control Engineering, 2nd Ed., K. Ogata (Prentice-Hall, Englewood Cliffs, NJ, 1990), Chap. 9

[25] H. Fujisaka, T. Yamada, Prog. Theor. Phys. 69 (1983) 32.

[26] M.G. Rosenblum, A.S. Pikovsky, J. Kurths, Phys. Rev. Lett. 76 (1996) 1804.

[27] M.G. Rosenblum, A.S. Pikovsky, J. Kurths, Phys. Rev. Lett. 78 (1997) 4193.

[28] N.F. Rulkov, M.M. Sushchik, L.S. Tsimring, H.D.I. Abarbanel, Phys. Rev. E 51 (1995) 980.

[29] R. Femat, G. Solis-Perales, Phys. Lett. A 262 (1999) 50.

[30] K. Bar-Eli, Physica (Amsterdam) 14D (1985) 242.

[31] D.G. Aronson, G.B. Ermentrout, N. Kopell, Physica (Amsterdam) 41D (1990) 403.

[32] D.V. Ramana Reddy, A. Sen, G.L. Johnston, Phys. Rev. Lett. 80 (1998) 5109.

[33] M. Yoshimoto, K. Yoshikawa, Y. Mori, Phys. Rev. E 47 (1993) 864.

[34] R. Herrero, M. Figueras, J. Rius, F. Pi, G. Orriols, Phys. Rev. Lett. 84 (2000) 5312.

[35] M. Crowley, I. Epstein, J. Phys. Chem. 93 (1989) 2496.

[36] S.H. Strogatz, Nature (London) 394 (1998) 316.

[37] J. Rayleigh, The Theory of Sound, Dover Publishers, New York, 1945.

[38] E.V. Appleton, Proc. Cambridge Phil. Soc. (Math. and Phys. Sci.) 21 (1922) 231.

[39] T. Kapitaniak, Phys. Rev. E 47 (1993) R2975.

[40] P.S. Landa, M.G. Rosenblum, Appl. Mech. Rev. 46 (1993) 141.

[41] J. Kozłowski, U. Parlitz, W. Lauterborn, Phys. Rev. E 51 (1995) 1861.

[42] H.-W. Yin, J.-H. Dai, H.-J. Zhang, Phys. Rev. E 58 (1998) 5683.

[43] S. Paul Raj, S. Rajasekar, K. Murali, Phys. Lett. A 264 (1999) 283.

[44] A.N. Pisarchik, Phys. Lett. A 242 (1998) 152.

[45] A. N. Pisarchik and R. Corbalán, "Shift of attractor boundaries in a system with a slow harmonic parameter perturbation," Physica D **150**, 14-24 (2001).

[46] J.M. Saucedo-Solorio, A.N. Pisarchik, V. Aboites, Phys. Lett. A 304 (2002) 21.

[47] H.G. Davies, K. Rangavajhula, Proc. Royal Society (London) A 457 (2001) 2965.

[48] H.G. Davies, K. Rangavajhula, Chaos, Solitons and Fractals 14 (2002) 293.

[49] A. N. Pisarchik, Phys. Lett. A (submitted).

[50] A. N. Pisarchik, and B. K. Goswami, "Annihilation of one of the coexisting attractors in a bistable system," Phys. Rev. Lett. **84**, 1423-1426 (2000).

[51] A.N. Pisarchik, Phys. Rev. E 64 (2001) 046203.

[52] S. Boccaletti, D.L. Valladeres, Phys. Rev. E 62 (2000) 7497.

[53] A. Pikovsky, M. Rosenblum, J. Kurths, Synchronization: A Universal Concept in Nonlinear Science, Cambridge University Press, New York, 2001.

[54] U. Parlitz, Int. J. Bifurcat. Chaos 3 (1992) 703.

[55] E.A. Spiedel, Ann. NY Acad. Sci. 617 (1981) 305.

[56] B.F. Kuntsevich, A.N. Pisarchik, Phys. Rev. E 64 (2001) 046221.

[57] Y. Pomeau and P. Manneville, Phys. Lett. A **75**, 1 (1979).

[58] H. Fujisaka, H. Kamifukumoto, and M. Inoue, Prog. Theor. Phys. **69**, 333 (1982).

[59] E. Ott, *Chaos in Dynamical Systems* (Cambridge University Press, Cambridge, 1993).

[60] N. Platt, E.A. Spiegel, C. Tresser, Phys. Rev. Lett. 70 (1993) 279.

[61] H. Fujisaka, T. Yamada, Prog. Theor. Phys. 74 (1985) 918.

[62] J. F. Heagy, N. Platt, and S. M. Hammel, Phys. Rev. E **49**, 1140 (1994).

[63] C. Toniolo, A. Provenzale, and E. A. Spiegel, Phys. Rev. E **66**, 066209 (2002).

[64] Y.-C. Lai and C. Grebogi, Phys. Rev. E **52**,R3313 (1995).

[65] Y. Nagai, X.-D. Hua, and Y.-C. Lai, Phys. Rev. E **54**,1190 (1996).

[66] T. Yamada, K. Fukushima, and T. Yazaki, Prog. Theor: Phys. Suppl. **99**, 120 (1989); P. W.Hammer, N. Platt, S. M. Hammel, J. F. Heagy, and B. D. Lee, Phys. Rev. Lett. **73**, 1095 (1994).

[67] D. L. Feng, C. X. Yu, J. L. Xie, and W. X. Ding, Phys. Rev. E **58**, 3678 (1998).

[68] F. Rödelsperger, A. Cenys, and H. Benner, Phys. Rev. Lett. **75**, 2594 (1995).

[69] T. John, R. Stannarius, and U. Behn, Phys. Rev. Lett. **83**, 749 (1999).

[70] A. N. Pisarchik and V. J. Pinto-Robledo, Phys Rev. E **66**,027203 (2002).

[71] Y.Nagai, X. Dong and Y. Lai.Phys Rev. E 54 (1996) 1190.

[72] P.W.Hammer, N.Platt, S. M. Hammel, J.F. Heagy and B. D. Lee, Phys. Rev. Lett. 73 (1994) 1095.

[73] A.N. Pisarchik and V.J.Pinto-Robledo,Phys Rev. E 66 (2002) 027203-1.

[74] R. Jaimes and A.N. Pisarchik,Phys Rev. E 69 (2004) 067203.

[75] E. Ott, C. Grebogi, and J. A. Yorke, Phys. Rev. Lett. **64**, 1196 (1990).

[76] R. Lima and M. Pettini, Phys. Rev. A **41**, 726 (1990).

[77] L. Fronzoni, M. Giocondo, and M. Pettini, Phys. Rev. A **43**, 6483 (1991).

[78] A. N. Pisarchik, V. N. Chizhevsky, R. Corbalán, and R. Vilaseca, Phys. Rev. E **55**, 2455 (1997); A. N. Pisarchik, B. F. Kuntsevich, and R. Corbalán, *ibid.* **57**, 4046 (1998).

[79] F. T. Arecchi, in *Instabilities and Chaos in Quantum Optics*, F. T. Arecchi and R. G. Harrison, eds., Vol. 34 of Springer Series on Synergetics (Springer, Berlin, 1987), pp. 9-48.

[80] E. Lacot, F. Stoeckel, and M. Chenevier, "Dynamics of an erbium-doped fiber laser," *Phys. Rev. A*, vol. 49, pp. 3997-4008, 1994.

[81] F. Sanchez, M. LeFlohic, G. M. Stephan, P. LeBoudec, and P.-L- Francois, "Quasi-periodic route to chaos in erbium-doped fiber laser," *IEEE J. Quantum Electron.*, vol. 31, pp. 481-488, 1995.

[82] L. Luo, T. J. Tee, and P. I. Chu, "Chaotic behavior in erbium-doped fiber-ring lasers," *J. Opt. Soc. Am. B*, vol. 15, pp. 972-978, 1998.

[83] L. Luo, T. J. Tee, and P. L. Chu, "Bistability of erbium-doped fiber laser," *Opt. Commun.*, vol. 146, pp. 151-157, 1998.

[84] Q. Mao and J. W. Y. Lit, "Optical bistability in an *L*-band dual-wavelength erbium-doped fiber laser with overlapping cavities," *IEEE J. Quantum Electron.*, vol. 14, pp. 1252-1254, 2002.

[85] J. M. Saucedo-Solorio, A. N. Pisarchik, A. V. Kir'yanov, and V. Aboites, "Generalized multistability in a fiber laser with modulated losses," *J. Opt. Soc. Am. B*, vol. 20, pp. 490-496, 2003.

[86] I. J. Sola, J. C. Martín, and J. M. Álvarez, "Nonlinear response of a unidirectional erbium-doped fiber ring laser to a sinusoidally modulated pump power," *Opt. Commun.*, vol. 212, pp. 359-369, 2002.

[87] I. J. Sola, J. C. Martín, J. M. Álvarez, and S. Jarabo, "Erbium doped fiber characterisation by laser transient behaviour analysis," *opt. Commun.*, vol. 193, pp. 133-140, 2001.

[88] A.V. Kiryanov, N.N. Ilichev, and Yu.O. Barmenkov, ´´ Excited-state absorption as a source of nonlinear thermo-induced lensing and self-Q-switching in an all-fiber Erbium laser" Laser Phys. Lett. 1, No. 4, 194198

[89] A. N. Pisarchik, A. V. Kir'yanov, Yu. O. Barmenkov, and R. Jaimes, to be published.

[90] E. Desurvire, *Erbium-doped fiber amplifier - Principles and applications* (Wiley & Sons, New-York - Chichester - Brisbane - Toronto - Singapore, 1994).

[91] C. O. Weiss and R. Vilaseca, *Dynamics of Lasers* (VCH, Weinheim, 1991).

[92] R.Jaimes ,A.V. Kiryanov, A.N. Pisarchik,, and Yu.O. Barmenkov,N.N. Ilichev (submitted).

[93] V. N. Chizhevsky, "Coexisting attractors in a CO_2 laser with modulated losses," J. Optics B: Quantum and Semiclass. Optics **2**, 711-717 (2000).

[94] A. N. Pisarchik and B. K. Goswami, Phys. Rev. Lett. **84**, 1423 (2000); A. N. Pisarchik, Phys. Rev. E **64**, 046203 (2001); A. N. Pisarchik, Yu. O. Barmenkov, and A. V. Kir'yanov, *ibid.* **68**, 066211 (2003).

[95] E. Brun, B. Derighetti, D. Meier, R. Holzner, and M. Ravani, "Observation of order and chaos in a nuclear spin-flip laser," J. Opt. Soc. Am. B **2**, 156-167 (1985).

[96] A. Uchida, T. Sato, and F. Kannari, "Suppression of chaotic oscillations in a microchip laser by injection of a new orbit into chaotic attractor," Optics Letters **23**, 460-462 (1998).

[97] A. Gavrielides, V. Kovanis, P. M. Varangis, T. Erneux, and G. Lythe, "Coexisting periodic attractors in injection locked diode lasers," Quantum Semiclass. Opt. **9**, 785-796 (1997).

[98] A. V. Kir'yanov, V. N. Filipov, and A. N. Starodumov, "Cw-pumped erbium-doped fiber laser passively Q switched with a Co^{2+}:ZnSe crystal: modeling and experimental study", J. Opt. Soc. Am. B **19,** 353-359 (2002).

[99] R. J. Mears, L. Reekie, I. M. Jauncey, and D. N. Payne, "Low noise erbium-doped fiber amplifier operating at 1.054 μm," Electron. Lett. **23**, 1026-1028 (1987).

[100] J. J. Degnan, "Theory of the optimally coupled Q-switched laser," IEEE J. Quantum. Electron. **25**, 214-220 (1989).

[101] X. Zhang, S. Zhao, Q. Wang, B. Ozygus, and H. Weber, "Modeling of diode-pumped actively Q-switched lasers," IEEE J. Quantum. Electron. **35**, 1912-1918 (1999).

[102] G. P. Agrawal and N. K. Dutta, *Long-wavelength semiconductor lasers* (Van Nostrand Reinhold, New York, 1986).

[103] C. Mayol, R. Toral, and C. R. Mirasso, "Lyapunov-potential description for laser dynamics," Phys. Rev. A **59**, 4690-4698 (1999).

[104] S. Yamashita and M. Nishihara, "L-band erbium-doped fiber amplifier incorporating an inline fiber grating laser," IEEE J. Select. Topics Quant. Electron. **7**, 44-48 (2001).

[105] R. Paschotta, R. Haring, E. Gini, H. Melchior, U. Keller, H. L. Offerhaus, and D. J. Richardson, "Passively Q-switched 0.1-mJ fiber laser system at 1.53 μm," Opt. Lett. **24**, 388-400 (1999).

[106] K. T. Alligood, T. D. Sauer, and J. A. Yorke, *Chaos - An Introduction to Dynamical Systems* (Springer-Verlag, New York, 1996).

[107] A. N. Pisarchik, B. F. Kuntsevich, and R. Corbalán, "Stabilizing unstable orbits by slow modulation of a control parameter in a dissipative dynamic system," Phys. Rev. E **57**, 4046-4053 (1998).

[108] V. N. Chizhevsky and P. Glorieux, "Targeting unstable periodic orbits," Phys. Rev. E **51**, R2701-R2704 (1995).

[109] C. Grebogi, E. Ott, and J. A. Yorke, "Chaotic attractors in crisis," Phys. Rev. Lett. **48**, 1507-1510 (1982).

[110] D. Dangoisse, P. Glorieux, and D. Hennequin, "Laser chaotic attractor in crisis," Phys. Rev. Lett. **57**, 2657-2660 (1986).

[111] E. A. Jackson, *Perspectives of nonlinear dynamics* (Cambridge University Press, Cambridge, 1989).

[112] C. Mayol, S. I. Turovets, R. Toral, C. R. Mirasso, and L. Pesquera, "Main resonances in directly modulated semiconductor lasers: effect of

spontaneous emission and gain saturation," IEE Proc. Optoelectron. **148**, 41-45 (2001).

[113] A. N. Pisarchik and B. F. Kuntsevich, "Control of multistability in a directly modulated diode laser," IEEE J. Quantum Electron. (2002) (accepted for publication).

[114] S. Adachi and Y. Koyamada, "High-performance OTDR using Q-switched erbium-doped fiber ring laser and pulse expander," Technical Digest of Opt. Fiber Commun. Conf., Anaheim, pp. 613-615 (OSA, Washington D.C., 2002).

[115] A. Uchida, S. Yoshimori, M. Shinozuka, T. Ogawa, and F. Kannari, "Chaotic on-off keying for secure communications," Optics Letters **26**, 866-868 (2001).

[116] Gerardo-Cruz, S. V., Martinez-Gomez, M.A., Kir'yanov, A.V. et al., in Technical Digest (11-th International Conference on Laser Optic, St.-Peterburg, Russian, July 2003-Paper # ThR3-p49), p64 (2003).

[117] A.V. Kiryanov, N.N. Ilichev, and Yu.O. Barmenkov, ´´ Excited-state absorption as a source of nonlinear thermo-induced lensing and self-Q-switching in an all-fiber Erbium laser" Laser Phys. Lett. 1, No. 4, 194198.

[118] U. Parlitz and W. Lauterborn, Phys. Lett. A 107, (1995) 351.

[119] N. Platt, S.M. Hammel, J.F. Heagy, Phys. Rev. Lett. 72 (1994) 3498.

[120] S. Boccaletti, J. Kurths, G. Osipov, D.L. Valladares, C. Zhou, Physics Reports 366 (2002) 1.

[121] C. Schafer, M.G. Rosenbum, J. Kurths, H.H. Abel, Nature (London) 392 (1998) 239; P. Tass, M.G. Rosenblum, J. Weule, J. Kurths, A. Pikovsky, J. Volkmann, A. Schnitzler, H.J. Freund, Phys. Rev. Lett. 81 (1998) 3291; A. Neiman, X. Pei, D. Russell, W. Wojtenek, L. Wilkens, F. Moss, H.A. Braun, M.T. Huber, K. Voigt, Phys. Rev. Lett. 82 (1999) 660.

[122] G.D. Van Wiggeren, R Roy, Science 279 (1998) 1198.

[123] M. Lakshmanan, K. Murali, Chaos in Nonlinear Oscillators, World Scientific, Singapore, 1996.

[124] A. Kenfack, arXiv:nlin.CD/0304022, v.1, 14 Apr. 2003.